Colossal magnetoresistance: spectral properties of the Holstein double-exchange model and application to manganites

Martin Hohenadler

DIPLOMARBEIT

zur Erlangung des akademischen Grades Diplomingenieur
der Studienrichtung Technische Physik an der

Technischen Universität Graz

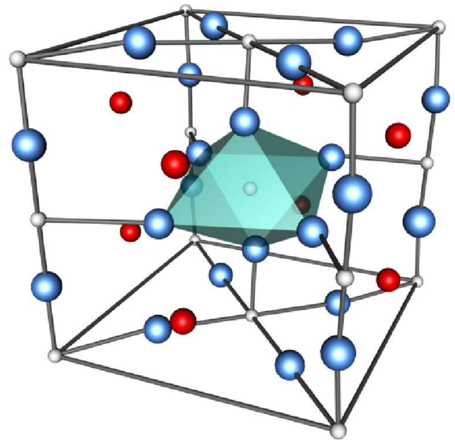

Betreuer:

O. Univ.-Prof. Dr. Wolfgang von der Linden
Institut für Theoretische Physik, TU Graz

Prof. David M. Edwards
Department of Mathematics, Imperial College, London

Dezember 2001

Second corrected edition. February 2002.

This document is available online at `www.itp.tu-graz.ac.at/~hohenadl`.

for Kathrin

Abstract

The many-body coherent potential approximation is used to calculate one-electron spectral functions, optical conductivity and spin-wave energy in the Holstein double-exchange model. The effect of electron-phonon coupling on these properties is studied in detail and comparison is made with experimental data on manganites. Satisfactory agreement is obtained with angle-resolved photoemission results on $La_{1.2}Sr_{1.8}Mn_2O_7$ and optical measurements on $Nd_{0.7}Sr_{0.3}MnO_3$. A pseudogap in the one-electron spectrum at the Fermi level plays an important role in both systems, but a small-polaron band is only predicted in the La system. A rigorous upper bound on spin-wave energies at $T = 0$ is derived. The spin-wave stiffness constant D decreases with increasing electron-phonon coupling g in a similar way to the Curie temperature T_{C}, but $D/(k_{\mathrm{B}}T_{\mathrm{C}})$ increases for large g (low T_{C}) as observed experimentally.

Contents

Physics is like sex: sure, it may give some practical results, but that's not why we do it.

(Richard Feynman)

1. Introduction

Recently interest has revived in manganites of the form $R_{1-x}A_xMnO_3$, where R is a trivalent rare-earth element such as La or Nd and A is a divalent alkaline earth ion such as Ca or Sr, which were first studied fifty years ago [1, 2].

The undoped ($x = 0$) compounds are antiferromagnetic insulators but upon doping, typically for $x \approx 0.2$–0.4, many of them become ferromagnetic metals. The origin of this metallic ferromagnetism has been explained soon after their discovery in terms of the double-exchange mechanism [3, 4]. However above the Curie temperature T_C many of the manganites become insulating, and this metal-insulator transition is unlike anything that occurs in ordinary ferromagnetic metals such as Fe, Co, Ni or Gd. Accompanying the metal-insulator transition is a large decrease in resistivity when a magnetic field is applied in the vicinity of T_C, which was first observed by Volger [5] in 1954.

There are competing theories of the metal-insulator transition in the manganites; the importance of electron-phonon coupling and the possible existence of small polarons or even bipolarons are hotly debated. Moreover the complex nature of these compounds, which is the result of the subtle interplay of a variety of physical effects, makes it extremely difficult to model them theoretically. Therefore, despite enormous experimental and theoretical effort, there are still many fundamental questions concerning, for example, the nature of the basic electronic structure.

Apart from the fascination of these systems from the theoretical point of view the sensitivity of their resistance to magnetic fields near T_C, which has been termed 'colossal magnetoresistance', gives rise to speculation about potential technical applications of the manganites.

A detailed overview on mixed-valence oxides is given by Coey [6]. Ramirez [7] reviews recent experimental results for manganites, and an extensive discussion of the importance of electron-phonon coupling and recent theoretical progress along these lines is by Edwards [8].

1.1. Electronic and crystal structure

In the undoped parent compound $LaMnO_3$, which is an antiferromagnetic insulator, each Mn ion has four d electrons. The approximately cubic crystal field splits the Mn

3d orbitals into energetically lower t_{2g} states, with d wavefunctions of xy, yz and zx type, and e_g states of $x^2 - y^2$ and $3z^2 - r^2$ symmetry. The spins of the four d electrons are aligned, by Hund's rule, leading to a $t_{2g}^3 e_g^1$ configuration of the Mn^{3+} ions with total spin $S = 2$. Doping removes x electrons per Mn atom. However there exist two pictures of the resulting electronic structure, depending on whether the electrons are removed from the O 2p band or from a narrow e_g band, resulting from hybridization of Mn d states with O 2p orbitals. This point is discussed in detail by Edwards [8]. Here we adopt the latter point of view, in which the remaining three t_{2g} electrons are regarded as forming a local spin of magnitude $S = 3/2$. In this case the e_g band contains $n = 1 - x$ electrons per atom with the possibility of metallic conduction. Strong Hund's rule coupling of the local spin and the e_g electrons, favouring 'high-spin' states with parallel local and itinerant moment, gives rise to strong electronic correlations. Double occupation of a Mn site is therefore strongly suppressed so that for $n = 1$ ($x = 0$) the system is a Mott insulator. For doping $x \approx 0.2$–0.4 the itinerant e_g electrons are completely spin-polarized and align the local Mn spins via the double-exchange mechanism (see section 2.1).

Manganites such as $LaMnO_3$ crystallize in a structure based on the ideal perovskite structure (see figure 1.1) which was first discovered in $CaTiO_3$. However the oxygen octahedra surrounding each Mn atom undergo two types of distortion; due to the La^{3+} ion being smaller than the O^{2-} ion they are rotated and tilted and, moreover, the Jahn-Teller (JT) effect (see section 1.2) leads to a tetragonal distortion. An important parameter in all manganites is the Mn–O–Mn bond angle which is less than 180° in a distorted structure. This reduction leads to reduced Mn–Mn hopping and hence to a narrowing of the e_g band.

We pointed out above that the undoped compound $LaMnO_3$ is an antiferromagnetic insulator. This antiferromagnetism results from the magnetic ordering of the Mn local spins, called A-type antiferromagnetic, with ferromagnetic basal planes arranged antiferromagnetically (see figure 1.1).

1.2. The Jahn-Teller effect

As mentioned in the last section the oxygen octahedra in the manganites undergo a tetragonal distortion due to the JT effect. This effect occurs as the cost in energy for a lattice deformation is a quadratic function of the linear displacement, x say, while the energy gained through the splitting of otherwise degenerate orbitals depends linearly on x. Hence it follows that for small enough distortions the split state is always favoured. In the manganites, the origin of the JT effect is the degenerate e_g^1 configuration of the Mn^{3+} ion; it splits the e_g level so as to lower the energy of the Mn $3z^2 - r^2$ orbital. The JT distortion in manganites such as $LaMnO_3$ is predominantly of the Q_2 type (see figure 1.1) in which each octahedron is stretched along one of the axes in the basal plane. The JT distortion also gives rise to orbital ordering in $LaMnO_3$

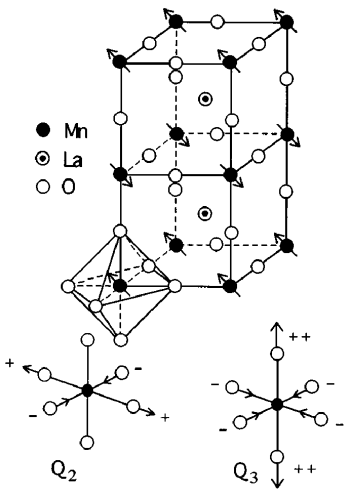

Figure 1.1.: The ideal cubic perovskite structure, showing the AF type A order for $LaMnO_3$. Also shown are the basal-plane distortion mode (Q_2) and the octahedral stretching mode (Q_3) which are present in the actual structure. (from reference [9])

with local $3z^2 - r^2$ orbitals pointing in alternate directions.

There is no evidence of the static JT effect discussed above in doped manganites such as $La_{0.7}Sr_{0.3}MnO_3$ [9]. Moreover the crystal structure of such doped compounds is much more nearly cubic, with a Mn–Mn spacing of 4–5Å [10]. However experiments indicate that a dynamical JT effect may occur as the e_g electron moves from site to site. The e_g electron carrying with it a local JT distortion of the surrounding oxygen octahedron is called a 'JT polaron'. We discuss polarons in section 2.3.1.

1.3. LSMO and LCMO

Most recent work has focused on the two manganites $La_{1-x}Sr_xMnO_3$ (LSMO) and $La_{1-x}Ca_xMnO_3$ (LCMO). Phase diagrams in the x-T plane of LSMO and LCMO are shown in figure 1.2. For $x < 0.5$ the two diagrams look very similar with a maximum Curie temperature T_C at $x \approx 0.33$. However a closer look reveals that the maximum T_C in LCMO (270K) is much lower than in LSMO (370K). Furthermore the paramagnetic state above T_C is insulating in LCMO and metallic in LSMO.

Here we restrict our discussion to the region $x \approx 0.33$ where T_C has its maximum, in the middle of the ferromagnetic regime. We are therefore not concerned with the existence of charge-ordering[1] for $x \approx 0.5$ or $x \lesssim 0.2$ (see figure 1.2), and it is usually assumed that the system is homogeneous. Phase separation with, for example, holes

[1] For quarter-filling $n = 0.5$, for example, interatomic Coulomb repulsion of e_g electrons leads to a configuration in which occupied and unoccupied Mn sites alternate in the entire lattice.

segregating in ferromagnetic metallic clusters has been proposed by Moreo et al. [11] and Nagaev [12]. However in most of the work along these lines models neglecting long-range Coulomb interaction have been employed, leading to unrealistic predictions of macroscopic phase separation [11].

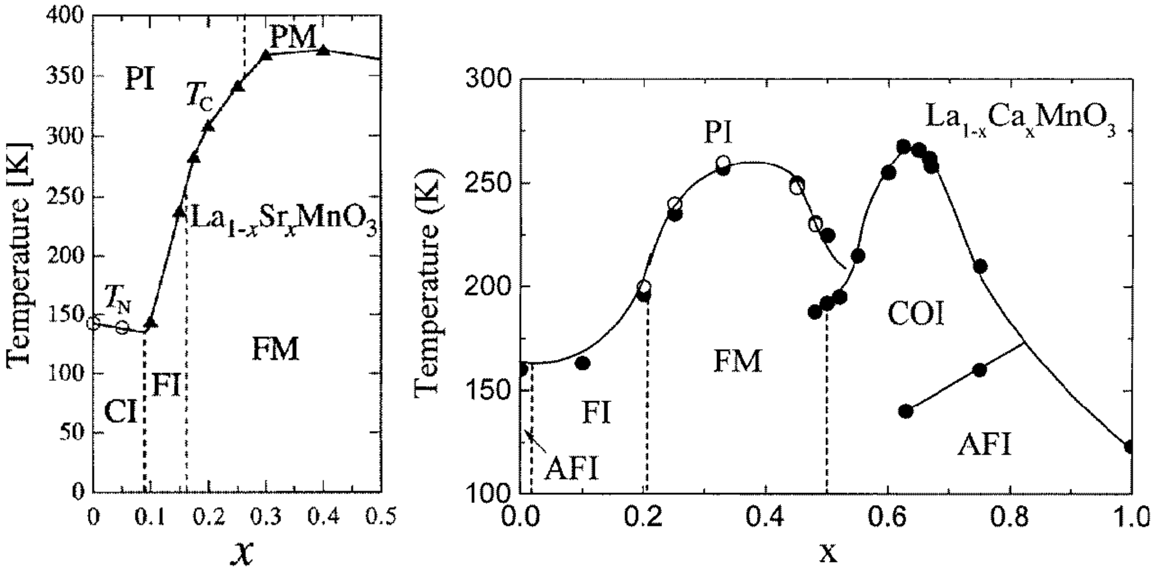

(a) (from reference [13]) (b) (from reference [14])

Figure 1.2.: Phase diagram for LSMO (a) and LCMO (b). The various states are: paramagnetic insulating (PI), paramagnetic metal (PM), canted insulating (CI), ferromagnetic insulating (FI), ferromagnetic metal (FM), antiferromagnetic insulating (AFI) and charge-ordered insulating (COI). T_C, T_N are Curie and Neél temperatures, respectively.

Figures 1.3 and 1.4 show the resistivity as a function of temperature for LSMO (figure 1.3) and LCMO (figure 1.4). Figure 1.4 clearly shows the metal-insulator transition in LCMO; for $T < T_C$ $\partial\rho/\partial T > 0$ as in a metal, while for $T > T_C$ $\partial\rho/\partial T < 0$ as in a semi-conductor or insulator. On the contrary in LSMO (figure 1.3, $x = 0.3$) $\partial\rho/\partial T > 0$ for all temperatures. Moreover the maximum resistivity in the paramagnetic state above T_C is about an order of magnitude larger in LCMO (~ 40mΩcm) than in LSMO (~ 4mΩcm).

A satisfactory theory of the manganites must be able to explain these huge differences between two apparently very similar materials.

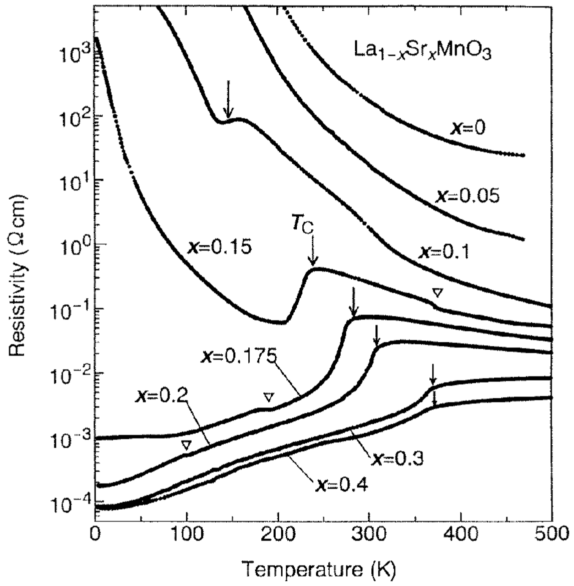

Figure 1.3.: Resistivity versus temperature for $La_{1-x}Sr_xMnO_3$ crystals. Arrows indicate the Curie temperature T_C for the ferromagnetic phase transition. (from reference [15])

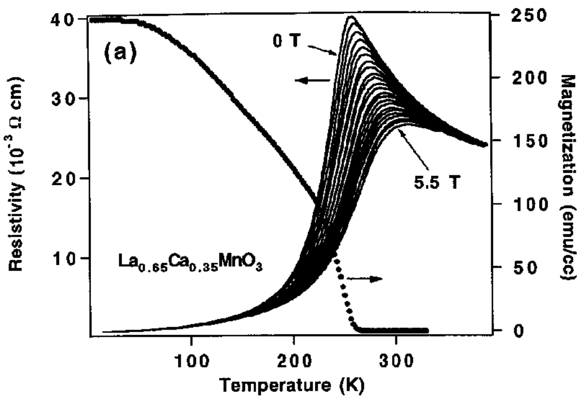

Figure 1.4.: Resistivity (solid lines) of $La_{0.65}Ca_{0.35}MnO_3$, acquired in applied fields ranging from 0 to 5.5T, and the bulk magnetization in an in-plane applied field of 50G (•), both as a function of temperature. (from reference [16])

1.4. The colossal magnetoresistance effect

The rediscovery of colossal magnetoresistance (CMR) in thin films of manganites such as LSMO or LCMO in the 1990's has inspired much of the recent research in this field. Figure 1.4 shows the resistivity and the magnetization of a $La_{0.65}Ca_{0.35}MnO_3$ crystal. The application of a magnetic field of 5.5 T for $T \approx T_C$ leads to a 30% reduction in resistivity. The CMR effect is much more remarkable in thin films with a maximum reduction in resistivity by a factor of up to 10^4.

The CMR effect may be used in a device to sense magnetic fields, or for magnetic storage devices. However the use of manganites for such applications strongly depends on a thorough understanding of the underlying physics, which allows the design of optimized materials.

1.5. Elements of condensed matter theory

This section summarizes some of the fundamental equations and relations of condensed matter theory which will be used in the following chapters.

1.5.1. Second quantization

In the second quantized form of quantum mechanics, which was introduced to simplify calculations involving many identical particles (see e.g. Nolting [17]), fermions and bosons are described in terms of so called creation (denoted by $a_r^\dagger$) and annihilation (a_r) operators. The wave function of a many-particle system can be described in the so-called Fock representation in terms of the number of particles occupying each of the available orbitals, which are labeled by a set of quantum numbers r, say.

The symmetry of the many-body wavefunction imposes commutation relations of the corresponding operators. In the notation of Nolting [17] these are ($\hbar = 1$)

$$[a_r, a_p]_{-\eta} = 0 \tag{1.1a}$$
$$[a_r^\dagger, a_p^\dagger]_{-\eta} = 0 \tag{1.1b}$$
$$[a_r, a_p^\dagger]_{-\eta} = \delta_{rp}\,, \tag{1.1c}$$

where $[A, B]_{-\eta} = AB - \eta BA$ and $\eta = +$ for bosons and $\eta = -$ for fermions.

Moreover, the following commutators for the particle number operator $n_r = a_r^\dagger a_r$ are useful

$$[n_r, a_p^\dagger]_- = \delta_{rp} a_p^\dagger \tag{1.2a}$$
$$[n_r, a_p]_- = -\delta_{rp} a_p\,. \tag{1.2b}$$

It is often convenient to use the notation $[\ ,\ ]_- = [\ ,\ ]$ and $[\ ,\ ]_+ = \{\ ,\ \}$.

1.5.2. Theory of Green functions

In this work we use the method of Green functions to calculate physical properties of the many-particle systems. We define the retarded Green function for fermion operators A and B with no explicit time-dependence by

$$G_{AB}^{\mathrm{ret}}(t) \equiv \langle\langle A; B\rangle\rangle_t = -\mathrm{i}\theta^+(t)\langle\{A(t), B\}\rangle\,, \tag{1.3}$$

and its Fourier transform by

$$\langle\langle A; B\rangle\rangle_\epsilon = \int_{-\infty}^{\infty} \mathrm{d}t \mathrm{e}^{\mathrm{i}\epsilon t}\langle\langle A; B\rangle\rangle_t\,. \tag{1.4}$$

Here $\theta^+(x) = 1$ for $x > 0$ and 0 otherwise and ϵ is restricted to the upper half of the complex plane. The latter Green function satisfies the equation of motion

$$\epsilon\langle\langle A; B\rangle\rangle_\epsilon = \langle\{A, B\}\rangle + \langle\langle [A, H]; B\rangle\rangle_\epsilon\,, \tag{1.5}$$

H being the Hamiltonian of the system. The angular brackets $\langle\ldots\rangle$ in the above equations denote thermal expectation values and are calculated via

$$\langle X\rangle = \frac{1}{Z}\mathrm{Tr}\left(\mathrm{e}^{-\beta\mathcal{H}}X\right)\,, \quad Z = \mathrm{Tr}\;\mathrm{e}^{-\beta\mathcal{H}}\,, \quad \mathcal{H} = H - \mu N \tag{1.6}$$

where N is the particle number operator and μ is the chemical potential.

We define the one-electron retarded Green function as[2]

$$G_{ij\sigma}(\epsilon) = \langle\langle a_{i\sigma}; a_{j\sigma}^\dagger\rangle\rangle_\epsilon \tag{1.7}$$

where $a_{j\sigma}^\dagger$ ($a_{i\sigma}$) creates (annihilates) an electron of spin σ on lattice site j (i), and its Fourier transform by

$$G_{\boldsymbol{k}\sigma} = \frac{1}{N}\sum_{\boldsymbol{R}_{ij}} \mathrm{e}^{\mathrm{i}\boldsymbol{k}\cdot\boldsymbol{R}_{ij}} G_{ij\sigma} \tag{1.8}$$

where $\boldsymbol{R}_{ij}$ is the lattice vector connecting sites i and j, and N is the number of unit cells.

For a system of interacting particles, the general form of the $\boldsymbol{k}$ dependent Green function is

$$G_{\boldsymbol{k}\sigma}(\epsilon) = \frac{1}{\epsilon - \epsilon_{\boldsymbol{k}} - \Sigma_{\boldsymbol{k}\sigma}(\epsilon)}\,, \tag{1.9}$$

$\epsilon_{\boldsymbol{k}}$ being the band energy. Here $\Sigma_{\boldsymbol{k}\sigma}(\epsilon)$ is the so-called self-energy which is zero for a system of non-interacting particles, but non-zero and complex in general. The self-energy directly contains all interaction and correlation effects. In the case of the retarded Green function ϵ in equation (1.9) has a small positive imaginary part. Finally, the one-particle density of states is defined by

$$N(\epsilon) = -\frac{1}{\pi}\mathrm{Im}\;G(\epsilon)\,. \tag{1.10}$$

[2]From now on we drop the superscript 'ret' since we exclusively use retarded Green functions in this work.

1.5.3. A useful relation

We will often encounter expressions containing a $\boldsymbol{k}$ sum over the first Brillouin zone, where the summand depends on $\boldsymbol{k}$ through $\epsilon_{\boldsymbol{k}}$ only. In this case the sum can be replaced by an energy integral using the relation

$$\frac{1}{N}\sum_{\boldsymbol{k}} F(\epsilon_{\boldsymbol{k}}) \to \int \mathrm{d}\epsilon D_0(\epsilon) F(\epsilon) \tag{1.11}$$

where $D_0(\epsilon)$ is the bare density of states per atom.

2. Models

Soon after their initial discovery by Jonker and van Santen [1, 2] more than fifty years ago Zener [3] suggested the so-called double-exchange (DE) mechanism as the origin of the metallic ferromagnetism in the manganites. DE was successful in explaining the crossover of, for example, $La_{1-x}Ca_xMnO_3$ from an antiferromagnetic insulator at $x = 0$ to a ferromagnetic metal for $x \gtrsim 0.3$. The DE mechanism was generalized by Anderson and Hasegawa [4] to the DE model (see section 2.2) which long seemed to be sufficient to describe the manganites. Although the model can account qualitatively and in some cases even quantitatively for some of the experimental results such as the magnetoresistance effect, the Curie temperature or the spin-wave spectrum, especially for LSMO, many predictions are not in agreement with measurements.

Millis et al. [18] pointed out that the DE model cannot account for the large resistivity of the manganites in the paramagnetic state above T_C and proposed that electron-phonon coupling may play an important role. Much experimental data on the manganites in both the paramagnetic and ferromagnetic state is interpreted in terms of standard Holstein small-polaron theory, which will be discussed briefly in section 2.3.1. Other authors, however, adopt a very different point of view. Furukawa [19], for example, completely neglects electron-phonon coupling and argues in favour of models of phase separation.

As pointed out by Green [20] and Edwards [8] many manganites fall in an intermediate electron-phonon coupling regime where standard small-polaron theory does not apply. Green's recent treatment of the so-called Holstein-DE model is the only theory so far that can describe this critical regime where a crossover from intermediate coupling to polaronic behaviour occurs and provides the basis of this work. It will therefore be presented in some detail in section 3.3.2.

We will show in chapter 4 that small-polaron theory is not compatible with optical data of pseudocubic manganites. However it does apply in quasi-two dimensional bilayer manganites such as $La_{1.2}Sr_{1.8}Mn_2O_7$. On the other hand experiments indicate that even in LSMO electron-phonon coupling is not negligible, in contrast to the arguments of Furukawa [19], so that the pure DE model is not sufficient. In summary a quantum-mechanical treatment of a model including DE and electron-phonon coupling (the Holstein-DE model) seems to give a reasonable description of the manganites, with doping $x \approx 0.3$.

As discussed in the last chapter, for $x \approx 0.2$–0.4, charge-ordering is expected not to occur and we assume the system to be homogeneous. Moreover in most of the recent theoretical work on the manganites further approximations are made which are not all generally accepted. The first of these is the use of a one-band model, neglecting the double degeneracy of the e_g band. However if one includes the intraatomic Coulomb interaction ('Hubbard U'), which is found experimentally to be large ($\sim$ 4eV), calculations using two-band models give results which are very similar to the simpler one-band calculations. Another simplification often made is to take the limit of strong Hund's rule coupling in which states with antiparallel local and e_g moment are completely suppressed. Although Hund's rule coupling is found to be large ($\sim$ 4eV) this approximation clearly affects the results for properties such as, for example, optical conductivity (see section 4.2). However the low-energy physics should still be reasonably described. Finally many authors take the limit of classical spins $S \to \infty$. In this limit spin-flip processes through exchange of angular momentum between local spins and conduction electrons cannot occur. Edwards et al. [21] has shown that, for example, in the DE model many results such as Curie temperature or resistivity do not vary enormously with S so that taking the classical limit $S = \infty$ is justified. The same insensitivity to changes in the value of S is expected in other models.

A detailed discussion of the validity of the models discussed in the sequel, as well as of recent theoretical progress in this field is given by Edwards [8].

2.1. The double-exchange mechanism

The DE mechanism is assumed to operate in mixed-valence systems of magnetic ions such as the manganites. As discussed in chapter 1 the undoped compound with nominal valence $La^{3+}Mn^{3+}O_3^{2-}$ ($x = 0$) is an antiferromagnetic insulator while $La_{1-x}A_xMnO_3$ (A = Ca, Sr, Pb) for $x \geq x_c \approx 0.2$ is a ferromagnetic metal. In the doped system x trivalent La ions per formula are replaced by divalent A ions. The missing third electron comes from a Mn ion leading to a mixed-valence state of the form

$$\left(La^{3+}_{1-x}A^{2+}_{x}\right) Mn^{3+}_{1-x}Mn^{4+}_{x}O_3 \, .$$

Zener [3] suggested that the onset of metallic ferromagnetism for $x \geq x_c$ is driven by hopping of the e_g electrons between neighbouring Mn sites. We shall see below that this hopping indeed leads to an effective ferromagnetic coupling of the localized spins.

As discussed in chapter 1 the magnetic ordering in undoped manganites such as $LaMnO_3$ is A-type antiferromagnetic (see figure 1.1). However, since the ferromagnetic coupling due to the DE mechanism appears to dominate, models for manganites in the CMR regime of doping often neglect this direct Mn–Mn coupling, but calculations including a superexchange interaction between local Mn spins exist.

We follow Nolting [22] and discuss the DE mechanism using a cluster model consisting of two Mn ions of valence 3+ and 4+ respectively, and an O^{2-} ion in between (see figure 2.1(a)). The excess electron of Mn^{3+}, electron 1 say, does not hop directly to Mn^{4+} but via the diamagnetic oxygen ion in between. According to Zener electron 1 hops to O^{2-} and at the same time one of the two O 2p electrons (the one with the same spin as electron 1) hops to Mn^{4+}. Since this process involves the simultaneous transfer of two electrons it has been termed 'double exchange'.

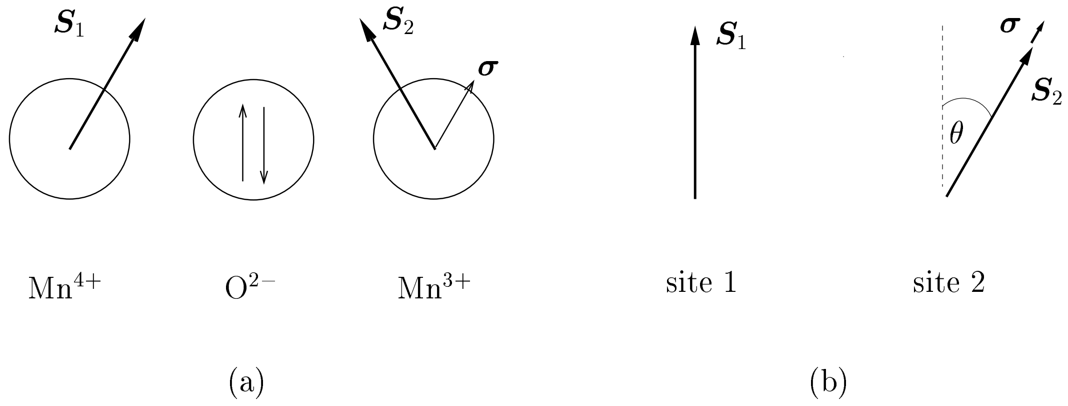

Figure 2.1.: The cluster model for the DE mechanism.

On a Mn site the electron with spin operator $\boldsymbol{\sigma}$ interacts with the local spin $\boldsymbol{S}$ through Hund's rule exchange coupling favouring parallel alignment. The interaction Hamiltonian for this cluster model is[1]

$$H_{\mathrm{sd}} = -J \sum_{i=1}^{2} \boldsymbol{\sigma}_i \cdot \boldsymbol{S}_i \,. \tag{2.1}$$

It is important to keep in mind that the e_g electron is not in a bound state (i.e. in an orbital) of the Mn ion but remains itinerant, interacting with the magnetic moment formed by the localized t_{2g} electrons.

In typical manganites the Hund's rule coupling J is large compared to the width of the conduction band so that the spin–spin interaction cannot be treated as a small perturbation of the e_g electrons. The local and itinerant spins can couple to a total spin of $S \pm \frac{1}{2}$ with energies $-JS/2$ and $J(S+1)/2$ respectively.

Let the classical vector $\boldsymbol{S}_1$, which describes the localized spin on site 1, define the axis of quantization (z-axis). Then the states of the itinerant electron on site 1 are

$$|\alpha\rangle = \begin{pmatrix} 1 \\ 0 \end{pmatrix}, \quad |\beta\rangle = \begin{pmatrix} 0 \\ 1 \end{pmatrix} . \tag{2.2}$$

[1] The subscript sd arises from the fact that in many DE systems s electrons form a conduction band and interact with localized d electrons.

If we denote the angle between the spins $\boldsymbol{S}_1$ and $\boldsymbol{S}_2$ by θ (see figure 2.1(b)), the corresponding states at site 2 are

$$
\begin{aligned}
|\alpha'\rangle &= \begin{pmatrix} \cos\theta/2 \\ \sin\theta/2 \end{pmatrix} = \cos\theta/2\,|\alpha\rangle + \sin\theta/2\,|\beta\rangle\ , \\
|\beta'\rangle &= \begin{pmatrix} \sin\theta/2 \\ -\cos\theta/2 \end{pmatrix} = \sin\theta/2\,|\alpha\rangle - \cos\theta/2\,|\beta\rangle\ .
\end{aligned} \tag{2.3}
$$

Hence, in our model consisting of only two lattice sites we may use the following complete basis

$$
\begin{aligned}
|1\rangle &= |1\alpha\rangle\ :\ \text{electron at site 1 in state}\,|\alpha\rangle\ , \\
|2\rangle &= |1\beta\rangle\ :\ \text{electron at site 1 in state}\,|\beta\rangle\ , \\
|3\rangle &= |2\alpha'\rangle\ :\ \text{electron at site 2 in state}\,|\alpha'\rangle\ , \\
|4\rangle &= |2\beta'\rangle\ :\ \text{electron at site 2 in state}\,|\beta'\rangle
\end{aligned}
$$

where we made use of our assumption that the spin of the electron is conserved in the hopping process.

At this point we can forget about the oxygen ion since it merely plays the role of a catalyst for the electron hopping. We are therefore left with a cluster of two Mn ions between which the DE mechanism operates. The complete Hamiltonian including the kinetic energy term is

$$H = H_0 + H_{\mathrm{sd}} \tag{2.4}$$

As shown in Nolting [22], if we define the transfer matrix element t by

$$\langle 1\alpha,\beta|H|2\alpha',\beta'\rangle = \langle 1\alpha,\beta|H_0|2\alpha',\beta'\rangle = t\langle\alpha,\beta|H|\alpha',\beta'\rangle\,, \tag{2.5}$$

the Hamiltonian in the basis $\{|1\rangle\,,|2\rangle\,,|3\rangle\,,|4\rangle\}$ becomes

$$H = \begin{pmatrix} -\frac{1}{2}JS & 0 & t\cos\theta/2 & t\sin\theta/2 \\ 0 & \frac{1}{2}J(S+1) & t\sin\theta/2 & -t\cos\theta/2 \\ t\cos\theta/2 & t\sin\theta/2 & -\frac{1}{2}JS & 0 \\ t\sin\theta/2 & -t\cos\theta/2 & 0 & \frac{1}{2}J(S+1) \end{pmatrix}\ . \tag{2.6}$$

Clearly H is not diagonal as the basis states we used are not eigenstates.

The Hamiltonian (2.6) can be diagonalized exactly. However, for brevity, we do not give the full derivation here but instead focus on the results. It may be shown [22] that we can derive an effective Hamiltonian which describes the DE mechanism in terms of a direct interaction of the localized Mn spins as in the Heisenberg model for magnetic insulators.[2] The result is

$$H_{\mathrm{eff}} = -t\sum_{n=0}^{\infty} J_n(S)\,(\boldsymbol{S}_1\cdot\boldsymbol{S}_2)^n\ . \tag{2.7}$$

[2]The Heisenberg model is discussed briefly in chapter 5.

Not all powers of the sum in H_{eff} are independent [22]. The number of terms depends on the magnitude of the local spins S. If we take $S = \frac{1}{2}$, for example, Hamiltonian (2.7) becomes

$$H_{1/2} = -\frac{3}{8}t - \frac{1}{2}t\frac{1}{\hbar^2}\left(\boldsymbol{S}_1 \cdot \boldsymbol{S}_2\right) . \tag{2.8}$$

The case $S = 3/2$ relating to the manganites gives a more complicated result. However it can be shown that the dominating bilinear term, corresponding to $n = 1$ in equation (2.7), always leads to ferromagnetic coupling of the spins.

2.2. The double-exchange model

In this section we will first discuss a general class of Hamiltonians often used to describe systems of magnetic ions interacting with each other as well as with itinerant electrons. In a certain range of parameters they constitute the DE model.

A model Hamiltonian for a system of localized magnetic moments and conduction electrons is

$$H = \sum_{ij\sigma} t_{ij} c_{i\sigma}^{\dagger} c_{j\sigma} + \sum_{ij} J_{ij} \boldsymbol{S}_i \cdot \boldsymbol{S}_j + J \sum_i \boldsymbol{\sigma}_i \cdot \boldsymbol{S}_i + h \sum_i (S_i^z + \sigma_i^z) \tag{2.9}$$

where $c_{i\sigma}^{\dagger}$ creates an electron of spin σ on lattice site i, $\boldsymbol{S}_i$ is a local spin operator and $\boldsymbol{\sigma}_i = (\sigma_i^x, \sigma_i^y, \sigma_i^z)$ is a conduction electron operator defined by

$$\sigma_i^+ = \sigma_i^x + i\sigma_i^y = c_{i\uparrow}^{\dagger} c_{i\downarrow} \, , \; \sigma_i^- = \sigma_i^x - i\sigma_i^y = c_{i\downarrow}^{\dagger} c_{i\uparrow} \, , \; \sigma_i^z = \frac{1}{2}\left(n_{i\uparrow} - n_{i\downarrow}\right) . \tag{2.10}$$

Here $n_{i\sigma} = c_{i\sigma}^{\dagger} c_{i\sigma}$ and t_{ij} is the hopping integral for hopping between sites i and j. J_{ij} and J are the coupling constants for coupling between localized and between localized and itinerant moments respectively. Finally, the last term describes the coupling of the system to an applied magnetic field, h being the Zeeman energy.

The third term in equation (2.9) can lead to very interesting effects. For example, it can cause an effective coupling of the localized spins $\boldsymbol{S}_i$ which is much stronger than the direct interaction described by the second term. Moreover scattering of conduction electrons by local spins can play a dominant role for the resistivity of the system.

As the direct coupling of local moments is often negligible[3] we will not consider it in the sequel. The exchange parameter J in equation (2.9) is negative if the local exchange coupling arises from hybridization between the localized and itinerant electrons. This is, for example, the case in anomalous rare-earth systems exhibiting heavy-fermion behaviour, and the Hamiltonian (2.9) is then usually called the Kondo lattice model.[4]

[3] As discussed in section 2.1, in the manganites neighbouring Mn spins are coupled antiferromagnetically. However the ferromagnetic coupling below T_{C} due to the DE effect is much stronger.

[4] This is due to its connection to the so-called Kondo impurity model which has a local spin on one lattice site only, to which the conduction electrons couple antiferromagnetically.

For $J > 0$ we shall distinguish two distinct physical regimes. If $J \ll W$, $2W$ being the width of the conduction band, the local exchange interaction can be treated as a small perturbation of the itinerant electrons. This gives rise to the Ruderman-Kittel-Kasuya-Yosida (RKKY) interaction, which oscillates in space and changes periodically from ferro- to antiferromagnetic [22]. In most rare-earth systems this leads to oscillatory or spiral configurations of the localized f (d) electron moments. The Hamiltonian in this weak-coupling regime is often called the s–f (s–d) model.

Clearly for $J \gg W$ perturbation theory is no longer applicable. A conduction electron can only hop onto a site with its spin parallel to the local moment. Moreover, if the conduction band is not completely filled double occupation of sites is strongly suppressed. If the system is half-filled (band filling $n = 1$) we have a so called Mott insulator, i.e. every site is occupied by one electron so that hopping would lead to energetically unfavourable double occupations. The limit $J \gg W$ is called the 'double exchange limit' and the model described by the Hamiltonian

$$H_{\mathrm{DE}} = \sum_{ij\sigma} t_{ij} c^{\dagger}_{i\sigma} c_{j\sigma} - J \sum_{i} \boldsymbol{S}_i \cdot \boldsymbol{\sigma}_i - h \sum_{i} (S^z_i + \sigma^z_i) \tag{2.11}$$

is referred to as the DE model.

In application to the manganites the first term in H_{DE} describes the hopping of the $\mathrm{e_g}$ electrons between neighbouring Mn sites, $\boldsymbol{S}_i$ corresponds to the localized moments of magnitude $S = 3/2$ formed by the three $\mathrm{t_{2g}}$ electrons and J is the Hund's rule exchange parameter coupling local and itinerant moments on the same Mn ion.

As discussed in section 2.1, the DE model incorporates the double-exchange mechanism. This is obvious if we take the limit of classical spins $S \to \infty$. In this case the effective hopping integral for hopping between neighbouring sites i and j becomes [4]

$$t = t_{ij} \cos{(\theta/2)} \tag{2.12}$$

where θ is the angle between the local spins $\boldsymbol{S}_i$ and $\boldsymbol{S}_j$. The cosine factor arises from the scalar product of two spin-$\frac{1}{2}$ eigenstates with different axes of quantization, as in the derivation of the effective Hamiltonian in section 2.1.

Clearly equation (2.12) favours parallel (i.e. ferromagnetic, $\theta = 0$) alignment of neighbouring spins as this allows the conduction electrons to gain kinetic energy (see figure 2.2). As the temperature is raised spin disorder will lead to a narrowing of the conduction band ($t = \frac{2}{3} t_{ij}$ in the paramagnetic state[5]) and therefore to an increase in resistivity. On the other hand application of a magnetic field near the Curie temperature polarizes the spins in the system and thereby reduces the resistivity. Hence it follows that the DE model can in principle explain the ferromagnetic to paramagnetic phase transition and the large increase in resistivity ρ in the paramagnetic state, as well as the sensitivity of ρ to an applied magnetic field. However, as pointed out at the

[5]This is the result of averaging $\cos\theta/2$ over the solid angle.

beginning of this chapter, the DE model cannot account for the very high resistivity in the manganites above T_C; also it cannot explain the huge differences between, for example, LSMO and LCMO.

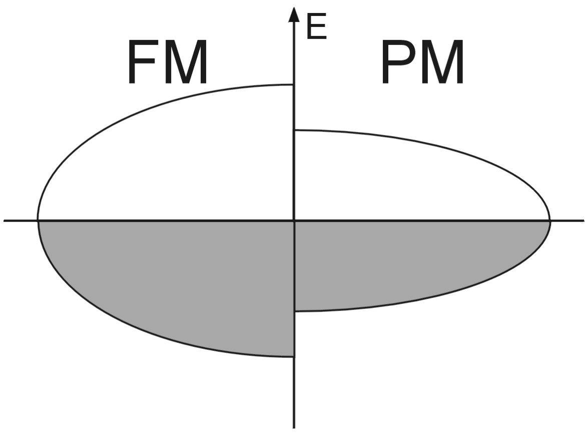

Figure 2.2.: In the case of a partially filled e_g band the band narrowing in the paramagnetic state leads to a reduced kinetic energy of the e_g electrons.

2.3. The Holstein and the Holstein-DE model

As discussed above the DE model is not sufficient to explain the physics of the manganites completely. Experimental evidence for unusually strong electron-phonon coupling lead to the formulation of an extended model including the coupling of the electrons to local phonons. While Millis et al. [23] treated the phonons classically, Green [20] considered a model with quantum phonons as in the Holstein model for small polarons. He called this extended model the Holstein-DE model.

2.3.1. The Holstein model and polarons

In chapter 1 we introduced the term 'polaron' for a charge carrier in a solid which is coupled to a local 'polarization' of the surrounding lattice. This 'polarization' can be, for example, a local lattice distortion, a real (electrostatic) polarization due to a displacement of the ions from their equilibrium positions or even a polarization of neighbouring spins (magnetic polaron). However in the context of the manganites we only consider the first of the above possibilities. The state of a carrier coupled to the local polarization has a binding energy which is called the polaron binding energy E_p.

As pointed out in chapter 1, in the manganites, strong electron-phonon coupling in combination with the JT effect gives rise to the formation of so-called JT polarons. The corresponding lattice distortion is predominantly of the Q_2 type (see figure 1.1). Before we formulate the Holstein-DE model for the manganites we give a short introduction to the Holstein model and to small-polaron theory. The latter is still widely used to interpret experimental data on manganites. However we will see in chapter 4 that standard small-polaron theory does not apply to pseudocubic manganites above or below T_{C}. The following discussion is based on Mahan's book [24].

Polarons become 'small' when they become localized which occurs for sufficiently strong electron-phonon coupling and a narrow conduction band. In contrast, weak electron-phonon coupling in combination with a broad band allows the electron to move in a coherent, Bloch-like motion. The effect of the phonons in this case is to slightly enhance its effective mass. This is sometimes called a 'large polaron'.

Small polarons are assumed to have a size comparable with atomic distances. Because of its localized state the polaron does no longer move in a translationally continuous way. Instead it hops from site to site whenever the necessary energy for the elastic lattice distortion is available. Thus the electron occupies an orbital state $\phi(\boldsymbol{r} - \boldsymbol{R}_i)$, say, centred on lattice site i which is the same on every ion in the periodic system. The electron may move from site to site due to the overlap or nonorthogonality of the orbitals on neighbouring ions, as in the tight-binding model. The phonons are coupled to the electron at whichever site it is on.

Holstein [25, 26, 24] considered the following model (the Holstein model) to study small polarons

$$H = \sum_{ij\sigma} t_{ij} c^\dagger_{i\sigma} c_{j\sigma} - g \sum_i n_i (b^\dagger_i + b_i) + \omega \sum_i b^\dagger_i b_i \tag{2.13}$$

where $b^\dagger_i$ creates an Einstein phonon[6] of energy ω which couples to the local electron occupation number $n_i = \sum_\sigma n_{i\sigma}$ with coupling strength g. We stress that the Holstein model is symmetric in the electron's spin σ. This will not be so in the Holstein-DE model discussed in the next section.

The model described by equation (2.13) exhibits the two different types of polaronic behaviour, namely small and large polarons, in the limit of strong or weak coupling, respectively. The most difficult regime to treat theoretically is the regime of intermediate electron-phonon coupling where a crossover from large to small polarons occurs. A detailed overview of the methods and results for the Holstein model is given by Mahan [24]. Here we merely reproduce some results of small-polaron theory which will be referred to in later chapters.

A very important result is that the dc conductivity σ_{dc} of the Holstein model in the small-polaron regime is thermally activated and has the form [24]

$$\sigma_{\mathrm{dc}} \propto \exp\left(-\frac{\bar{\Delta}}{k_{\mathrm{B}}T}\right) . \tag{2.14}$$

[6] In this model the phonons have a constant (i.e., independent of wave-vector $\boldsymbol{k}$) dispersion relation $E = \hbar\omega$, as in Einstein's model for lattice vibrations in a crystal.

Here $\bar{\Delta}$ is an activation energy, equal to half the polaron binding energy E_{p}, which has its origin in the energy necessary to deform the lattice when an electron hops onto a site. Equation (2.14) shows that with rising temperature T the conductivity increases as more and more conduction electrons have enough thermal energy to overcome the hopping barrier $\bar{\Delta}$.

As shown in Mahan [24] there is also a relation between the real part of the optical conductivity $\sigma(\nu)$ and the dc conductivity

$$\sigma(\nu) = \sigma_{\mathrm{dc}} \frac{1 - \mathrm{e}^{-\beta\nu}}{\beta\nu} \exp\left[-\frac{(\nu - \beta\gamma)^2}{4\gamma} + \frac{\bar{\Delta}}{k_{\mathrm{B}}T} \right] \tag{2.15}$$

where $\beta = (k_{\mathrm{B}}T)^{-1}$ as usual and $\gamma = 4\bar{\Delta} k_{\mathrm{B}} T$. According to equation (2.15) the optical conductivity is a Gaussian with its maximum located at $\nu_{\mathrm{max}} = \beta\gamma = 4\bar{\Delta}$. This is an important test for the validity of small-polaron theory in the manganites. We will show in chapter 4 that the above results are not consistent with experimental data.

Despite its simplicity the Holstein model actually applies in some cases to conduction bands of semi-conductors and ionic solids which have their minimum at the Γ point and have an isotropic effective mass.

2.3.2. The Holstein-DE model

Green [20] combined the two models discussed in the previous sections with the intention to obtain a model capable of describing the physics of the manganites for doping $x \approx 0.3$. He called this model, in which the electrons of the DE model also couple to local phonons as in the Holstein model, the Holstein-DE model. The Hamiltonian is

$$\begin{aligned} H_{\mathrm{HDE}} = & \sum_{ij\sigma} t_{ij} c^{\dagger}_{i\sigma} c_{j\sigma} - J \sum_i \boldsymbol{S}_i \cdot \boldsymbol{\sigma}_i - h \sum_i \left(S^z_i + \sigma^z_i \right) \\ & - g \sum_i n_i \left(b^{\dagger}_i + b_i \right) + \omega \sum_i b^{\dagger}_i b_i \,. \end{aligned} \tag{2.16}$$

As in the DE model the double degeneracy of the $\mathrm{e_g}$ band is neglected. However we pointed out in chapter 1 that the JT effect splits the $\mathrm{e_g}$ band. Consequently, within the Holstein-DE model, we only consider the lower-lying $\mathrm{e_g}$ orbital so that the JT effect always lowers the energy of the $\mathrm{e_g}$ electron.

The electron-phonon coupling term in equation (2.16) is of the breathing-mode form $-g' \sum_i n_i x_i$, where x_i is the displacement of a shell of atoms surrounding site i.[7] However if we choose the phonon energy ω appropriately we may regard it as an

[7] This can easily be seen if we look at the definition of the displacement operator x for the case of a single harmonic oscillator. In second-quantized form we have

$$x = \sqrt{\frac{\hbar}{2m\omega}} (b^{\dagger} + b) \,.$$

effective JT coupling to the Q_2 mode (see figure 1.1). The last term in equation (2.16) corresponds to vibrations of the O_6 octahedra about the central Mn with frequency ω.

An unfortunate feature of the pure Holstein model is that its ground state consists of unphysical[8] singlet bipolarons with two electrons bound to the same site. However this problem does not appear in the Holstein-DE model since for $J \gg W$ (the DE limit) double occupation is strongly suppressed.

Both the DE and the Holstein-DE model neglect the effect of A-site disorder due to doping where, for example, La ions are replaced by Ca or Sr and which gives rise to scattering of the e_g electrons.

The following discussion of previous theoretical results for the Holstein-DE model is cited from Green [20].

citation

Hamiltonian (2.16) was first studied by Röder et al. [27], who treated the Hund coupling using a mean-field approximation and the electron-phonon coupling using a variational Lang-Firsov approximation. The same authors later used a similar method to study a more realistic model for CMR systems incorporating two e_g bands [28]. Lee and Min [29] extended this approach to deal with transport properties. These treatments concentrate on the coherent polaron band for which the phonon occupation numbers do not change as the electron hops. In the present paper we stress the importance of incoherent processes which become dominant as the temperature increases. Such processes are also neglected by Alexandrov and Bratkovsky [30]. In their picture the coherent polaron band narrows with increasing temperature until for $k_{\mathrm{B}}T \approx \omega/2$ there is a crossover to thermally activated hopping. However we show that in this temperature range the most significant effect is a rapid growth in the importance of incoherent processes, where phonon occupation numbers change as the electron hops, leading to increasing electron mobility and decreasing resistivity.

In this paper we treat both the Hund and the electron-phonon coupling using an extension of a many-body coherent potential approximation (CPA) previously derived for the DE model [21, 31]. The CPA treats the Hund coupling much better than mean-field theory, introducing strong correlation between electrons, and enables us to study the complete electronic spectrum, not just the polaron band of the Lang-Firsov treatments. For sufficiently strong electron-phonon coupling at $T = 0$ the spectrum consists of a number of polaronic subbands, including the central coherent band at the Fermi level, which lie within a gap in a continuous spectrum whose width is comparable with the bare bandwidth. As T increases the widths and weights of the polaronic bands increase until the gap is filled and we recover a picture similar to that of Millis et al. [23, 32], who treat the phonons classically. The absence of polaron bands

[8] The model does not include the intraatomic Coulomb repulsion which would suppress double occupation of a site.

within the gap in Millis et al.'s classical treatment means that their resistivity shows a spurious divergence as $T \to 0$ in the strong-coupling case. Ranninger [33] considers scattering of coherent polarons by phonons, which leads to polaron sidebands, but his treatment does not include the incoherent processes discussed above which are important at higher temperature. In the limit of classical spins and phonons Millis et al. [23, 32] used dynamical mean-field theory (DMFT) to study a model with two e_g bands. However they neglect on-site Coulomb interactions so that the model does not yield a Mott insulator correctly for the undoped compound $LaMnO_3$, with one electron per atom in the conduction band. The one-band model (2.16) automatically gives the correct behaviour in this limit for large Hund's rule coupling J.

Very recently Held and Vollhardt [34] considered the two-band DE model within DMFT, including an on-site Coulomb interaction U. Their main result, the variation of the Curie temperature T_C with band occupation, is very similar to the one we obtained in the simpler one-band model [31]. In the two-band Holstein-DE model of Millis et al., without U, the true ground state in a quantum treatment would consist of unphysical bipolarons with two electrons bound on the same site.

Our approach has many similarities with analytical studies of the Holstein model using DMFT, which have been carried out for the classical phonon [35] and empty-band [36] limits in which the model is a one-electron problem. Indeed the standard dynamical CPA is equivalent to DMFT for one-electron problems such as the binary alloy [37], the DE and Holstein models in the empty-band limit [36, 38, 39], and the DE model with classical local spins [31]. DMFT should be regarded as the correct extension of the CPA to many-body problems [40]. However in the many-body case DMFT cannot be carried through analytically and numerical work [41] on the Holstein model has been aimed mostly at understanding superconductivity temperatures and charge-density-wave instabilities rather than polaron physics. For the current many-body problem we regard our CPA as an approximate solution of DMFT, or as an extrapolation from the one-electron case. The CPA has the advantage of relative analytic simplicity, but does not treat the many-body dynamics as well as DMFT, retaining too much one-electron character.

2.4. Model parameters

The models discussed in this chapter all have some parameters which have to be chosen appropriately to describe the manganites. However we will see in chapter 3 that it is sometimes convenient to use values which differ from experiments as this often simplifies calculations considerably.

In the DE and the Holstein-DE model we have the following parameters:

band filling n: as discussed in chapter 1 the maximum CMR effect occurs for doping

$x \approx 0.3$ corresponding to $n = 1 - x \approx 0.7$ e_g electrons per atom. However, to simplify the calculations, we will always use $n = 0.5$ since then the chemical potential is fixed for all temperatures.

band-width W**:** first-principle band structure calculations suggest a value of $W =$ 1eV for the half-width of the e_g band.

phonon energy ω**:** experimentally the transverse optical phonons have energies $\omega \approx$ 40–70meV and we use $\omega = 50$meV in our calculations.

Hund's rule exchange coupling J**:** for simplicity we take the strong Hund's rule coupling limit $J \to \infty$; experiments suggest a value of $J \approx 3$eV.[9]

magnitude S **of the local spins:** the three t_{2g} electrons in the manganites form a localized spin of magnitude $S = 3/2$. We mainly work in the limit of classical spins $S = \infty$ but a discussion of the effect of the value of S on optical conductivity is given in chapter 4.

electron-phonon coupling strength g**:** we will see in chapter 3 that this is the only free parameter in the Holstein-DE model. The choice of g will be made so as to get agreement with experimental data on the manganites.

[9] We mentioned at the beginning of this chapter that this is a reasonable simplification if we are interested only in the low-energy properties of the model.

3. The coherent potential approximation

This chapter begins with an introduction to the standard coherent potential approximation (CPA) for disordered alloys. We then review Hubbard's original equation-of-motion (EOM) approach to the Hubbard model which is equivalent to the CPA method developed much later. The resulting CPA equations are the same as for a simplified case of the many-body CPA for the DE and the Holstein-DE model which is discussed in section 3.3.

3.1. CPA for disordered alloys

The CPA method was originally developed to treat disordered alloys which consist of two or more different sorts of atoms, randomly distributed over the lattice. Such systems are clearly not translationally invariant and therefore Bloch's theorem does not hold. It is obvious that the disorder and its consequences make calculations much more difficult than for ordered systems.

We follow Gasser et al. [42] and consider an alloy consisting of atoms A and B with potentials V^A and V^B respectively, described by the Hamiltonian

$$H = \sum_{ij\sigma} t_{ij} c_{i\sigma}^{\dagger} c_{j\sigma} + \sum_{i\sigma} V_i n_{i\sigma} \,, \tag{3.1}$$

where $n_{i\sigma} = c_{i\sigma}^{\dagger} c_{i\sigma}$ as usual and V_i takes the values

$$V_i = \begin{cases} V^A \,, & \text{atom A on site } i \\ V^B \,, & \text{atom B on site } i \,. \end{cases} \tag{3.2}$$

Moreover we only consider the case of so-called 'diagonal' disorder, in which the band-energy does not depend on the type of atom (A or B) so that we have

$$t_{ij} = \sum_{\boldsymbol{k}} \epsilon_{\boldsymbol{k}} \mathrm{e}^{\mathrm{i}\boldsymbol{k}(\boldsymbol{R}_i - \boldsymbol{R}_j)} \,. \tag{3.3}$$

The probability to find an atom of type A (B) on a site is c $(1-c)$, where c $(1-c)$ is the concentration of atoms A (B) in the system.

The fundamental idea of the CPA method is to replace the random potential V_i by a so-called 'coherent potential' $\Sigma_\sigma(\epsilon)$, uniform in space but (in general) complex and energy-dependent. This restores translational invariance and allows standard methods (e.g. the EOM method) to be applied. In fact Σ_σ is just the electron self-energy and once the coherent potential is known the Green function of the so-called 'effective medium' can be obtained from

$$G^{\text{eff}}_{\boldsymbol{k}\sigma}(\epsilon) = \frac{1}{\epsilon - \epsilon_{\boldsymbol{k}} - \Sigma_\sigma(\epsilon)}\,. \tag{3.4}$$

So far we have not simplified our task to deal with the disordered system as we do not know the coherent potential. An exact determination of Σ_σ would be equivalent to the solution of the original problem. However we now set out to find an approximation for Σ_σ which describes the properties of the disordered system reasonably well but still requires less effort in calculating physical properties.

Since we want our approximation to be exact for ordered systems we have the boundary conditions

$$\Sigma_\sigma = \begin{cases} V^A\,, & c = 1 \\ V^B\,, & c = 0\,. \end{cases} \tag{3.5}$$

The simplest approach for Σ_σ is to take the arithmetic mean $\Sigma_\sigma = cV^A + (1-c)V^B$. However it is easy to see that this does not take into account the most important effect of the disorder in the system, namely to break translational invariance.

In the actual CPA approach we require the one-electron Green function of the effective medium to satisfy

$$G^{\text{eff}}_{ij\sigma}(\epsilon) = \overline{G_{ij\sigma}(\epsilon)}\,, \quad G_{ij\sigma}(\epsilon) = \langle\langle c_{i\sigma}; c^\dagger_{j\sigma}\rangle\rangle_\epsilon\,, \tag{3.6}$$

where the bar denotes averaging over all possible configurations of atoms A and B with fixed concentrations c and $1-c$, respectively. This step is obvious since the physics of the system described by $G_{ij\sigma}$ cannot depend on a particular distribution of the alloy components.

The Green function $G_{ij\sigma}$ for one frozen configuration obeys the equation of motion (cf. equation (1.5))

$$\sum_l \{[\omega - \Sigma_\sigma]\delta_{ij} - t_{ij}\}\,\langle\langle c_{l\sigma}; c^\dagger_{j\sigma}\rangle\rangle_\omega = \delta_{ij} + \widetilde{V}_{i\sigma}\langle\langle c_{i\sigma}; c^\dagger_{j\sigma}\rangle\rangle_\omega\,. \tag{3.7}$$

This can be written as [42]

$$G_{ij\sigma}(\epsilon) = G^{\text{eff}}_{ij\sigma}(\epsilon) + \sum_l G^{\text{eff}}_{il\sigma}(\epsilon)\widetilde{V}_{l\sigma}G_{lj\sigma}(\epsilon) \tag{3.8}$$

where we defined $\widetilde{V}_{i\sigma} = (V_i - \Sigma_\sigma) n_{i\sigma}$.

We introduce the so-called **t-matrix** (or scattering matrix)

$$\widetilde{V}_{l\sigma} G_{lj\sigma}(\epsilon) = \sum_m \widetilde{T}_{lm\sigma} G^{\text{eff}}_{mj\sigma}(\epsilon) . \tag{3.9}$$

Inserting equation (3.9) in equation (3.8) and averaging over all configurations gives

$$\overline{G_{ij\sigma}(\epsilon)} = G^{\text{eff}}_{ij\sigma}(\epsilon) + \sum_{lm} G^{\text{eff}}_{ij\sigma}(\epsilon) \overline{\widetilde{T}_{lm\sigma}} G^{\text{eff}}_{mj\sigma}(\epsilon) = G^{\text{eff}}_{ij\sigma}(\epsilon) . \tag{3.10}$$

Clearly equation (3.6) is satisfied if we determine the coherent potential so that

$$\overline{\widetilde{T}_{lm\sigma}} = 0 . \tag{3.11}$$

Until now we have not made any approximations and our theory would still be exact if we could satisfy equation (3.11) exactly. However this is not possible as we do not know $\widetilde{T}$ explicitly. Nevertheless the t-matrix can be calculated approximately by iteration. Equation (3.8) gives the following equation to determine $\widetilde{T}$ [42]

$$\widetilde{T}_{lm\sigma} = \widetilde{t}_{i\sigma} \delta ij + \widetilde{t}_{i\sigma} \sum_{l \neq i} G^{\text{eff}}_{il\sigma}(\epsilon) \widetilde{T}_{lj\sigma} , \tag{3.12}$$

with the single-site or atomic t-matrix

$$\widetilde{t}_{i\sigma} \equiv \frac{1}{1 - \widetilde{V}_{i\sigma} G^{\text{eff}}_\sigma(\epsilon)} \widetilde{V_{i\sigma}} , \tag{3.13}$$

depending on the local potential and the local Green function G^{eff}_σ only. Equation (3.13) can be solved iteratively and if the occupation of sites with atoms of type A or B is uncorrelated[1] it may be shown that equation (3.11) can approximately be satisfied by [17]

$$\overline{\widetilde{t}_{i\sigma}} = 0 . \tag{3.14}$$

For our example of a two-component alloy we obtain the **CPA equation** [42]

$$0 \stackrel{!}{=} c \frac{V^A - \Sigma_\sigma}{1 - (V^A - \Sigma_\sigma) G^{\text{eff}}_\sigma(\epsilon)} + (1-c) \frac{V^B - \Sigma_\sigma}{1 - (V^B - \Sigma_\sigma) G^{\text{eff}}_\sigma(\epsilon)} , \tag{3.15}$$

from which the coherent potential Σ_σ has to be computed self-consistently.

In the general case of an alloy of α components, with concentrations c_m and potentials V^m, $m = 1, \ldots, \alpha$, the CPA equation becomes [17]

$$0 \stackrel{!}{=} \sum_{m=1}^{\alpha} c_m \frac{V^m - \Sigma_\sigma}{1 - (V^m - \Sigma_\sigma) G^{\text{eff}}_\sigma(\epsilon)} . \tag{3.16}$$

[1] This simplest CPA approach is known as the **single-site approximation**.

Although the CPA method was originally introduced to treat disordered alloys we can take a different point of view to end up with the following recipe which can basically be applied to any Hamiltonian.

1. Calculate the atomic limit ($t_{ij} = 0$) one-electron Green function G^{AL}. This can be done exactly using the EOM method possibly in combination with some other tricks as for example canonical transformations of the Hamiltonian.[2]

2. Identify the poles of G^{AL} as components of an alloy, with the weights of the poles being the concentrations c_m.[3]

3. Solve equation (3.16) numerically to determine the electron self-energy Σ and thereby the effective medium.

4. Once the coherent potential is known the one-electron Green function G for finite band-width as well as other physical properties which are related to G can be obtained.[4]

3.2. CPA for the Hubbard model

Edwards [8] has shown that for a simplified case (details will be given in the next section) the many-body CPA for the DE and the Holstein-DE model gives the same CPA equations as in Hubbard's one-electron CPA for the Hubbard model with Hamiltonian

$$H = \sum_{ij\sigma} t_{ij} c^{\dagger}_{i\sigma} c_{j\sigma} + U \sum_{i} n_{i\uparrow} n_{i\downarrow} \,. \tag{3.17}$$

Here the first term describes the hopping of electrons and the second term represents the Coulomb interaction of two electrons on the same site[5], with a Hubbard $U > 0$. The Hubbard model is a simpler model for a system of strongly correlated electrons than the DE and the Holstein-DE model, as the Coulomb interaction in equation (3.17) takes a much simpler form than the coupling to local spins or phonons in the other models.

[2] In section 3.3.2 we shall use the so-called Lang-Firsov transformation to decouple electrons and phonons in the Holstein-DE model.

[3] There exist cases in which the Green function has an infinite number of poles (cf. equation (3.39)). In order to apply the CPA to such systems, further approximations (e.g. neglecting high-energy excitations) are necessary to reduce the number of components of the alloy, and to obtain a numerically solvable CPA equation.

[4] Physical properties such as, for example, the dc conductivity, which includes the two-electron current-current response function, can be obtained within a CPA method if one sets out to calculate the corresponding higher Green functions instead of G.

[5] Since there is only one orbital per atom in this model, two electrons on the same site must have opposite spins.

Hubbard [43] used the EOM method and the idea of the alloy analogy described below to calculate the one-electron Green function. His result becomes exact in the atomic limit $t_{ij} = 0$. It turns out that Hubbard's approach is equivalent to the CPA method developed later [44] which we discussed in section 3.1.

The idea of the **alloy analogy**, which provides the connection to the original CPA method for alloys, consists in considering the $\uparrow$ spin electrons, say, to move in a random potential due to a static configuration of the $\downarrow$ spin electrons in the system which must be averaged over. Thus, in equation (3.17), we replace $n_{i\downarrow}$ by

$$\langle n_{i\downarrow} \rangle = \begin{cases} 1 & \text{with probability } n_\downarrow \\ 0 & \text{with probability } 1 - n_\downarrow \, , \end{cases} \tag{3.18}$$

n_σ being the number of electrons with spin σ per atom, to obtain an one-electron Hamiltonian. In the spirit of section 3.1 we therefore have a two-component alloy with potentials $V^A = U$ and $V_B = 0$ and concentrations $c^A = n_\downarrow$ and $c^B = 1 - n_\downarrow$, respectively. In the alloy analogy for the Hubbard model, a σ spin electron moves in a random potential given by U on $n_{\bar\sigma}$ sites and 0 on $1 - n_{\bar\sigma}$ sites.

Instead of insisting on a zero average t-matrix we can equivalently determine the coherent potential Σ_σ if we put the local Green function of the effective medium equal to the average of the Green functions for each type of atom of the alloy

$$G_\sigma = n_{\bar\sigma} \frac{G_\sigma}{1 - (U - \Sigma_\sigma) \, G_\sigma} + (1 - n_{\bar\sigma}) \frac{G_\sigma}{1 + \Sigma_\sigma G_\sigma} \tag{3.19}$$

where

$$G_\sigma(\epsilon) = \frac{1}{N} \sum_{\boldsymbol{k}} \frac{1}{\epsilon - \epsilon_{\boldsymbol{k}} - \Sigma_\sigma(\epsilon)} = G_0 \left(\epsilon - \Sigma_\sigma(\epsilon) \right) \, . \tag{3.20}$$

Here the Green function for non-interacting electrons is given by (cf. equation (1.11))

$$G_0(\epsilon) = \frac{1}{N} \sum_{\boldsymbol{k}} \frac{1}{\epsilon - \epsilon_{\boldsymbol{k}}} = \int \mathrm{d}\epsilon' \frac{D_0(\epsilon')}{\epsilon - \epsilon'} \, , \tag{3.21}$$

where D_0 is the density of states per atom and $\epsilon_{\boldsymbol{k}} = \sum_j t_{ij} \exp[\mathrm{i}\boldsymbol{k}(\boldsymbol{R}_i - \boldsymbol{R}_j)]$. Equation (3.19) can be written as

$$G_\sigma = \frac{n_{\bar\sigma}}{\Sigma_\sigma + G_\sigma^{-1} - U} + \frac{1 - n_{\bar\sigma}}{\Sigma_\sigma + G_\sigma^{-1}} \, . \tag{3.22}$$

Comparison with Hubbard's results for the atomic limit Green function [43]

$$G_\sigma^{\mathrm{AL}}(\epsilon) = \frac{n_{\bar\sigma}}{\epsilon - U} + \frac{1 - n_{\bar\sigma}}{\epsilon} \tag{3.23}$$

yields

$$G_\sigma(\epsilon) = G_\sigma^{\mathrm{AL}} \left(\Sigma_\sigma + G_\sigma^{-1} \right) \, . \tag{3.24}$$

Clearly this CPA equation becomes exact in the atomic limit when $D_0(\epsilon) = \delta(\epsilon)$ and it follows from equation (3.21) that $\Sigma_\sigma + G_\sigma^{-1} = \epsilon$. Solution of the CPA equation becomes simple if we use an elliptic density of states

$$D_{\mathrm{e}}(\epsilon) = \frac{2}{\pi W^2}\sqrt{W^2 - \epsilon^2}\,, \tag{3.25}$$

where $2W$ is the bandwidth, and we can calculate G_0 from equation (3.21)

$$G_0(\epsilon) = \frac{2}{W^2}\left[\epsilon - \left(\epsilon^2 - W^2\right)^{1/2}\right]. \tag{3.26}$$

Combining equations (3.20) and (3.26) and solving for $\epsilon - \Sigma_\sigma(\epsilon)$ we find

$$\Sigma_\sigma + G_\sigma^{-1} = \epsilon - W^2 G_\sigma/4\,. \tag{3.27}$$

3.3. Many-body CPA

The CPA method considered so far allows us to reduce the Hamiltonian of a many-particle system to a one-electron Hamiltonian using, for example, the alloy analogy as discussed for the Hubbard model. Nevertheless such one-electron problems are in general very challenging and solutions only exist for simplified cases in which further approximations have been made.

However many interesting effects arise from strong correlations between electrons in a many-particle system. It would therefore be considerably more satisfactory to develop a many-body theory which takes into account such correlations. The many-body CPA method described in the sequel represents such an extension of Hubbard's one-electron CPA.

In contrast to the method introduced in section 3.1, the many-body CPA is an analytic method; it uses the EOM method similar to Hubbard [43] to calculate the one-electron Green function. However owing to the more complicated form of DE and Holstein-DE model an extension of the original method is necessary.

The general derivation is quite involved making use of various mathematical techniques, which are beyond the scope of this work, to obtain the one-electron Green function, the Curie temperature as well as other quantities [21, 31, 20].

Here we will therefore restrict ourselves to a special case in which the CPA equations obtained for the Hubbard model hold. To this end we assume the system to be in the paramagnetic state[6] ($n_\uparrow = n_\downarrow = n/2$), without an external magnetic field ($h = 0$), and take the limit of strong Hund's rule coupling $J \to \infty$. In the limit of classical spins $S \to \infty$ the results of the many-body CPA become identical to results obtained within dynamical mean field theory (DMFT), which has so far only been implemented for classical spins. The many-body CPA therefore represents an analytic extension of DMFT to the case of quantum spins [31, 20].

[6] We will see later, however, that we can also consider a saturated ferromagnetic state with a simple modification of the atomic limit Green function.

3.3.1. Many-body CPA for the DE model

As this work is mainly concerned with the Holstein-DE model, we will only briefly discuss the results of Edwards et al. [21] for the pure DE model. The main features of the many-body CPA for the DE model are as follows.

- It correctly reduces to Kubo's one-electron CPA [38] in the empty-band limit $n \to 0$.
- Edwards et al. recovered the right atomic limit Green function as $t_{ij} \to 0$, for arbitrary band filling n.

In the zero-field ($h = 0$) paramagnetic state the one-electron Green function G[7] can be obtained from the atomic limit G^{AL} and equation (3.24) just as in the case of the Hubbard model. Taking the band to be of the elliptic form (3.25) the CPA equation becomes

$$G(\epsilon) = G^{\mathrm{AL}}\left(\epsilon - W^2 G/4\right) , \tag{3.28}$$

with G^{AL} given by [21]

$$\begin{aligned} G^{\mathrm{AL}}_{\uparrow}(\epsilon) = \frac{1}{2S+1} &\left[\frac{nS/2 - \langle \boldsymbol{S}\cdot\boldsymbol{\sigma}\rangle}{\epsilon + J(S+1)/2} + \frac{S(1-n/2) - \langle \boldsymbol{S}\cdot\boldsymbol{\sigma}\rangle}{\epsilon - J(S+1)/2} \right. \\ &\left. + \frac{(S+1)(1-n/2) + \langle \boldsymbol{S}\cdot\boldsymbol{\sigma}\rangle}{\epsilon + JS/2} + \frac{n(S+1)/2 + \langle \boldsymbol{S}\cdot\boldsymbol{\sigma}\rangle}{\epsilon - JS/2} \right] , \end{aligned} \tag{3.29}$$

where the angle brackets denote thermal averages. The four poles in equation (3.29) correspond to energies to add or remove an electron from the atom. Since we can have a maximum of two electrons (with opposite spins) per atom in the one-band DE model there are four possible states with energies

$$E = \begin{cases} E_1 = -JS/2, & \text{one electron with spin parallel to } \boldsymbol{S} \\ E_2 = 0, & \text{no electron} \\ E_3 = 0, & \text{two electrons with opposite spins} \\ E_4 = J(S+1)/2, & \text{one electron with spin antiparallel to } \boldsymbol{S}\,. \end{cases}$$

In the strong coupling limit $J \to \infty$ we are left with only one pole in the Green function[8] and equation (3.29) reduces to

$$G^{\mathrm{AL}}(\epsilon) = \epsilon^{-1}(S+1-n/2)/(2S+1)\,. \tag{3.30}$$

Equation (3.28) then becomes a quadratic equation for G with solution

$$G(\epsilon) = \alpha^2 \frac{2}{D^2}\left[\epsilon - \sqrt{\epsilon^2 - D^2}\right] \tag{3.31}$$

[7] We omit the spin index σ as there is no spin dependence in the paramagnetic state.
[8] States 3 and 4 are not allowed for $J = \infty$

where $\alpha^2 = (S+1-n/2)/(2S+1)$ and $D = \alpha W$. The resulting density of states is a single elliptic band of width $2\alpha W$ and weight α^2 (cf. equations (3.25) and (3.26)). For classical spins $S = \infty$ the band is narrowed by a factor $\alpha \to 1/\sqrt{2} \simeq 0.707$ compared to the bare band. This is close to the classical result of 2/3, obtained by averaging $\cos(\theta/2)$ in equation (2.12) over all angles, and represents the DE effect.

The use of an elliptic bare density of states instead of the exact density of states of the simple cubic tight binding band simplifies the calculations. In figure 3.1 we reproduce the results of Edwards et al. [21] for the density of states for the DE model. The plot shows that the elliptic band D_{e} should be a reasonable approximation to D_{c}. Moreover Edwards et al. also used the simple-cubic density of states and compared, for example, results for the resistivity. They concluded that the approximation does indeed not influence the results dramatically.

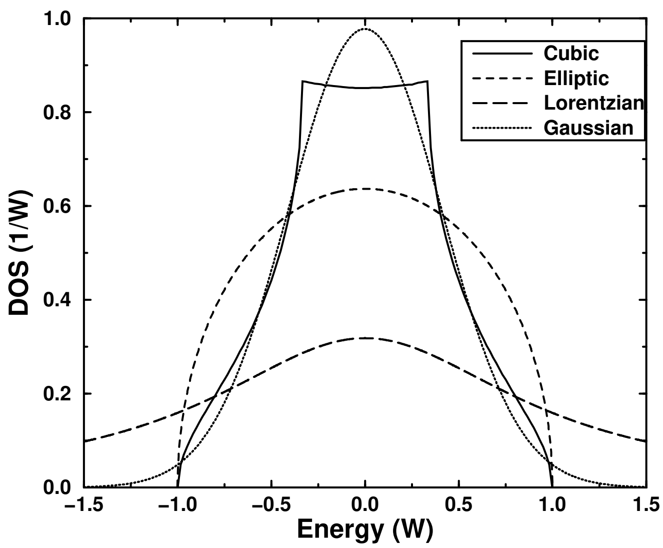

Figure 3.1.: Various densities of states in the DE model plotted in units of W. Reproduced from Edwards et al. [21].

3.3.2. Many-body CPA for the Holstein-DE model

The following discussion is based on Green's [20] recent many-body CPA treatment of the Holstein-DE model. A more detailed discussion of the method and its application to the manganites is by Edwards [8] and details of the calculations can be found in Green's paper [20].

In contrast to other work which focused on either the weak or the strong coupling limit, or treated the phonons classically, the many-body CPA is able to describe the crossover from weak to strong electron-phonon coupling, as well as from quantum phonons to classical phonons as temperature and/or model parameters are varied.

The results of Green [20] for the Holstein-DE model become exact in the atomic limit $t_{ij} \to 0$, for any n, as for the DE model. However due to the more complicated form of the model the DMFT/one-electron CPA results are no longer recovered as $n \to 0$. The method is therefore cruder for the Holstein-DE than for the DE model.

The following derivation and discussion of the many-body CPA for the Holstein-DE model is cited from Edwards [8].

citation

We start by deriving the Green function for the Holstein-DE model in the atomic limit. The Hamiltonian H_{AL} in this limit is given by equation (2.16) with the first term omitted and with site indices and summation suppressed. We remove the electron-phonon coupling by the standard canonical transformation [24] $\tilde{H} = \mathrm{e}^{s} H_{\mathrm{AL}} \mathrm{e}^{-s}$ where $s = -(g/\omega)n(b^\dagger - b)$. Under this transformation $b \to b + (g/\omega)n$ and the Hamiltonian separates into a fermionic and bosonic component:

$$\tilde{H} = H_{\mathrm{f}} + H_{\mathrm{b}} \tag{3.32}$$

$$H_{\mathrm{f}} = -J\boldsymbol{S}\cdot\boldsymbol{\sigma} - h\left(S^z + \sigma^z\right) - \left(g^2/\omega\right) n^2\,,\; H_{\mathrm{b}} = \omega b^\dagger b\,. \tag{3.33}$$

The transformation corresponds to a displacement of the equilibrium position of the phonon harmonic oscillator in the presence of an electron and the downward energy shift g^2/ω is a polaron binding energy which we write as $\lambda\omega$, where $\lambda = g^2/\omega^2$. If two electrons occupy the site ($n = 2$), which will not occur for large J, the energy shift becomes $4g^2/\omega^2$ corresponding to an on-site bipolaron. Writing out explicitly the thermal average in the definition of the one-particle retarded Green function we have

$$\begin{aligned} G_\sigma^{\mathrm{AL}}(t) &= -\mathrm{i}\theta(t)\left\langle \left[c_\sigma(t), c_\sigma^\dagger\right]_+ \right\rangle \\ &= -\mathrm{i}\theta(t)\frac{\mathrm{Tr}\left\{\mathrm{e}^{-\beta H_{\mathrm{AL}}}\left[c_\sigma(t), c_\sigma^\dagger\right]_+\right\}}{\mathrm{Tr}\left\{\mathrm{e}^{-\beta H_{\mathrm{AL}}}\right\}} \end{aligned} \tag{3.34}$$

and the canonical transformation introduced above can be carried out within the traces, using the property of cyclic invariance. Thus $H_{\mathrm{AL}} \to \tilde{H}$, $c_\sigma^\dagger \to X^\dagger c_\sigma^\dagger$ and $c_\sigma(t)$ becomes

$$\mathrm{e}^{\mathrm{i}\tilde{H}t} X c_\sigma \mathrm{e}^{-\mathrm{i}\tilde{H}t} \tag{3.35}$$

where $X = \exp\{g(b^\dagger - b)/\omega\}$. Using equation (3.32), we can write the traces in equation (3.34) as products of fermionic and bosonic traces. Hence we find

$$G_\sigma^{\mathrm{AL}}(t) = -\mathrm{i}\theta(t)\left\{\left\langle c_\sigma(t)c_\sigma^\dagger\right\rangle_{\mathrm{f}} F(t) + \left\langle c_\sigma^\dagger c_\sigma(t)\right\rangle_{\mathrm{f}} F^*(t)\right\} \tag{3.36}$$

where $F(t) = \langle X(t)X^{\dagger}\rangle_{\mathrm{b}}$ and the thermal averages $\langle\ \rangle_{\mathrm{f}}$, $\langle\ \rangle_{\mathrm{b}}$ correspond to the systems with Hamiltonians H_{f} and H_{b} respectively. It may be shown [24] that

$$F(t) = \mathrm{e}^{-\lambda(2b+1)} \exp\left\{2\lambda\left[b(b+1)\right]^{1/2}\cos\left[\omega(t+i\beta/2)\right]\right\} \tag{3.37}$$

where $b = b(\omega) = \left\{\mathrm{e}^{\beta\omega} - 1\right\}^{-1}$ is the Bose function with $\beta = (k_{\mathrm{B}}T)^{-1}$. The last factor is of the form $\exp\left(z\cos\phi\right)$ which generates the modified Bessel functions $\mathrm{I}_r(z)$:

$$\exp\left(z\cos\phi\right) = \sum_{r=-\infty}^{\infty} \mathrm{I}_r(z)\mathrm{e}^{\mathrm{i}r\phi}\,. \tag{3.38}$$

To evaluate the fermionic averages we consider for simplicity the limit $J \to \infty$ in zero field ($h = 0$). Then the last term in H_{f} may be written $-(g^2/\omega)n$, since $n = 0$ or 1 only, and this may be absorbed into the chemical potential which is finally determined to give the correct number of electrons n per atom. Thus H_{f} is just the DE Hamiltonian in the atomic limit and the sum of the two fermionic averages corresponds to the function $G^{\mathrm{AL}}(t)$ whose Fourier transform is given by equation (3.30). It is easy to see that the first and second thermal averages in equation (3.36) take constant values $(1-n)(S+1)/(2S+1)$ and $n(S+1/2)(2S+1)$ respectively. Hence, from equations (3.36)-(3.38), we obtain the Fourier transform of G^{AL}, with $J \to \infty$ and $h = 0$, in the form

$$G^{\mathrm{AL}}(\epsilon) = \sum_{r=-\infty}^{\infty} \frac{\mathrm{I}_r\{2\lambda\left[b(\omega)(b(\omega)+1)\right]^{1/2}\}}{(2S+1)\exp\{\lambda\left[2b(\omega)+1\right]\}} \frac{(2S+1)\frac{n}{2}\mathrm{e}^{r\beta\omega/2} + (S+1)(1-n)\mathrm{e}^{-r\beta\omega/2}}{\epsilon + r\omega}\,. \tag{3.39}$$

The density of states $-\pi^{-1}\mathrm{Im}\ G^{\mathrm{AL}}(\epsilon)$ is shown in figure 3.2 for the classical spin limit $S \to \infty$ at quarter-filling $n = 0.5$. It consists of delta-function peaks separated in energy by ω and the envelope curves show the weight distribution at low and high temperature. W is an energy unit which, when we go beyond the atomic limit, will be the half-width of the itinerant electron band, as usual. The values adopted for the parameters ω/W and g/W relate to the manganites. The symmetry of the spectrum about zero energy is due to the choice of filling $n = 0.5$; in general at $T = 0$ the lower and upper 'bands' have weights n and $1-n$ respectively. By counting weights it may be seen that for any n the chemical potential lies in the peak at $\epsilon = 0$, which has very small weight $\mathrm{e}^{-\lambda}/2$ per spin. The shape of the envelope function at $T = 0$, with two maxima and very small values at the centre of the pseudogap between them, may be understood physically as follows. The delta-function at $\epsilon = r\omega$ ($r \geq 0$) corresponds to an excitation from the ground state, with no electron and the undisplaced oscillator in its ground state, to a state with one electron and the displaced oscillator in its r^{th} excited state. The strength of the delta-function depends on the square of the overlap integral between the displaced and undisplaced oscillator wave functions. Clearly this is very small for $r = 0$ and goes through a maximum with increasing r as the normalized displaced wave function spreads out. At $T = 0$ it is easily seen from equation (3.39), using $\mathrm{I}_r(z) \sim (z/2)^{|r|}/|r|!$ for small z, that the weight of the delta-functions at $\epsilon = \pm r\omega$ is proportional to $\lambda^r/r!$. Hence the maxima in the envelope curve occur at $\epsilon \approx \pm\lambda\omega$, which is the polaron binding energy.

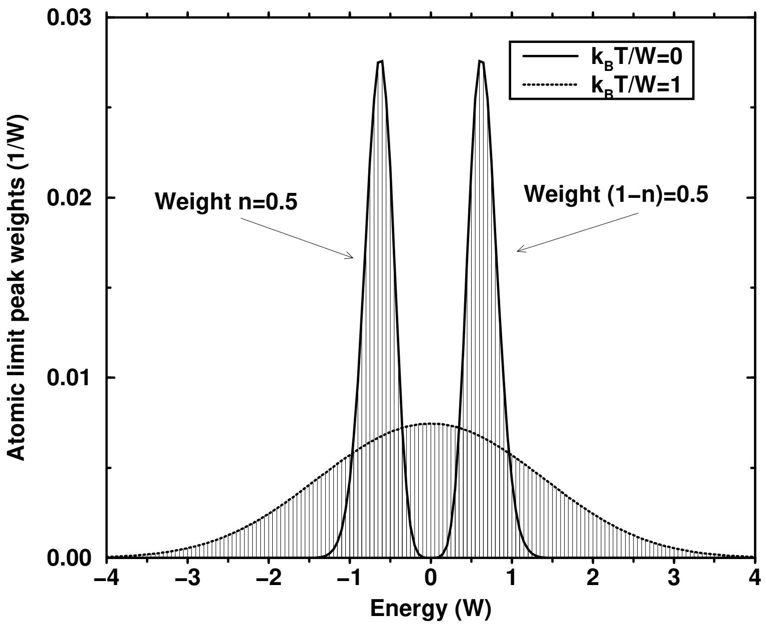

Figure 3.2.: One-electron spectra of the Holstein-DE model in the atomic limit at zero and very high temperature. They consist of delta-functions, with energy spacing ω, whose strength is indicated by the envelope curves. The plots are for the paramagnetic state with $S = J = \infty$, $h = 0$, $n = 0.5$, $\omega/W = 0.05$ and $g/W = 0.18$, where W is a unit of energy later to be identified with the half-width of the electron band in the full Hamiltonian. Reproduced from Green [20].

We now turn to the Holstein-DE model with finite band-width. As for the DE model it is necessary to use the full equation of motion method to derive the many-body CPA in the presence of a magnetic field and/or magnetic order [20]. In the present case it is very difficult to determine self-consistently all the expectation values which appear. We therefore approximate them by their values in the atomic limit. It then turns out that in the zero field paramagnetic state, for $J = \infty$ and with the elliptic band, the CPA Green function G again satisfies equation (3.28), with G^{AL} now given by equation (3.39).

The densities of states calculated for $T = 0$ using equations (3.39) and (3.28) with

$S = \infty$, $n = 0.5$, $\omega/W = 0.05$ and various values of g/W are shown in figure 3.3. Apart from lacking the perfect symmetry about the chemical potential $\mu = 0$ the results are qualitatively similar for other values of n not too close to 0 or 1. For $g = 0$ we recover the elliptic band with half-width $W/\sqrt{2}$ as for the DE model with $J = \infty$, $S = \infty$. As g increases the density of states broadens and small subbands are split off from the band edges. As g increases further a pseudogap develops near the chemical potential. At a critical value $g = g_c$ a gap appears which contains a small polaron band around the chemical potential. Increasing g further causes more bands to be formed in the gap, with weights similar to those of the relevant atomic limit. It should be pointed out that the paramagnetic state considered here at $T = 0$ is not the actual ground state, which is ferromagnetic. We discuss the magnetic state later. The effect of increasing temperature on the density of states in the gap region is shown in figure 3.4 for $g = 0.18W > g_c$. With increasing T the polaron bands grow rapidly and eventually merge to fill the gap.

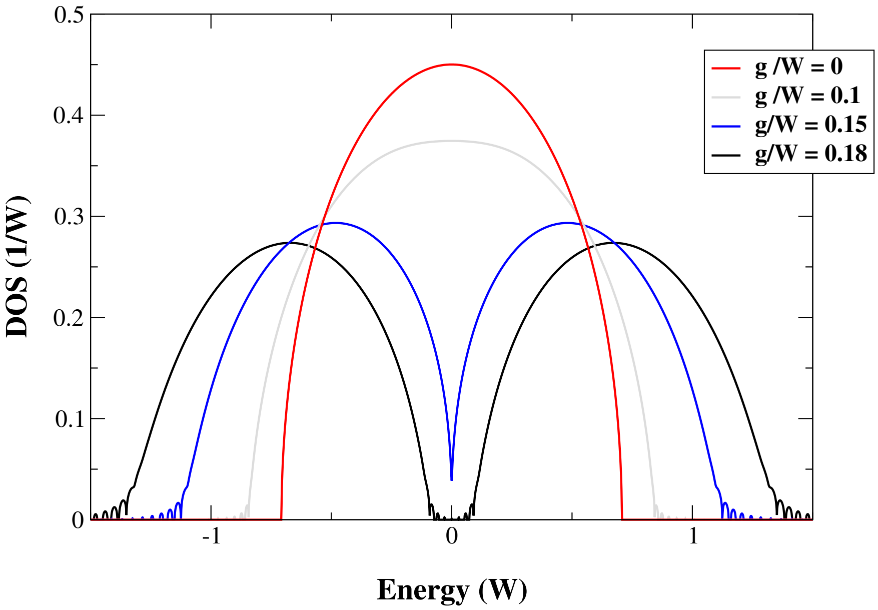

Figure 3.3.: The one-electron density of states (DOS) for the Holstein-DE model with half-bandwidth W, for the hypothetical paramagnetic state at $T = 0$, with various strengths of electron-phonon coupling g/W. Other parameters as in figure 3.2. Reproduced from Green [20].

It is important to compare these results with the standard small-polaron theory developed by Holstein [25, 26]. Holstein distinguished between 'diagonal transitions', in which the number of phonons is unchanged as the electron moves from site to site, and 'nondiagonal transitions' in which phonon occupation numbers change. The former give rise to a coherent Bloch-like polaron band of half-width $W\mathrm{e}^{-\lambda(2b+1)}$ which decreases with increasing temperature. The nondiagonal transitions are inelastic processes which destroy phase coherence and the polaron moves by diffusive hopping. The hopping probability increases with temperature so that polaron motion crosses over from coherent Bloch-like at $T = 0$ to diffusive hopping as $k_\mathrm{B}T$ approaches the phonon energy ω. The paramagnetic state of the Holstein-DE model differs from this standard picture in one important respect. There are no well-defined Bloch states, owing to strong scattering by the disordered local spins, so no coherent polaron band will form. This is fortunate because the CPA treatment of electron-phonon scattering will never lead to coherent states of infinite lifetime at the Fermi surface at $T = 0$. However in the presence of strong spin disorder it should be satisfactory. We interpret the central band around the chemical potential in figure 3.4 as an incoherent polaron band whose increasing width as the temperature rises is due to life-time broadening of the atomic level. The life-time decreases as the hopping probability increases with rising temperature.

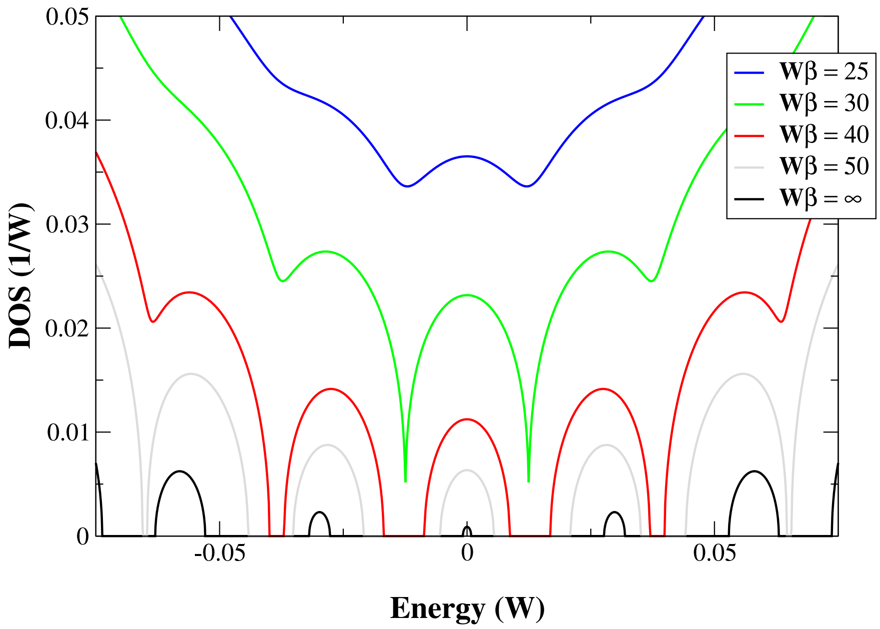

Figure 3.4.: Evolution with temperature $\beta = (k_\mathrm{B}T)^{-1}$ of the polaron subbands in the pseudogap around the chemical potential $\mu = 0$ for $g/W = 0.18$. These subbands at $T = 0$ can just be seen in figure 3.3. All parameters as in figure 3.2. Reproduced from Green [20].

To substantiate this picture we study the central polaron band in the limit of very strong electron-phonon coupling. In this limit it can be shown that we need retain only the $r = 0$ term in equation (3.39) and it is then easy to solve equation (3.28) for

G. The result is of the same form as equation (3.31) but with

$$D^2 = \frac{1}{2} W^2 \mathrm{e}^{-\lambda(2b+1)} \mathrm{I}_0 \left(2\lambda \left[b(b+1)\right]^{1/2}\right) \tag{3.40}$$

and $\alpha^2 = D^2/W^2$ in the case $S = \infty$. The central band is thus elliptical with half-width D and weight D^2/W^2. It is now easy to calculate the conductivity and, using $D^2 \ll W^2$, we find

$$\sigma = \frac{\pi \mathrm{e}^2}{6\hbar a} \frac{D^2}{W^2} \approx \frac{\pi \mathrm{e}^2}{12\hbar a} \left(\frac{\beta\omega}{4\pi\lambda}\right)^{1/2} \mathrm{e}^{-\beta\lambda\omega/4} \,. \tag{3.41}$$

The last step follows by using the asymptotic forms for strong coupling and high temperature $\mathrm{I}_0(z) \sim (2\pi z)^{-1/2} \exp z$ and $b \sim (\beta\omega)^{-1}$. This form of σ is similar to that for small polaron hopping conduction in the adiabatic limit ($W \gg \omega$) [45] but with activation energy $\lambda\omega/4$ equal to one quarter, instead of one half, of the polaron binding energy. Nevertheless this establishes the link between the many-body CPA and standard small polaron theory in the strong coupling limit. However the results shown in figure 3.4, with parameters relevant to typical manganites, are far from this limit. They correspond to intermediate coupling and in the actual paramagnetic state above the Curie temperature the polaron bands are largely washed out. In this regime, with increasing temperature, there is a crossover from polaronic behaviour to a situation where the phonons behave classically, the case considered by Millis et al. [23]. For electron-phonon coupling greater than a critical value these authors find a gap in the density of states which gradually fills with increasing temperature. However in their classical treatment there are no polaron bands in the gap so that the link with standard polaron physics is not established.

Apart from the symmetry about $\epsilon = 0$ the above results for $n = 0.5$ are not untypical of the general case. For general n the main lower and upper bands, separated by a gap for $g > g_\mathrm{c}$, have approximate weights n and $1 - n$ respectively. The chemical potential at $T = 0$ is always confined to the polaron band arising from the $r = 0$ term of equation (3.39), and moves from the bottom at $n = 0$ to the top at $n = 1$, so that we correctly have an insulator in these limits.

Magnetism/magnetic order can be taken into account within the many-body CPA using a DMFT result for the Heisenberg model with classical spins which was empirically extended to the case of quantum spins [20]. This allows to calculate the required correlation functions in the magnetized state. Without this trick, however, the CPA equations never yield a ferromagnetic solution except for the case of classical spins $S \to \infty$ which we discuss later.[9]

[9]This is a general problem of CPA methods: they usually do not give states with spontaneous

In figure 3.5 we show Green's results for the Curie temperature as a function of the electron-phonon coupling strength g/W. The suppression of T_{C} with increasing coupling comes from the localization of the conduction electrons and the resulting narrowing of the band. This makes the DE mechanism less effective in lowering the kinetic energy and weakens the ferromagnetic coupling of neighbouring local spins.

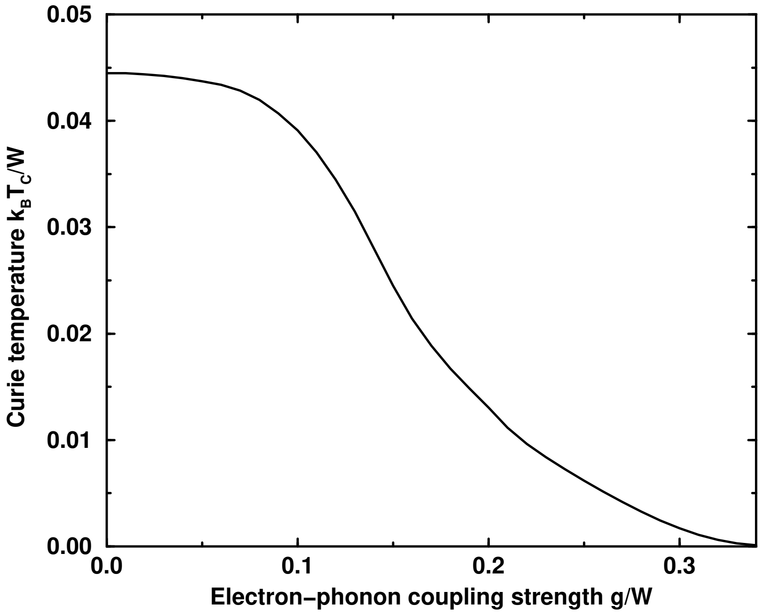

Figure 3.5.: Suppression of the Curie temperature of the Holstein-DE model with increasing electron-phonon coupling g/W. The plot is for $S = J = \infty$, $h = 0$, $n = 0.5$. Reproduced from Green [20].

Green's theory can explain the huge differences between LCMO and LSMO by assuming that the electron-phonon coupling strength changes from $g/W = 0.10$, or slightly greater, in LSMO to $g/W = 0.16$ in LCMO [20]. These values give a Curie temperature and a resistivity comparable with experiments (see section 1.3). Figure 3.6 shows the resistivity ρ as a function of temperature for $g/W = 0.16$. The reduction of ρ in the magnetic field h is the CMR effect, and we see that there is a metal-insulator transition at T_{C} as observed experimentally for LCMO. In contrast, in figure 3.7, $g/W = 0.10$ and the system remains metallic (i.e. $\partial\rho/\partial T > 0$) for all temperatures. The main differences between theory and experiment are:

magnetization for systems of quantum spins. Another common way to describe magnetic order is to empirically assume a magnetization law (e.g. a Curie law). However this approach does not allow to calculate the inherent Curie temperature of the model so that temperature dependent quantities can only be obtained as a function of T/T_{C}.

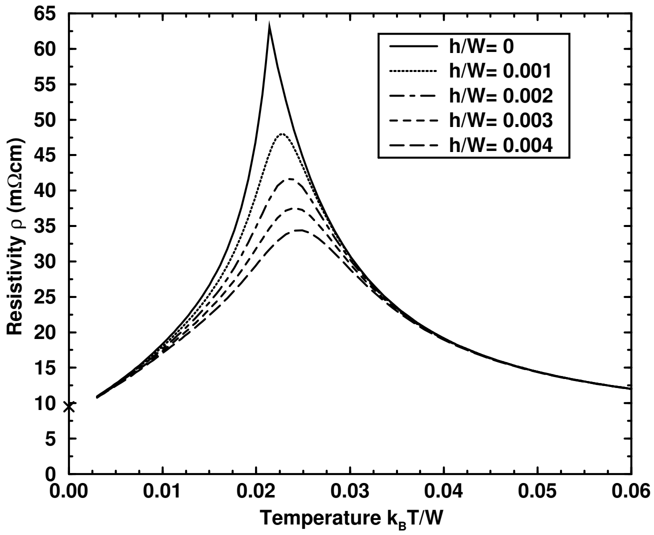

Figure 3.6.: Resistivity ρ versus temperature for the Holstein-DE model with $S = J = \infty$, $n = 0.5$, $\omega/W = 0.05$, intermediate coupling $g/W = 0.16$ and various applied fields h. Reproduced from Green [20].

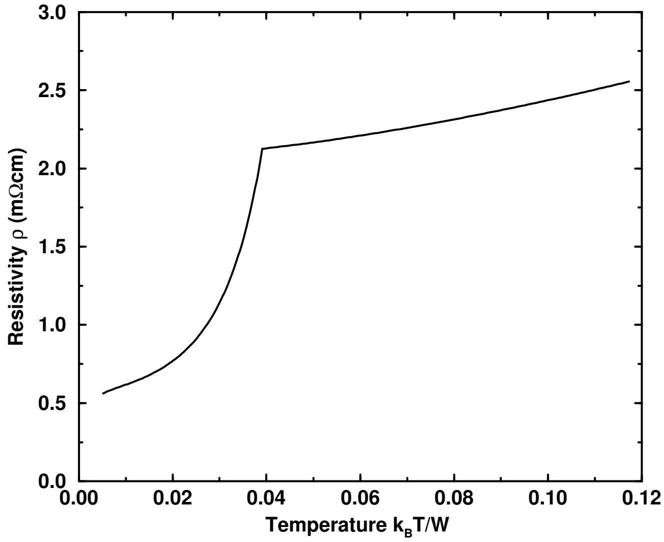

Figure 3.7.: The same plot as figure 3.6 but for weak electron-phonon coupling $g/W = 0.10$. Reproduced from Green [20].

- The fields required to achieve a certain CMR effect in the theoretical resistivity are too high by a factor 4 (see figures 1.4 and 3.6).
- The predicted drop in resistivity below T_C is too slow.

These two discrepancies might be remedied by introducing a dependence of g on ρ, corresponding to more efficient screening of the electron-phonon interaction with increasing metallization [8]. However it is not clear whether the the above failures of the theory arise from the CPA method or from the Holstein-DE model itself.

Apart from the paramagnetic state we shall also consider the case of a completely saturated ferromagnetic state at zero temperature, with all local and itinerant spins aligned. Then the second term in equation (2.16) becomes a constant shift in energy and the Hamiltonian is equivalent to that of the pure Holstein model. Within the many-body CPA the saturated state is actually the self-consistent ground state only for $S = \infty$ [20], and we shall mainly consider this limit in the sequel. In the saturated ferromagnetic state at $T = 0$ (the derivation of G^{AL} at $T = 0$ is given below), with all n electrons per atom having $\uparrow$ spin, the local Green function $G_\uparrow(\epsilon)$ again satisfies equation (3.28) with G^{AL} replaced by

$$G_\uparrow^{\mathrm{AL}} = \mathrm{e}^{-\lambda} \left\{ \frac{1}{\epsilon} + \sum_{r=1}^{\infty} \frac{\lambda^r}{r!} \left(\frac{n}{\epsilon + \omega r} + \frac{1-n}{\epsilon - \omega r} \right) \right\} . \tag{3.42}$$

We conclude this chapter with the derivation of the atomic limit Green function G^{AL} (equation (3.39) in the limit of zero temperature and/or classical spins. These expressions have been used in the calculations of chapters 4 and 5.

Zero-temperature limit for G^{AL}

The modified Bessel functions appearing in equation (3.39) are defined as [46]

$$\mathrm{I}_n(x) = \sum_{\nu=0}^{\infty} \frac{1}{v!\Gamma(n+\nu+1)} \left(\frac{x}{2}\right)^{2\nu+n} .$$

For small arguments x and integral order n we find

$$\mathrm{I}_n(x) \sim \frac{1}{|n|!} \left(\frac{x}{2}\right)^{|n|} .$$

For $\beta = (k_{\mathrm{B}}T)^{-1} \to \infty$ the Bose function can be expanded and we obtain $b(\omega) = \left[\mathrm{e}^{\beta\omega} - 1\right]^{-1} \sim \mathrm{e}^{-\beta\omega}$. Finally we make the substitution $[b(b+1)]^{1/2} \sim \mathrm{e}^{-\beta\omega/2}$ retaining terms to leading order in β only. Inserting these expressions into (3.39) we have

$$G_{\mathrm{T}=0}^{\mathrm{AL}} = \lim_{\beta\to\infty} \sum_{r=-\infty}^{\infty} \frac{\frac{1}{|r|!}\{\lambda \mathrm{e}^{-\beta\omega/2}\}^{|r|}}{(2S+1)\exp\lambda} \frac{(2S+1)\frac{n}{2}\mathrm{e}^{r\beta\omega/2} + (S+1)(1-n)\mathrm{e}^{-r\beta\omega/2}}{\epsilon + r\omega} .$$

Splitting up the sum into positive and negative r, cancelling identical terms in numerator and denominator, replacing $r \to -r$ and using $\mathrm{I}_r = \mathrm{I}_{-r}$ we obtain the desired limit of G^{AL}

$$G^{\mathrm{AL}}_{\mathrm{T}=0} = \mathrm{e}^{-\lambda} \left\{ \frac{S+1-n/2}{(2S+1)\epsilon} + \sum_{r=1}^{\infty} \frac{\lambda^r}{r!} \left[\frac{n/2}{\epsilon + r\omega} + \frac{(S+1)(1-n)}{2S+1} \frac{1}{\epsilon - r\omega} \right] \right\} . \tag{3.43}$$

Limit of classical spins $S \to \infty$ for G^{AL}

As discussed earlier it is often convenient to work in the limit of infinite (i.e. classical) spins $S \to \infty$. For completeness we therefore state the corresponding limits of the Green functions (equation (3.39) and (3.43)).

$$G^{\mathrm{AL}} = \sum_{r=-\infty}^{\infty} \frac{\mathrm{I}_r \left\{ 2\lambda [b(\omega)(b(\omega)+1)]^{1/2} \right\}}{\exp\{\lambda[2b(\omega)+1]\}} \frac{\frac{n}{2}\mathrm{e}^{r\beta\omega/2} + \frac{(1-n)}{2}\mathrm{e}^{-r\beta\omega/2}}{\epsilon + r\omega}, \tag{3.44}$$

$$G^{\mathrm{AL}}_{\mathrm{T}=0} = \mathrm{e}^{-\lambda} \left\{ \frac{1}{2\epsilon} + \sum_{r=1}^{\infty} \frac{\lambda^r}{r!} \left[\frac{n/2}{\epsilon + r\omega} + \frac{(1-n)/2}{\epsilon - r\omega} \right] \right\} . \tag{3.45}$$

4. Optical properties

There have been numerous optical investigations of the manganites in recent years. Measurements of optical conductivity and angle-resolved photoemission spectroscopy provide valuable insight into the physics of these compounds. They reveal, for example, the structure of the density of states and the dynamical Jahn-Teller effect.

In section 4.1 we calculate the one-electron spectral function which relates to observed ARPES spectra. In section 4.2 we derive a formula for the optical conductivity within the many-body CPA for the DE and the Holstein-DE model. We discuss the theoretical results and confront them with experimental data. Moreover we compare our findings with other theoretical work on the same models.

4.1. Angle-resolved photoemission spectroscopy

The decreasing resistivity of LCMO as the temperature increases above T_{C} is, according to Millis et al. [23] and Green [20], due to the gradual filling of a pseudogap in the density of states. In Green's work the pseudogap contains well-defined polaron subbands in the (hypothetical) paramagnetic state at $T = 0$ but above T_{C}, with parameters appropriate to LCMO, these are smeared out so as to resemble the classical picture of Millis et al. (see figure 3.4). The pseudogap should be observable in ARPES measurements and in optical conductivity. In an excellent paper on ARPES for the bilayer manganite $\mathrm{La_{1.2}Sr_{1.8}Mn_2O_7}$, nominally with $n = 0.6$, Dessau et al. [47] interpret their results very much in the spirit of the Holstein model. In this section we present some calculations of the spectral functions in the low temperature ferromagnetic state to compare with this experimental data. For convenience we take $n = 0.5$ and also $S = J = \infty$, as discussed in previous chapters. A half-width $W = 1\mathrm{eV}$ is consistent with the $\mathrm{e_g}$ bands crossing the Fermi level in the calculations of Dessau et al. [47], shown in figure 4.4. The low $T_{\mathrm{C}} = 126\mathrm{K}$ in this bilayer manganite is partly due to quasi-two dimensional fluctuations, but the large resistivity $\rho \simeq 3\mathrm{m}\Omega\mathrm{cm}$ at low temperatures indicates that small-polaron bands might exist even in the ferromagnetic state. Consequently the electron-phonon coupling should be stronger than in cubic manganites like LCMO and we choose $g/W = 0.2$.

The one-electron spectral function is given by

$$
\begin{aligned}
A_{\boldsymbol{k}}(\epsilon) &= -\pi^{-1}\mathrm{Im}\,[\epsilon - \epsilon_{\boldsymbol{k}} - \Sigma(\epsilon)]^{-1} \\
&= -\pi^{-1}\Sigma''_\epsilon/[(\epsilon - \epsilon_{\boldsymbol{k}} - \Sigma'_\epsilon)^2 + \Sigma''^2_\epsilon]
\end{aligned}
\tag{4.1}
$$

where Σ'_ϵ, Σ''_ϵ are the real and imaginary parts of the self-energy $\Sigma(\epsilon)$ and $\epsilon_{\boldsymbol{k}}$ is the band energy for wave-vector $\boldsymbol{k}$. In the ferromagnetic state at $T = 0$ the local Green function $G_\uparrow(\epsilon)$ is calculated from equation (3.28), with G^{AL} defined by equation (3.42), and $\Sigma(\epsilon)$ follows from equation (3.27). As discussed in section 3.3 these equations assume an elliptic density of states which we here regard as an approximation to the density of states for a band which takes the form $\epsilon_{\boldsymbol{k}} = -W\cos\pi y$ for $\boldsymbol{k} = \pi(1, y)$, $0 \leq y \leq 1$. This band is shown as a full line in figure 4.3 and crosses the Fermi level E_{F} at $\boldsymbol{k} = \pi(1, \frac{1}{2})$. It roughly models one of the $x^2 - y^2$ bands in figure 4.4. The calculated results for $A_{\boldsymbol{k}}$ are shown in figure 4.1. Well away from the Fermi level, a well-defined peak exists which broadens as $\boldsymbol{k}$ approaches the Fermi momentum at $y = 0.5$. For larger y the weight below the Fermi level is strongly reduced. The peaks never approach the Fermi level closely which is an important feature of the observed spectra [47] reproduced in figure 4.2. The theoretical curves in figure 4.1 resemble quite closely the data of figure 4.2(c). There is a pseudogap in the calculated spectra extending about 0.1eV on each side of the Fermi level. In fact this pseudogap contains polaron bands like those shown in figure 3.4. However, their amplitude is too small to show up in figure 4.1 and in the experimental data. Nevertheless, it is the central polaron band around the Fermi level which is presumably responsible for the low but finite conductivity of the system. The positions of the peaks in figure 4.1 are plotted in figure 4.3 and comparison can be made with the right half of figure 4.4 reproduced from Dessau et al. [47]. Filled and unfilled symbols correspond to high and low weights, respectively, obtained by integration of the spectral function up to the Fermi energy. This comparison between theory and experiment supports the conclusion of Dessau et al. [47] that, in the manganites with a layered structure, strong electron-phonon coupling (with the appearance of a pseudogap) is already important below T_{C}. This contrasts with the usual pseudocubic manganites where the pseudogap only appears above T_{C}. Previous work related to ours is the calculation by Perebeinos and Allen [48] of ARPES spectra in a two-band model of undoped $LaMnO_3$. It should be mentioned that Moreo et al. [49] interpret the observed pseudogap not as an intrinsic property but in terms of phase separation.

4.2. Optical conductivity

The response of a system, described by the change of an observable $\hat{A}$, to a time-dependent perturbation V_t, coupling to the observable $\hat{B}$ as $V_t = \hat{B}F_t$, is described

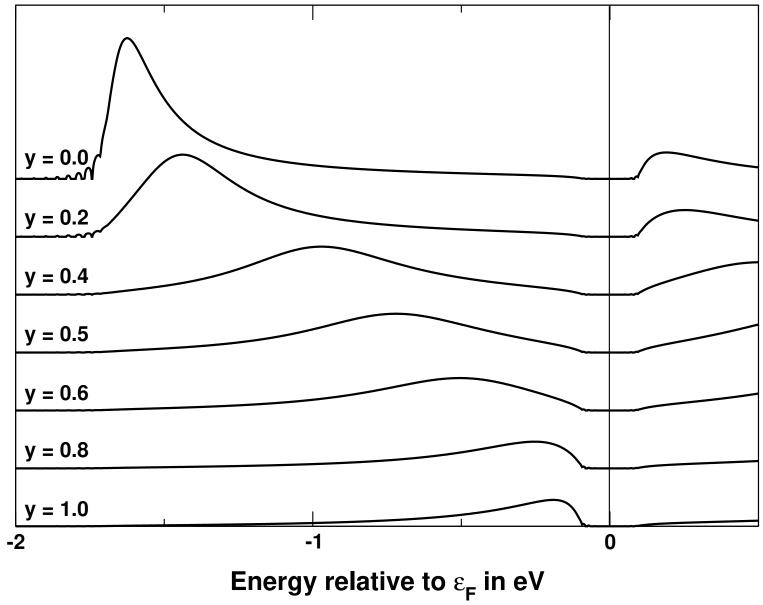

Figure 4.1.: The spectral function $A_{\boldsymbol{k}}(\epsilon)$ in the ferromagnetic state at $T = 0$ for $J = S = \infty$, $n = 0.5$ and strong electron-phonon coupling $g/W = 0.20$, with $\boldsymbol{k} = \pi(1, y)$.

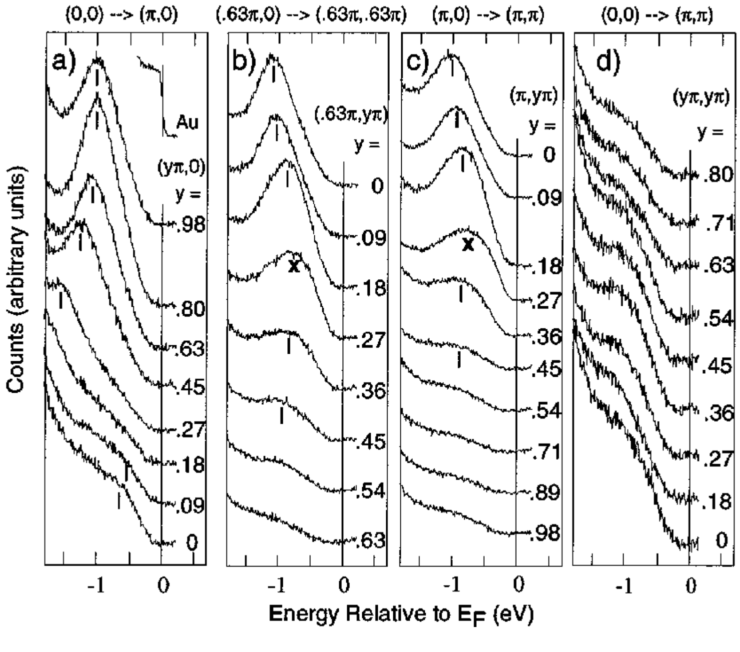

Figure 4.2.: ARPES spectra of $La_{1.2}Sr_{1.8}Mn_2O_7$ ($T_C = 126K$) in the ferromagnetic state at $T = 10K$, reproduced from Dessau et al. [47].

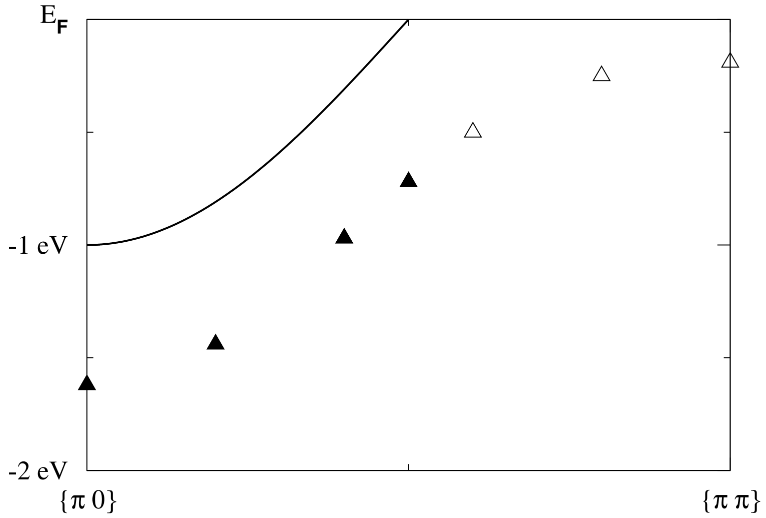

Figure 4.3.: The band energy $\epsilon_{\boldsymbol{k}}$ (——) and the position of the peak centres in figure 4.1. Different symbols denote high (▲) and low (△) spectral weight obtained by integration over the spectral function up to the Fermi energy E_{F}.

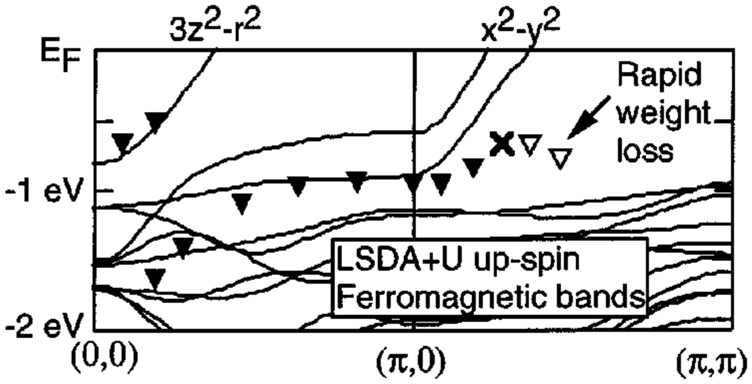

Figure 4.4.: Virtual crystal LSDA+U majority spin bands for $La_{1.2}Sr_{1.8}Mn_2O_7$ with experimental peaks from figure 4.2, reproduced from [47].

within Linear Response Theory by [17]

$$\Delta A_t = \int_{-\infty}^{\infty} \mathrm{d}t' F_{t'} G^{\mathrm{ret}}_{AB}(t,t') \tag{4.2}$$

where $G^{ret}_{AB}(t,t') = \langle\langle A(t); B(t')\rangle\rangle$ is the time-dependent retarded Green function. Fourier transformation leads to the well-known *Kubo* formula:

$$\Delta A_t = \frac{1}{2\pi}\int_{-\infty}^{\infty} \mathrm{d}\nu F(\nu) G^{\mathrm{ret}}_{AB}(\nu) \exp\left[-\mathrm{i}(\nu + \mathrm{i}0^+)t\right] \tag{4.3}$$

Using equation (4.3) for a small electric field uniform in space but oscillating in time with frequency ν, $\boldsymbol{E}(\boldsymbol{r},t) = \boldsymbol{E}_0 \exp(-\mathrm{i}\nu t)$, it may be shown [17] that the induced current density is (*Ohm's Law*)

$$\langle J^\alpha\rangle = \frac{1}{2\pi}\sum_\beta \int_{-\infty}^{\infty} \mathrm{d}\nu \exp\left[-\mathrm{i}(\nu + \mathrm{i}0^+)t\right] \sigma_{\alpha\beta}(\nu) F^\beta(\nu)\,, \tag{4.4}$$

where the conductivity tensor $\sigma_{\alpha\beta}$ which corresponds to a retarded Green function is given by

$$\sigma^{\alpha\beta}(\nu) = \frac{\mathrm{i}e^2}{a^3 m\nu}\delta_{\alpha\beta} + \frac{\mathrm{i}Na^3}{\hbar\nu}\left\langle\langle J_\alpha; J_\beta\rangle\right\rangle_\nu\ . \tag{4.5}$$

Here $\left\langle\langle J_\alpha; J_\beta\rangle\right\rangle_\nu$ is the current-current response function, a^3 is the volume of the unit cell, N is the number of lattice sites, and m and $-e$ are the electron mass and charge, respectively. We define the current density operator $\boldsymbol{J}$ as [21]

$$\boldsymbol{J} = -\frac{e}{Na^3}\sum_{\boldsymbol{k}\sigma} \boldsymbol{v}_{\boldsymbol{k}} n_{\boldsymbol{k}\sigma}\,, \tag{4.6}$$

where $\boldsymbol{v}_{\boldsymbol{k}} = \nabla\epsilon_{\boldsymbol{k}}$, and $n_{\boldsymbol{k}\sigma} = c^\dagger_{\boldsymbol{k}\sigma} c_{\boldsymbol{k}\sigma}$.

As we assume our system to have cubic symmetry the conductivity tensor reduces to a scalar. Hence the real part of the optical conductivity is

$$\sigma(\nu) := \mathrm{Re}\ \left[\sigma_{xx}(\nu)\right] = -\frac{Na^3}{\hbar\nu}\mathrm{Im}\ \left\langle\langle J_x; J_x\rangle\right\rangle_\nu . \tag{4.7}$$

Using equation (4.6) we obtain

$$\left\langle\langle J_x; J_x\rangle\right\rangle_\nu = \frac{e^2}{3\left(Na^3\right)^2}\sum_{\boldsymbol{k}\boldsymbol{k}'\sigma\sigma'} \boldsymbol{v}_{\boldsymbol{k}}\cdot\boldsymbol{v}_{\boldsymbol{k}}\left\langle\langle n_{\boldsymbol{k}\sigma}; n_{\boldsymbol{k}'\sigma'}\rangle\right\rangle_\nu\ . \tag{4.8}$$

In the local approximation of CPA or DMFT there is no vertex correction in the current-current response function which may thus be expressed in terms of the one-particle spectral function defined by equation (4.1). Consequently we have [21]

$$\left\langle\langle n_{\boldsymbol{k}\sigma}; n_{\boldsymbol{k}\sigma}\rangle\right\rangle_\nu = \int \mathrm{d}\epsilon \int \mathrm{d}\eta \frac{A_{\boldsymbol{k}\sigma}(\epsilon)A_{\boldsymbol{k}\sigma}(\epsilon+\eta)}{\nu - \eta + i0^+}\left[f(\epsilon) - f(\epsilon+\nu)\right]\,, \tag{4.9}$$

where $f(\epsilon) = \{\exp[\beta(\epsilon - \mu)] + 1\}^{-1}$ is the Fermi function. Inserting equations (4.8) and (4.9) into equation (4.7) we get

$$\sigma(\nu) = -\frac{e^2}{3Na^3\hbar\nu}\sum_{\boldsymbol{k}\sigma} \boldsymbol{v}_{\boldsymbol{k}}^2 \mathrm{Im} \int \mathrm{d}\epsilon \int \mathrm{d}\eta \frac{A_{\boldsymbol{k}\sigma}(\epsilon)A_{\boldsymbol{k}\sigma}(\epsilon+\eta)}{\nu - \eta + i0^+}\left[f(\epsilon) - f(\epsilon+\nu)\right] . \quad (4.10)$$

Using Dirac's well-known identity

$$\frac{1}{\nu - \nu_0 \pm \mathrm{i}0^+} = \mathrm{PV}\frac{1}{\nu - \nu_0} \mp \mathrm{i}\pi\delta(\nu - \nu_0)\,, \quad (4.11)$$

we find for the optical conductivity in the paramagnetic state

$$\sigma(\nu) = \frac{2\pi e^2}{3Na^3\hbar}\sum_{\boldsymbol{k}} \boldsymbol{v}_{\boldsymbol{k}}^2 \int \mathrm{d}\epsilon A_{\boldsymbol{k}\sigma}(\epsilon)A_{\boldsymbol{k}\sigma}(\epsilon+\nu)\frac{f(\epsilon) - f(\epsilon+\nu)}{\nu} \quad (4.12)$$

which is identical to the formula given by Pruschke et al. [50]. Since $A_{\boldsymbol{k}}$ depends on $\boldsymbol{k}$ through $\epsilon_{\boldsymbol{k}}$ only we may define a function $\phi(\epsilon_{\boldsymbol{k}})$ such that

$$\phi'(\epsilon_{\boldsymbol{k}}) = A_{\boldsymbol{k}}(\epsilon)A_{\boldsymbol{k}}(\epsilon+\nu), \quad (4.13)$$

where the dependence of ϕ on ϵ and ν has been suppressed in the notation. Writing

$$\sum_{\boldsymbol{k}} \boldsymbol{v}_{\boldsymbol{k}}^2 A_{\boldsymbol{k}}(\epsilon)A_{\boldsymbol{k}}(\epsilon+\nu) = \sum_{\boldsymbol{k}} \left(\nabla\epsilon_{\boldsymbol{k}}\right)^2 \phi' = \sum_{\boldsymbol{k}} \left(\nabla\epsilon_{\boldsymbol{k}}\right)\nabla\phi$$

and using the identity

$$\mathrm{div}\left(\phi \cdot \boldsymbol{A}\right) = \phi\ \mathrm{div}\boldsymbol{A} + \nabla\phi \cdot \boldsymbol{A}$$

we can apply Gauss's Theorem:

$$\begin{aligned}\int \mathrm{d}\boldsymbol{k}\nabla\phi\nabla\epsilon_{\boldsymbol{k}} &= \int \mathrm{d}\boldsymbol{k}\left[\mathrm{div}\left(\phi\nabla\epsilon_{\boldsymbol{k}}\right) - \phi\Delta\epsilon_{\boldsymbol{k}}\right] \\ &\overset{\text{(Gauss's Thm.)}}{=} \int_S \mathrm{d}S\phi\nabla\epsilon_{\boldsymbol{k}} - \int \mathrm{d}\boldsymbol{k}\phi\Delta\epsilon_{\boldsymbol{k}}\,.\end{aligned}$$

The first integral in the last line is over the surface of a simple cubic unit cell and vanishes since $\nabla\epsilon_{\boldsymbol{k}}$ has reversed signs on opposite faces of the cell. The sum in equation (4.12) can therefore be written as

$$\sum_{\boldsymbol{k}} \nabla\epsilon_{\boldsymbol{k}} \cdot \nabla\phi(\epsilon_{\boldsymbol{k}}) = -\sum_{\boldsymbol{k}} \phi(\epsilon_{\boldsymbol{k}})\nabla^2\epsilon_{\boldsymbol{k}}\,. \quad (4.14)$$

For a simple cubic tight binding band

$$\epsilon_{\boldsymbol{k}} = -2t\left(\cos(k_x a) + \cos(k_y a) + \cos(k_z a)\right) \quad (4.15)$$

$\Delta\epsilon_{\boldsymbol{k}} = -a^2\epsilon_{\boldsymbol{k}}$. Then the summand in equation (4.14) is a function of $\epsilon_{\boldsymbol{k}}$ only and by replacing the $\boldsymbol{k}$ sum by an integral over energy (see equation (1.11)) equation (4.12) becomes

$$\sigma(\nu) = \frac{2\pi \mathrm{e}^2}{3a\hbar}\sum_{\sigma}\int \mathrm{d}\epsilon \int \mathrm{d}E D_{\mathrm{c}}(E) E\phi(E)\frac{f(\epsilon)-f(\epsilon+\nu)}{\nu} \tag{4.16}$$

where $D_{\mathrm{c}}(E)$ is the density of states for the simple cubic band. By using equation (4.1) in the definition of $\phi'(\epsilon_{\boldsymbol{k}})$ and integrating with respect to $\epsilon_{\boldsymbol{k}}$ we obtain[1]

$$\begin{aligned}\phi = \frac{1}{\pi^2}&\frac{1}{\left((\Sigma''_{\epsilon}-\Sigma''_{\epsilon+\nu})^2+O^2\right)\left((\Sigma''_{\epsilon}+\Sigma''_{\epsilon+\nu})^2+O^2\right)}\\ &\times\left\{\Sigma''_{\epsilon+\nu}\left({\Sigma''_{\epsilon+\nu}}^2-\Sigma''^2_{\epsilon}+O^2\right)\arctan P+\right.\\ &\left.+\,\Sigma''_{\epsilon}\left[\left(\Sigma''^2_{\epsilon}-{\Sigma''_{\epsilon+\nu}}^2+O^2\right)\arctan Q+\Sigma''_{\epsilon+\nu}O\log R\right]\right\},\end{aligned} \tag{4.17}$$

with

$$O = \Sigma'_{\epsilon}-\Sigma'_{\epsilon+\nu}+\nu \qquad P = \frac{\Sigma'_{\epsilon}-\epsilon+\epsilon_{\boldsymbol{k}}}{\Sigma''_{\epsilon}}$$

$$Q = \frac{\Sigma'_{\epsilon+\nu}-\nu-\epsilon+\epsilon_{\boldsymbol{k}}}{\Sigma''_{\epsilon+\nu}} \qquad R = \frac{\Sigma''^2_{\epsilon}+\left(\Sigma'_{\epsilon}-\epsilon+\epsilon_{\boldsymbol{k}}\right)^2}{{\Sigma''_{\epsilon+\nu}}^2+\left(\Sigma'_{\epsilon+\nu}-\nu-\epsilon+\epsilon_{\boldsymbol{k}}\right)^2}\,.$$

Since we calculate the self-energy Σ using the elliptic density of states $D_{\mathrm{e}}(\epsilon)$, as discussed in chapter 3, it is reasonable to approximate $D_{\mathrm{c}}(E)$ in equation (4.16) by $D_{\mathrm{e}}(E)$. The integral over E can then be carried out by parts so that, using the definition of ϕ', we find

$$\sigma(\nu) = \frac{2\pi e^2}{3a\hbar}\int \mathrm{d}\epsilon \int \mathrm{d}E\frac{W^2-E^2}{3}D_{\mathrm{e}}(E)A_E(\epsilon)A_E(\epsilon+\nu)\frac{f(\epsilon)-f(\epsilon+\nu)}{\nu} \tag{4.18}$$

with $A_E(\epsilon)$ given by equation (4.1), $\epsilon_{\boldsymbol{k}}$ being replaced by E. This is of the form given by Chung and Freericks [51] and Chattopadhyay et al. [52]. If $D_{\mathrm{c}}(E)$ in equation (4.16) is replaced by a Gaussian, corresponding to a hypercubic lattice in infinite dimensions, the factor $(W^2-E^2)/3$ in equation (4.18) is replaced by a constant [53, 21]. In the sequel we use equation (4.18) which is consistent with Edwards et al.'s previous calculations of $\sigma(0)$ [21, 20]. This expression satisfies the correct one-band sum rule [52, 54] that

$$\frac{2}{\pi}\int_0^{\infty}\sigma(\nu)\mathrm{d}\nu = -\frac{Ke^2}{3a\hbar}\,, \tag{4.19}$$

where the 'kinetic energy' K is the thermal average per lattice site of the first term in the Hamiltonian (2.16).

[1] The integration has been done using MATHEMATICA®.

We take $J = S = \infty$ and, as in previous papers [21, 20], $a = 5$Å, which is slightly larger than the Mn–Mn distance in perovskite manganites. It is again convenient to take $n = 0.5$, so that for $J = S = \infty$ the chemical potential μ is fixed at the centre of the occupied band for all temperatures, by symmetry. In the ferromagnetic state at $T = 0$ the spin-degeneracy factor 2 in equation (4.18) is omitted. Computational details of the calculation of $\sigma(\nu)$ are given in appendix A.

Although we will mainly consider the limit of classical spins $S = \infty$, it is interesting to study the effect of the value of S on the optical conductivity. The results for $\sigma(\nu)$ for $S = 1/2, 3/2, 5/2$ and ∞ are shown in figure 4.5. Clearly the value of S does not change $\sigma(\nu)$ dramatically. Moreover, since our model is fairly simple compared to the complexity of the real manganites, we can only expect to get order of magnitude agreement with experimental data. It is therefore sensible to take the limit $S = \infty$, instead of $S = 3/2$ appropriate to the manganites, to simplify the calculations.

Before we confront our results with experimental data, we discuss the influence of the electron-phonon coupling strength g/W on optical conductivity. To this end, in figure 4.6, we plot $\sigma(\nu)$ for different values of g/W in the paramagnetic state at $T = 0$. For $g = 0$, the pure DE model, $\sigma(\nu)$ has a maximum at $\nu = 0$ and goes to zero at $\nu \simeq 1.25$eV. With increasing electron-phonon coupling the optical conductivity curve broadens and the maximum shifts to higher photon energies. For $g/W = 0.16$ there is a gap in the optical conductivity for very small energies, which grows as the coupling increases further.

To understand this behaviour of $\sigma(\nu)$ we plot the density of states as well as the optical conductivity for $g/W = 0.1$, 0.13 and 0.19 in the ferromagnetic state at $T = 0$, the paramagnetic state at $T = T_{\mathrm{C}}$ and $T = 1.5T_{\mathrm{C}}$. The values of T_{C} for various electron-phonon coupling parameters are given in table 4.1. Figures 4.7, 4.9 and 4.11 show that with increasing g/W a pseudogap develops which has become a real gap in the paramagnetic state for $g/W = 0.19$, and which broadens with increasing g/W (see also section 3.3.2). Since the peak in the optical conductivity is due to transitions across the gap this evolution of the density of states explains the change in $\sigma(\nu)$ when g/W is varied (figure 4.6).

From figures 4.7, 4.9 and 4.11 we see that the gap/pseudogap gradually fills in as the system becomes ferromagnetic. The reason is the increased conduction band-width $2W$ in the ferromagnetic state due to the DE effect (see section 2.1), reducing the electron-phonon coupling g/W. Again this evolution of the density of states is reflected in the corresponding curves for the optical conductivity, which show a dramatic increase of $\sigma(\nu)$ in the magnetized state.

A closer look at figures 4.8, 4.10 and 4.12 reveals the metal-insulator transition of the dc conductivity discussed in section 3.3.2. In figure 4.8 $\sigma(0)$ for $T = T_{\mathrm{C}}$ is larger than for $T = 1.5T_{\mathrm{C}}$, i.e. we have $\partial\sigma_{\mathrm{dc}}/\partial T < 0$ and $\partial\rho/\partial T > 0$, while in figures 4.10 and 4.12 $\partial\rho/\partial T < 0$ above T_{C} as in figure 3.6 for the dc resistivity. Hence g/W can be slightly larger than 0.10, the value suggested for LSMO in section 3.3.2, still giving metallic behaviour for all temperatures as observed in experiments.

Table 4.1.: Curie temperature T_C for different electron-phonon coupling parameters g/W (from figure 3.5). Absolute temperatures are for $W = 1$eV.

g/W	$k_\mathrm{B}T_\mathrm{C}/W$	T_C/K
0.10	0.038	440
0.13	0.031	360
0.16	0.021	240
0.19	0.015	170
0.20	0.013	150

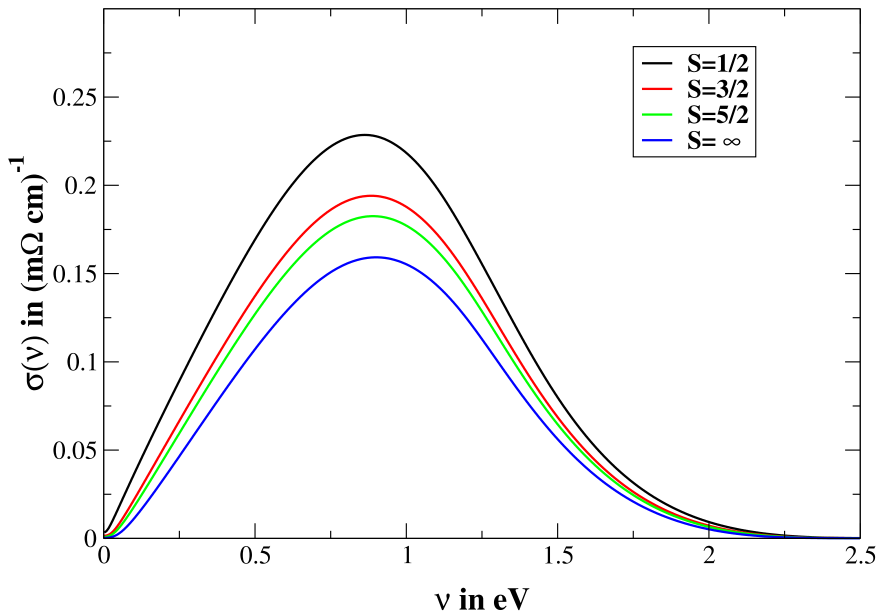

Figure 4.5.: Calculated optical conductivity for different values of the localized spin S in the paramagnetic state at $T = 0$. The plot is for $g/W = 0.16$, $J = \infty$, $n = 0.5$, $\omega/W = 0.05$ and $a = 5$Å.

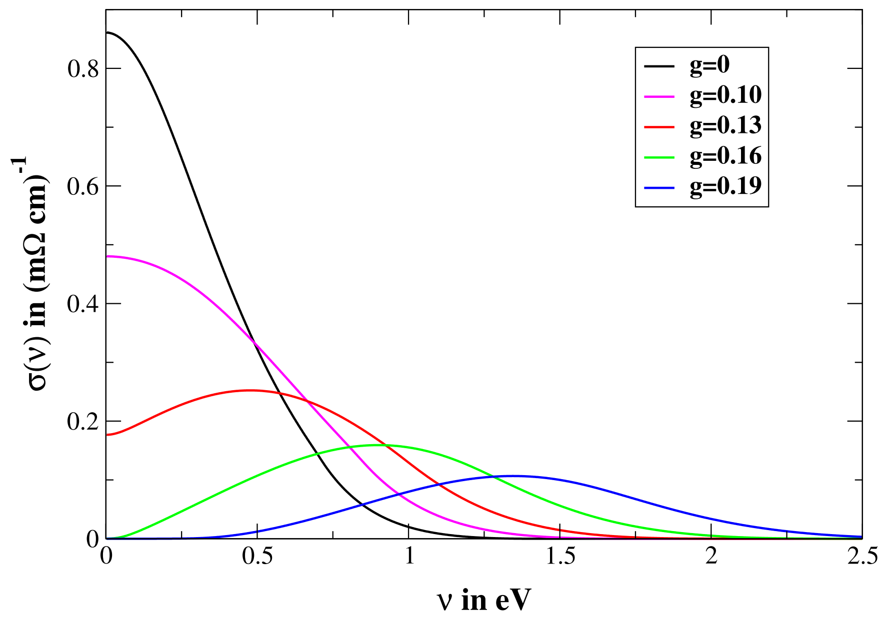

Figure 4.6.: Calculated optical conductivity for different electron-phonon coupling strengths g/W in the paramagnetic state at $T = 0$. The plot is for $J = S = \infty$, $n = 0.5$, $\omega/W = 0.05$ and $a = 5\text{Å}$.

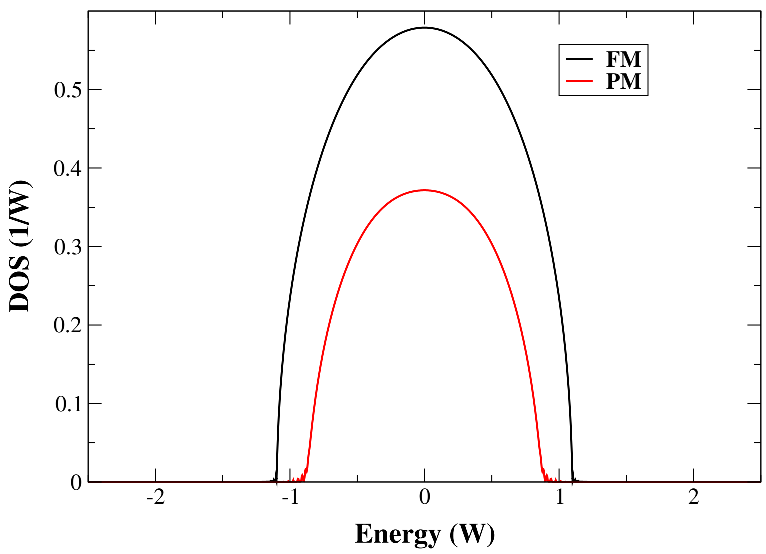

Figure 4.7.: The density of states (DOS) for $g/W = 0.1$ in the ferromagnetic state at $T = 0$ and the paramagnetic state at $T = T_{\mathrm{C}}$. All other parameters as in figure 4.6.

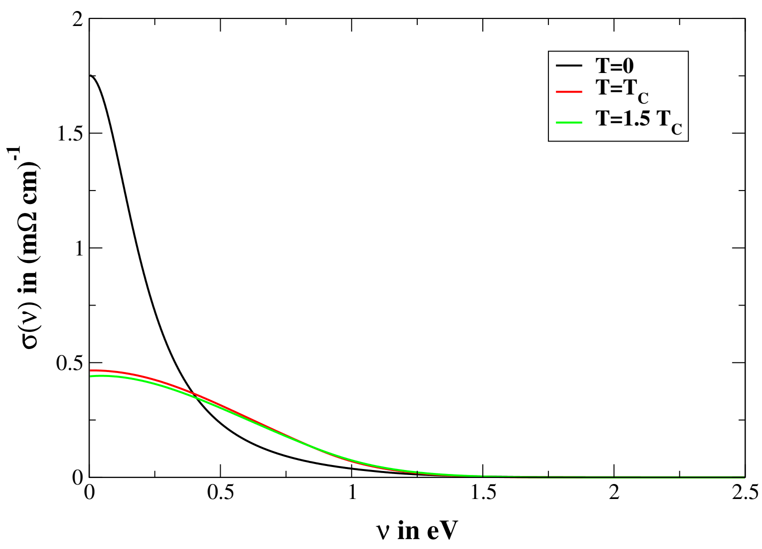

Figure 4.8.: Calculated optical conductivity for $g/W = 0.10$ in the ferromagnetic state at $T = 0$, the paramagnetic state at $T = T_{\mathrm{C}}$ and the paramagnetic state at $T = 1.5T_{\mathrm{C}}$. All other parameters as in figure 4.6.

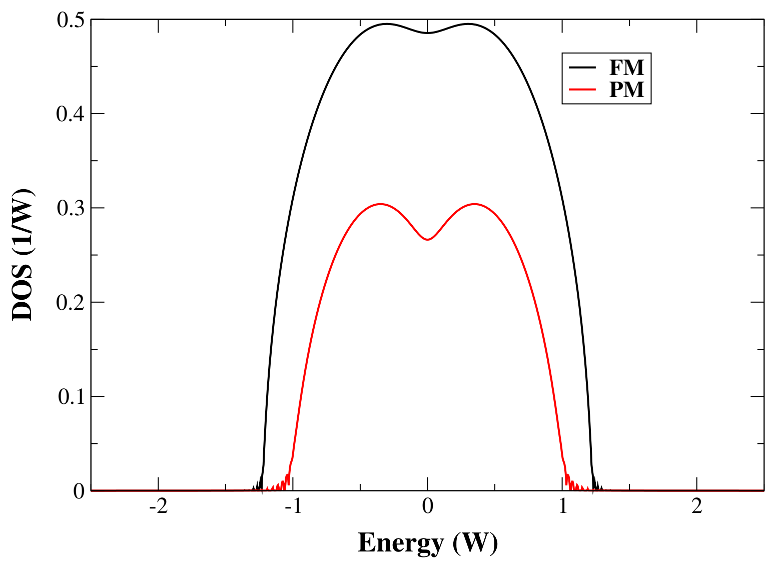

Figure 4.9.: The density of states (DOS) for $g/W = 0.13$ in the ferromagnetic state at $T = 0$ and the paramagnetic state at $T = T_{\mathrm{C}}$. All other parameters as in figure 4.6.

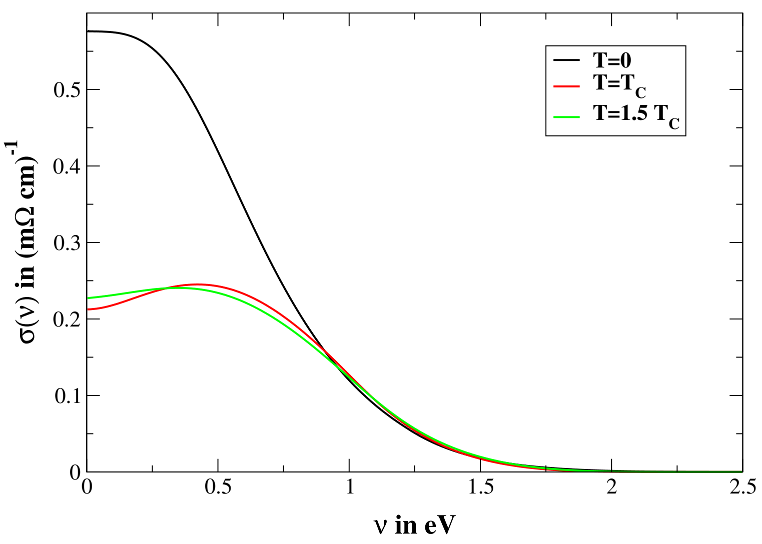

Figure 4.10.: Calculated optical conductivity for $g/W = 0.13$ in the ferromagnetic state at $T = 0$, the paramagnetic state at $T = T_\mathrm{C}$ and the paramagnetic state at $T = 1.5T_\mathrm{C}$. All other parameters as in figure 4.6.

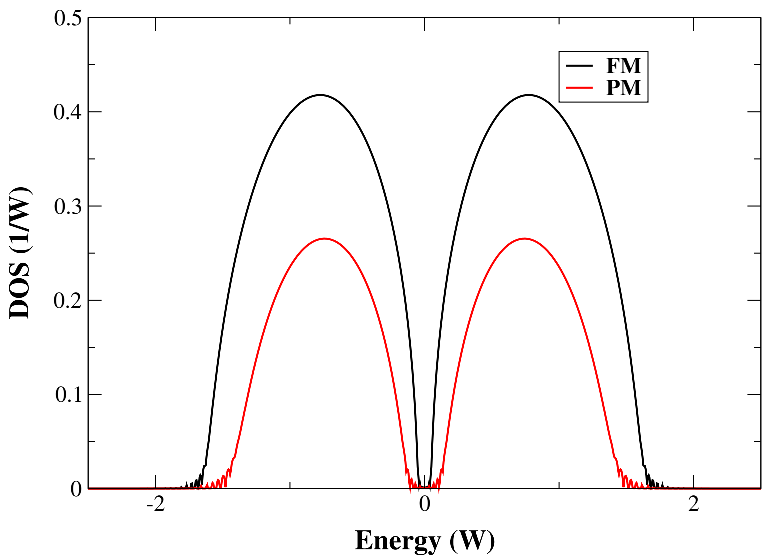

Figure 4.11.: The density of states (DOS) for $g/W = 0.19$ in the ferromagnetic state at $T = 0$ and the paramagnetic state at $T = T_\mathrm{C}$. All other parameters as in figure 4.6.

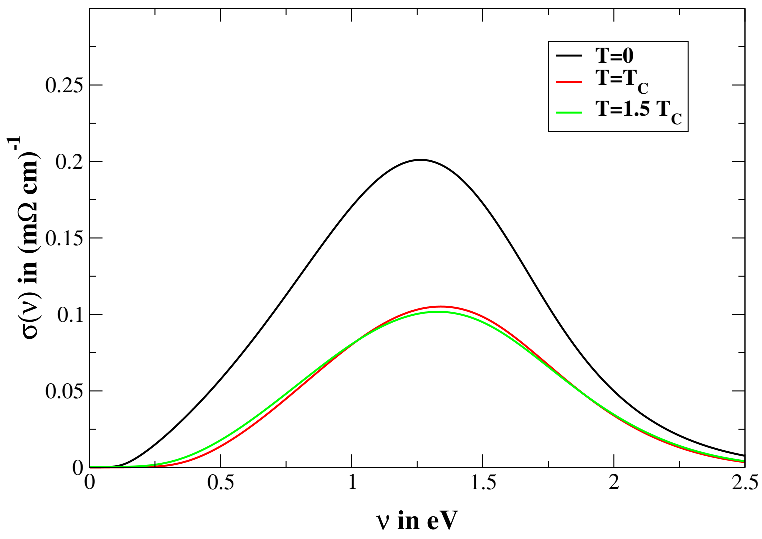

Figure 4.12.: Calculated optical conductivity for $g/W = 0.19$ in the ferromagnetic state at $T = 0$, the paramagnetic state at $T = T_{\mathrm{C}}$ and the paramagnetic state at $T = 1.5T_{\mathrm{C}}$. All other parameters as in figure 4.6.

We now discuss experimental results for optical conductivity of the manganites. Figure 4.13 shows typical curves for $\sigma(\nu)$. In general they exhibit a three-peak structure. The peak at about 1eV is interpreted as transitions between occupied JT split Mn^{3+} ions and neighbouring unoccupied unsplit Mn^{4+}. The second peak, usually centered at 3eV, is ascribed to interband transitions between the Hund's rule split $\mathrm{e_g}$ bands. Finally the third peak presumably arises from charge-transfer transitions between Mn $\mathrm{e_g}$ orbitals and O 2p orbitals, with a photon energy of about 4eV.

The latter peak does not appear in our one-band model and our assumption of $J = \infty$ eliminates the upper Hund's rule band. Our calculated $\sigma(\nu)$ is therefore only non-zero in the region $\nu < 2.5$eV and in general exhibits one peak. We shall focus the discussion by considering one material, $\mathrm{Nd_{0.7}Sr_{0.3}MnO_3}$ (NSMO), which has been investigated by at least two experimental groups. In the paramagnetic state above T_{C} there is one feature common to data on both thin films [55, 54] and single crystals [56]. This is a broad peak at about 1.2eV with a maximum conductivity $\sigma_{\max} \approx 0.7$–$0.9(\mathrm{m\Omega cm})^{-1}$. However in NSMO films T_{C}, as deduced from the maximum in the resistivity $\rho(T)$, is larger in oxygen-annealed films ($T_{\mathrm{C}} \approx 230$K) than in an unannealed sample ($T_{\mathrm{C}} \approx 180$K) [54, 55] (see also figure 4.13). In a NSMO single crystal, on the other hand, $\rho(T)$ is essentially the same ($T_{\mathrm{C}} \approx 200$K) in polished and annealed samples but the peak in the polished sample is shifted to $\nu \simeq 1$eV with a reduced $\sigma_{\max} \approx 0.3(\mathrm{m\Omega cm})^{-1}$. Since $\rho(T)$ and $\sigma(\nu)$ are quantitatively quite similar in NSMO and LCMO [54] we model NSMO with electron-phonon coupling $g/W = 0.16$, the same value as proposed by Green [20] for LCMO. The dc conductivity $\sigma(0)$ at $T = 10$K is also very similar in annealed NSMO and LCMO films, 2.9 and

$3.3(\text{m}\Omega\text{cm})^{-1}$ respectively [54]. The value for NSMO agrees well with a measured $\sigma(0)$ of 3.2 $(\text{m}\Omega\text{cm})^{-1}$ at $T = 15\text{K}$ in a NSMO single crystal [56].

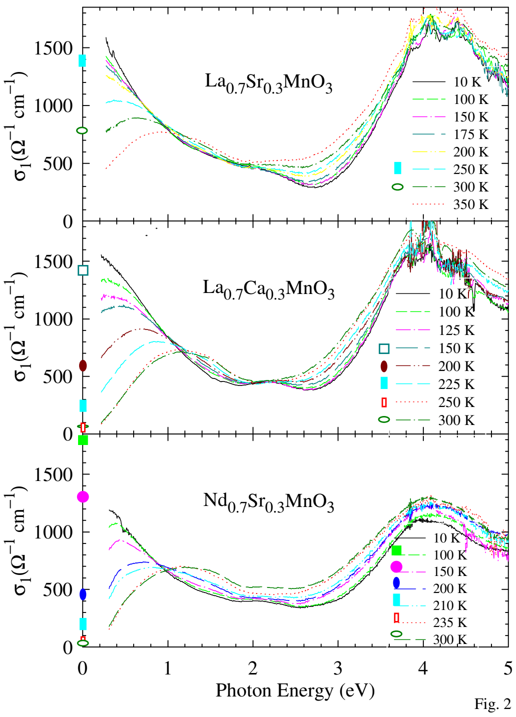

Fig. 2

Figure 4.13.: Optical conductivity of different manganites and at different temperatures, reproduced from Quijada et al. [54].

Using the parameters discussed above the Curie temperature of the model is about 240K (see table 4.1) and in figure 4.14 we plot the calculated optical conductivity for the ferromagnetic state at $T = 0$ and the paramagnetic state at $T = T_\text{C}$ and $T = 1.5T_\text{C}$. The low dc conductivity of $0.11(\text{m}\Omega\text{cm})^{-1}$ at $T = 0$ is due to the inadequate treatment of the coherent ground state in the CPA. Fortuitously the incoherent scattering introduced by the CPA seems to model quite well the low temperature incoherent scattering in the unannealed NSMO sample of Kaplan et al. [55] which has a dc conductivity of about $0.15(\text{m}\Omega\text{cm})^{-1}$ at $T = 15\text{K}$. This optical data is reproduced in figure 4.15 for comparison with the calculated results of figure 4.14. In annealed NSMO films [54], and in single crystals [56], $\sigma(\nu)$ in the low temperature ferromagnetic state continues to rise with decreasing ν down to much lower photon energy, and $\sigma(0) \approx 3(\text{m}\Omega\text{cm})^{-1}$.

As pointed out above, $\sigma(\nu)$ is much less sample-dependent in the paramagnetic state above T_C and a quantitative comparison with theory is meaningful. In figure 4.14 $\sigma_{\max} \approx 0.15(\text{m}\Omega\text{cm})^{-1}$ and it must be remembered that this curve is the contribution

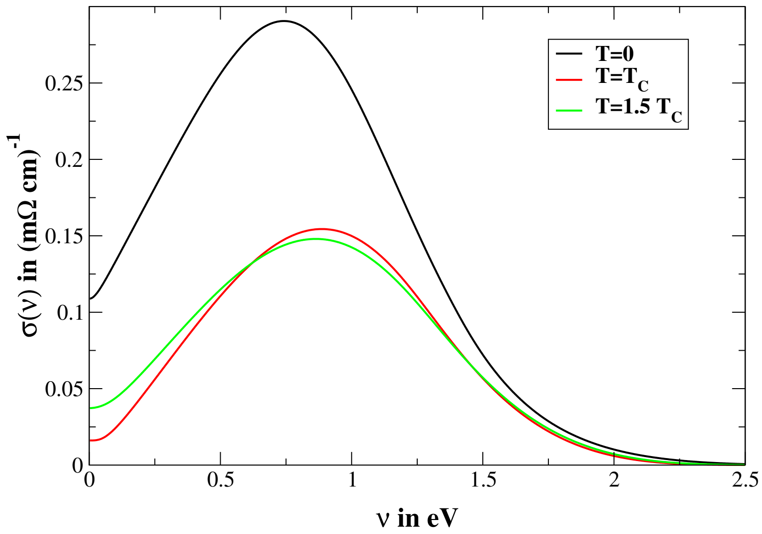

Figure 4.14.: Calculated optical conductivity for strong electron-phonon coupling $g/W = 0.16$ in the ferromagnetic state at $T = 0$, the paramagnetic state at $T = T_\mathrm{C}$ and the paramagnetic state at $T = 1.5T_\mathrm{C}$. All other parameters as in figure 4.6.

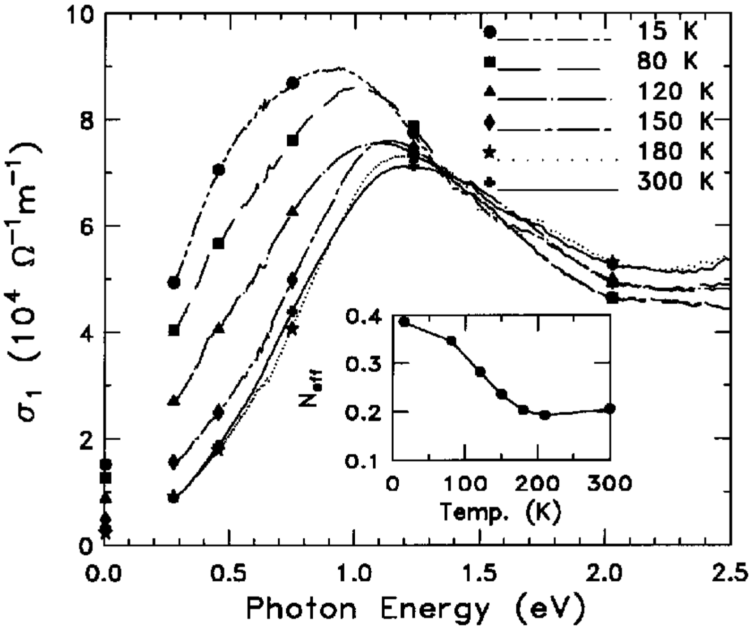

Figure 4.15.: The optical conductivity of $Nd_{0.7}Sr_{0.3}MnO_3$ at different temperatures, reproduced from Kaplan et al. [55].

of optical transitions within the e_g band only. To compare with the data of figure 4.15 one should subtract the background due to other transitions which might leave an effective $\sigma_{\max} \approx 0.3(\mathrm{m}\Omega\mathrm{cm})^{-1}$. Bearing in mind the simplicity of the one-band model, this order-of-magnitude agreement between theory and experiment is satisfactory. Our calculated results are quite similar to those of figure 7d in Millis et al. [23]. Clearly, for the present intermediate electron-phonon coupling strength, their classical treatment of phonons is sufficient to obtain the essential features of the optical conductivity. The calculated peak in $\sigma(\nu)$ with $\nu \approx 1$eV arises from $\boldsymbol{k}$-conserving transitions across the type of pseudogap discussed in section 4.1. During the process an electron moves from one site to a neighbouring one which was previously unoccupied. The electron motion is accompanied by a lattice distortion, of Jahn-Teller type, which corresponds to a displacement of the local phonon oscillator coordinate in the Holstein-DE model (see section 3.3.2). When an electron enters (leaves) a site the final displaced (undisplaced) oscillator is generally in an excited state with typical excitation energy g^2/ω. This is the atomic-limit polaron binding energy and for the parameters assumed here is about 0.5eV. Thus the peak in $\sigma(\nu)$ occurs at about twice the polaron binding energy just as in the standard small-polaron theory (see section 2.3.1). However for the present intermediate electron-phonon coupling $g/W = 0.16$ polaron bands near the Fermi level are largely washed out above T_C [20], as standard small-polaron theory is not expected to apply to $\sigma(\nu)$ for low photon energies. In fact an activation energy in the dc conductivity of 0.25eV half the polaron binding energy, as predicted by small-polaron theory [24], is about a factor 4 larger than one deduced from Green's [20] numerical calculations (see figure 3.6). Green's calculation of the dc resistivity above T_C is in reasonable agreement with experiments on NSMO where an activation energy of about 0.08eV is found [57]. Lee et al. [56] quote an activation energy of about 0.15eV and, with undue reliance on small-polaron theory, expect to have a peak in $\sigma(\nu)$ at about 0.6eV. Although there is no sign of such a peak in their data they claim that their one broad peak near 1.2eV should be interpreted in terms of a two-peak structure, one near 1.5eV and the other below 1eV. Our interpretation of the 1.2eV peak in $\sigma(\nu)$ for $T > T_C$ is broadly in line with that of several other previous authors [23, 54, 55]. However we stress again that, for moderate electron-phonon coupling standard small-polaron theory does not hold at low photon energy, where only states around the Fermi level are involved, so no simple link between peak position and the activation energy of the dc conductivity can be made. Below T_C the peak in $\sigma(\nu)$ shifts to lower frequency as the pseudogap rapidly fills in. However in our calculations this shift is held up due to spurious incoherent scattering in the ground state, which limits the low-temperature dc conductivity. The same effect actually occurs in unannealed NSMO films (figure 4.15) but in annealed films and single crystals the peak shifts almost to zero frequency [54, 56]. The theoretical situation could be improved by introducing screening effects in the electron-phonon interaction so that g/W decreases with decreasing resistivity, as mentioned at the end of section 3.3.2. The spurious residual resistivity at $T = 0$ drops from 9mΩcm to 0.5mΩcm as g/W decreases from 0.16 to 0.10 [20, 58]. Ishihara et al. [59] and Mack and Horsch [60] have given an alternative interpretation of the broad low energy peak at $T = 0$ in terms of orbital degrees of freedom in the doubly-degenerate e_g band. They propose that strong correlation, with the constraint of no doubly occupied sites, leads to incoherent motion of the carriers.

5. Spin waves

In this chapter we derive a simple approximate formula for the spin-wave spectrum of the Holstein-DE model. Our aim is to calculate the spin-wave stiffness constant D in the saturated ferromagnetic state at zero temperature. We will discuss the behaviour of D as a function of electron-phonon coupling strength and compare with the corresponding behaviour of the Curie temperature T_{C}. We also discuss results of inelastic neutron scattering experiments and how they relate to our findings. Section 5.1 introduces the idea of spin waves in the Heisenberg model.

5.1. Spin waves in the Heisenberg model

We follow Nolting [17] and introduce the concept of spin waves for the case of the Heisenberg model for magnetic insulators, which often exhibit a spontaneous magnetization below a critical temperature. Since there are no itinerant electrons in these systems the only possible interaction is the direct exchange of electrons between neighbouring sites. This exchange due to Coulomb interaction can be described in terms of a spin–spin interaction using the Hamiltonian

$$H = -\sum_{ij} J_{ij} \boldsymbol{s}_i \cdot \boldsymbol{s}_j - g_{\mathrm{J}} \mu_{\mathrm{B}} B_0 \sum_i s_i^z . \tag{5.1}$$

Here $\boldsymbol{s}_i$[1] is a local magnetic moment or spin on lattice site i, and the second term describes the coupling to an external magnetic field B_0, with $\hbar = 1$. The so-called exchange matrix elements J_{ij}, which are positive for the common case of a ferromagnet, vanish for $i = j$. For isotropic exchange coupling in a translational invariant system the matrix elements depend on the distance of i and j only, i.e. $J_{ij} = J(\boldsymbol{R}_i, \boldsymbol{R}_j) = J(|\boldsymbol{R}_i - \boldsymbol{R}_j|)$.

The spin operators in equation (5.1) are defined as $\boldsymbol{s}_i = (s_i^x, s_i^y, s_i^z)$. Introducing spin raising/lowering operators $s^\pm = s^x \pm \mathrm{i} s^y$, we can write the scalar product as

$$\boldsymbol{s}_i \cdot \boldsymbol{s}_j = s_i^z s_j^z + \frac{1}{2}\left(s_i^+ s_j^- + s_i^- s_j^+\right) . \tag{5.2}$$

[1] We use lower-case letters for spin operators in this section to avoid confusion with the notation for the Holstein-DE model in section 5.2.

With the Fourier transform for spin operators

$$s^{\alpha}(\boldsymbol{k}) = \sum_i \mathrm{e}^{-\mathrm{i}\boldsymbol{k}\cdot\boldsymbol{R}_i} s_i^{\alpha} \tag{5.3a}$$

$$s_i^{\alpha} = \frac{1}{N}\sum_{\boldsymbol{k}} \mathrm{e}^{\mathrm{i}\boldsymbol{k}\cdot\boldsymbol{R}_i} s^{\alpha}(\boldsymbol{k})\,, \tag{5.3b}$$

where N is the number of lattice sites, $\alpha = x, y, z, +, -$, and the well-known commutation relations

$$[s_i^x, s_j^y] = \mathrm{i}\delta_{ij} s_i^z \text{ and cyclic permutations} \tag{5.4a}$$

$$[s_i^z, s_j^{\pm}] = \pm\delta_{ij} s_i^{\pm} \tag{5.4b}$$

$$[s_i^+, s_j^-] = 2\delta_{ij} s_i^z \tag{5.4c}$$

and in momentum space

$$[s^+(\boldsymbol{k}), s^-(\boldsymbol{p})] = 2s^z(\boldsymbol{k}+\boldsymbol{p}) \tag{5.5a}$$

$$[s^z(\boldsymbol{k}), s^{\pm}(\boldsymbol{p})] = \pm s^{\pm}(\boldsymbol{k}+\boldsymbol{p}) \tag{5.5b}$$

$$\left(s^+(\boldsymbol{k})\right)^{\dagger} = s^-(-\boldsymbol{k})\,, \tag{5.5c}$$

it is straight forward to transform Hamiltonian (5.1) to $\boldsymbol{k}$ space. The result is

$$H = -\frac{1}{N}\sum_{\boldsymbol{k}} J(\boldsymbol{k})\left\{s^+(\boldsymbol{k})s^-(-\boldsymbol{k}) + s^z(\boldsymbol{k})s^z(-\boldsymbol{k})\right\} - g_{\mathrm{J}}\mu_{\mathrm{B}}B_0 s^z(0) \tag{5.6}$$

where

$$J(\boldsymbol{k}) = \frac{1}{N}\sum_{ij} J_{ij}\mathrm{e}^{\mathrm{i}\boldsymbol{k}\cdot(\boldsymbol{R}_i-\boldsymbol{R}_j)}\,. \tag{5.7}$$

For ferromagnetic coupling $J_{ij} > 0$ the ground state of the Heisenberg model is a saturated ferromagnetic state with all spins having the same orientation. We denote this state as $|F\rangle$. Because of the perfect alignment of the spins, application of a spin raising operator $s^+(\boldsymbol{k})$ to $|F\rangle$ gives zero. We also have

$$s_i^z\,|F\rangle = s\,|F\rangle\;, \quad s^z(\boldsymbol{k})\,|F\rangle = \delta_{\boldsymbol{k},0} N s\,|F\rangle$$

where the second relation follows from the first and equation (5.3a).

The energy of the ground state can easily be calculated using the above relations and we obtain

$$H\,|F\rangle = E_0\,|F\rangle$$
$$E_0 = -NJ_0 s^2 - N g_{\mathrm{J}}\mu_{\mathrm{B}}B_0 s\,, \tag{5.8}$$

with $J_0 = \sum_i J_{ij}$. The state

$$|q\rangle = s^-(\boldsymbol{q})\,|F\rangle \tag{5.9}$$

is an eigenstate of Hamiltonian (5.1) with energy $E(\boldsymbol{q})$ [17]

$$\begin{aligned} H\,|q\rangle &= E(\boldsymbol{q})\,|q\rangle \\ E(\boldsymbol{q}) &= E_0 + \omega(\boldsymbol{q})\,. \end{aligned} \tag{5.10}$$

It may be shown that the excitation energy $\omega(\boldsymbol{q})$ is given by

$$\omega(\boldsymbol{q}) = g_{\mathrm{J}}\mu_{\mathrm{B}}B_0 + 2s(J_0 - J(\boldsymbol{q}))\,.$$

This excitation energy can may be ascribed to a quasi-particle with energy ω and momentum $\boldsymbol{q}$, called **magnon**. The first term, which describes the coupling to the external field B_0, reveals that the total magnetic moment of the system in the excited state $|q\rangle$ is changed by $g_{\mathrm{J}}\mu_{\mathrm{B}}$ compared to the ground state. Hence it follows that the magnon is a particle of spin 1 (a boson).

Finally, using the commutation relations (5.5), it is simple to calculate the expectation value

$$\langle q|\, s_i^z\,|q\rangle = s - \frac{1}{N} \tag{5.11}$$

for any i or $\boldsymbol{q}$. Compared to the ferromagnetic ground state, for which we have $\langle F|\, s_i^z\,|F\rangle = s$, the z component of the local moment is reduced by a fraction $1/N$ on every lattice site in the crystal. This leads to the idea of a spin wave corresponding to a collective excitation of the system in which the z component of the total spin is reduced by s, and s^z on each site is reduced by $1/N$. In a vector model of the local spins, which precess around the z axis, each spin therefore has a z component $s - 1/N$ and neighbouring spins on sites i and j have a phase difference of $\boldsymbol{q}\cdot(\boldsymbol{R}_i - \boldsymbol{R}_j)$ (see figure 5.1). This may be interpreted as a spin wave of momentum $\boldsymbol{q}$ and energy $\omega(\boldsymbol{q})$, with the magnons playing the same role as the phonons for vibrations in a crystal lattice.

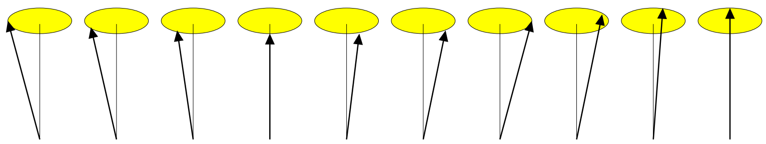

Figure 5.1.: Visualization of a spin wave.

If we are only interested in the spin-wave dispersion for small values of $|\boldsymbol{q}|$ we may expand $\omega(\boldsymbol{q})$ in the form

$$\omega(\boldsymbol{q}) = Dq^2\,. \tag{5.12}$$

Here D is called 'spin-wave stiffness' and for the ferromagnetic ground state to be stable we must have $D > 0$. Otherwise the systems could lower its energy by exciting spin waves. D is usually difficult to calculate as it depends, in general, on the band structure, the electron density and the temperature. At low temperatures, however, we may assume that the interaction between magnons is negligible. In this case the spin-wave stiffness of the simple cubic Heisenberg model becomes [61]

$$D = 2sJza^2 \tag{5.13}$$

where z is the number of nearest neighbours in the lattice and a is the lattice constant as usual. Finally the Curie temperature of the spin s nearest neighbour simple cubic Heisenberg model, obtained within mean-field theory, is [61]

$$k_\mathrm{B}T_\mathrm{C} = \frac{2}{3}s(s+1)Jz^2\,. \tag{5.14}$$

These results will be used in the next section.

5.2. Spin waves in the Holstein-DE model

Quijada et al. [54] considered the spin-wave stiffness constant D in the saturated ferromagnetic state at $T = 0$ and its relation to optical conductivity. However, their derivation of an expression for D was restricted to the DE model.

In the limit $J \to \infty$ the local and itinerant spins are locked together as we make the ansatz

$$|q\rangle = \left(S_{\boldsymbol{q}}^- + \sigma_{\boldsymbol{q}}^-\right)|F\rangle \tag{5.15}$$

for the state (unnormalized as yet) with a magnon of wave-vector $\boldsymbol{q}$ excited. Here $|F\rangle$ is the exact ferromagnetic ground state, which we assume to be one of complete spin alignment, and the spin lowering operators are defined by

$$S_{\boldsymbol{q}}^- = \sum_i \mathrm{e}^{\mathrm{i}\boldsymbol{q}\cdot\boldsymbol{R}_i} S_i^-\,, \quad \sigma_{\boldsymbol{q}}^- = \sum_i \mathrm{e}^{\mathrm{i}\boldsymbol{q}\cdot\boldsymbol{R}_i}\sigma_i^-\,, \tag{5.16}$$

where $\boldsymbol{R}_i$ is the position of lattice site i.

Actually we do not know the state $|F\rangle$ exactly for the Holstein-DE model, unlike the DE model, but we shall only approximate it at a later stage. The spin-wave energy is given by

$$\omega_{\boldsymbol{q}} = \frac{\langle q|\,H\,|q\rangle}{\langle q\mid q\rangle} - E_0 \tag{5.17}$$

where E_0 is the exact ground state energy, so that $H\,|F\rangle = E_0\,|F\rangle$. By the variational principle, this is an upper bound on $\omega_{\boldsymbol{q}}$. Using the definition of $|q\rangle$ (equation (5.15)) we can write equation (5.17) as

$$\omega_{\boldsymbol{q}} = \frac{\langle q|\,[H, S_{\boldsymbol{q}}^- + \sigma_{\boldsymbol{q}}^-]\,|F\rangle}{\langle q\mid q\rangle}\,. \tag{5.18}$$

To evaluate the denominator in equation (5.18) we again use equation (5.15) and write

$$\begin{aligned}\langle q \mid q\rangle &= \langle F| \left(S^{+}_{-\boldsymbol{q}} + \sigma^{+}_{-\boldsymbol{q}}\right) \left(S^{-}_{\boldsymbol{q}} + \sigma^{-}_{\boldsymbol{q}}\right) |F\rangle \\ &= \langle F| \left[S^{+}_{-\boldsymbol{q}} + \sigma^{+}_{-\boldsymbol{q}}, S^{-}_{\boldsymbol{q}} + \sigma^{-}_{\boldsymbol{q}}\right] |F\rangle \ , \end{aligned} \tag{5.19}$$

where we exploited $(S^{+}_{\boldsymbol{q}} + \sigma^{+}_{\boldsymbol{q}}) |F\rangle = 0$, which is due to the fact that $|F\rangle$ is the state of maximum total spin. As shown in appendix B the result is

$$\langle q \mid q\rangle = N(2S + n) \tag{5.20}$$

where S is the magnitude of the localized spin $\boldsymbol{S}_i$. Only the first term in the Hamiltonian (2.16) makes a non-zero contribution to the commutator in equation (5.18) (see appendix B). This one-electron term may be written as $H_0 = \sum_{\boldsymbol{k}\sigma} \epsilon_{\boldsymbol{k}} n_{\boldsymbol{k}\sigma}$ where $n_{\boldsymbol{k}\sigma}$ is the occupation number for the Bloch state $\boldsymbol{k}\sigma$. Hence we are left with the commutator

$$[H_0, \sigma^{-}_{\boldsymbol{q}}] = \sum_{\boldsymbol{k}\sigma} \epsilon_{\boldsymbol{k}} [n_{\boldsymbol{k}\sigma}, \sigma^{-}_{\boldsymbol{q}}] \,. \tag{5.21}$$

Using

$$\sigma^{-}_{\boldsymbol{q}} = \sum_{\boldsymbol{k}} c^{\dagger}_{\boldsymbol{k}\downarrow} c_{\boldsymbol{k}+\boldsymbol{q}\uparrow} \tag{5.22}$$

we get

$$\langle q| \left[H, S^{-}_{\boldsymbol{q}} + \sigma^{-}_{\boldsymbol{q}}\right] |F\rangle = \sum_{\boldsymbol{k}} \left(\epsilon_{\boldsymbol{k}} - \epsilon_{\boldsymbol{k}+\boldsymbol{q}}\right) \langle q| \, c^{\dagger}_{\boldsymbol{k}\downarrow} c_{\boldsymbol{k}+\boldsymbol{q}\uparrow} |F\rangle \ . \tag{5.23}$$

Once again, using equation (5.15), the expectation value can be written in terms of a commutator, namely

$$\langle q| \, c^{\dagger}_{\boldsymbol{k}\downarrow} c_{\boldsymbol{k}+\boldsymbol{q}\uparrow} |F\rangle = \langle F| \left[\sigma^{+}_{-\boldsymbol{q}}, c^{\dagger}_{\boldsymbol{k}\downarrow} c_{\boldsymbol{k}+\boldsymbol{q}\uparrow}\right] |F\rangle \ . \tag{5.24}$$

With $[\sigma^{+}_{-\boldsymbol{q}}, c_{\boldsymbol{k}+\boldsymbol{q}\uparrow}] = -c_{\boldsymbol{k}\downarrow}$ and $[\sigma^{+}_{-\boldsymbol{q}}, c_{\boldsymbol{k}\downarrow}] = c^{\dagger}_{\boldsymbol{k}+\boldsymbol{q}\uparrow}$, it follows

$$\langle q| \left[H, S^{-}_{\boldsymbol{q}} + \sigma^{-}_{\boldsymbol{q}}\right] |F\rangle = \sum_{\boldsymbol{k}} \left(\epsilon_{\boldsymbol{k}} - \epsilon_{\boldsymbol{k}+\boldsymbol{q}}\right) \left(\langle n_{\boldsymbol{k}+\boldsymbol{q}\uparrow}\rangle - \langle n_{\boldsymbol{k}\downarrow}\rangle\right) \ . \tag{5.25}$$

The expectation values are evaluated in the ferromagnetic ground state $|F\rangle$ so that we have $\langle n_{\boldsymbol{k}\downarrow}\rangle = \langle F| \, n_{\boldsymbol{k}\downarrow} |F\rangle = 0$. Finally, replacing $\boldsymbol{k} \to -\boldsymbol{k}$ and using the fact that $\epsilon_{\boldsymbol{k}}$ and $\langle n_{\boldsymbol{k}}\rangle$ are even functions of momentum, we have

$$\omega_{\boldsymbol{q}} = \frac{1}{N(n+2S)} \sum_{\boldsymbol{k}} \left(\epsilon_{\boldsymbol{k}+\boldsymbol{q}} - \epsilon_{\boldsymbol{k}}\right) \langle n_{\boldsymbol{k}\uparrow}\rangle \,. \tag{5.26}$$

Assuming a simple cubic tight binding band $\epsilon_{\boldsymbol{k}} = -t \sum_{\boldsymbol{R}} \mathrm{e}^{\mathrm{i}\boldsymbol{k}\cdot\boldsymbol{R}}$, the sum being over 6 nearest neighbour sites, we find

$$\omega_{\boldsymbol{q}} = -\frac{t}{N(n+2S)} \sum_{\boldsymbol{R}} \left(\mathrm{e}^{\mathrm{i}\boldsymbol{q}\cdot\boldsymbol{R}} - 1\right) \sum_{\boldsymbol{k}} \mathrm{e}^{\mathrm{i}\boldsymbol{k}\cdot\boldsymbol{R}} \langle n_{\boldsymbol{k}\uparrow}\rangle \,. \tag{5.27}$$

Since $\langle n_{\boldsymbol{k}\uparrow}\rangle$ has cubic symmetry in $\boldsymbol{k}$-space, the $\boldsymbol{k}$ sum in equation (5.27) is independent of the particular neighbour $\boldsymbol{R}$. By including the factor $-t$ it may therefore be written as $(1/6)\sum_{\boldsymbol{k}} \epsilon_{\boldsymbol{k}}\langle n_{\boldsymbol{k}\uparrow}\rangle$. Hence

$$\begin{aligned}\omega_{\boldsymbol{q}} &= \frac{D}{a^2}\sum_{\boldsymbol{R}}\left(1-\mathrm{e}^{\mathrm{i}\boldsymbol{q}\cdot\boldsymbol{R}}\right) \\ &= \left(2D/a^2\right)\left(3-\cos q_x a-\cos q_y a-\cos q_z a\right)\,, \end{aligned} \tag{5.28}$$

where $\boldsymbol{q}=(q_x,q_y,q_z)$ and

$$D=-\frac{a^2}{6N(n+2S)}\sum_{\boldsymbol{k}}\epsilon_{\boldsymbol{k}}\langle n_{\boldsymbol{k}\uparrow}\rangle=-\frac{Ka^2}{6(n+2S)}\,. \tag{5.29}$$

Here K is the expectation value of the kinetic energy which appears in the optical sum rule (equation (4.19)). By expanding equation (5.28) in powers of $\boldsymbol{q}$ to second order, we find

$$\omega_{\boldsymbol{q}}=Dq^2 \tag{5.30}$$

as that D defined by equation (5.29) is the spin-wave stiffness constant.

At this stage, with the expectation value $\langle n_{\boldsymbol{k}\uparrow}\rangle$ calculated in the exact ground state, equation (5.28) is a rigorous upper bound on the magnon energy for arbitrary J and S. This is no longer the case when we proceed to evaluate it within the many-body CPA. Clearly, equations (5.28) and (5.29) apply equally to the Holstein-DE and the DE model. However, we shall show that electron-phonon coupling in the former model has a strong influence via $\langle n_{\boldsymbol{k}\uparrow}\rangle$. In the limit $J\to\infty$, equation (5.29) is equivalent to results derived by Nagaev [62, 63], Kubo and Ohata [64], Furukawa [65, 19], Wang [66] and Quijada et al. [54] for the DE model. The K defined in the latter paper is one-third of our kinetic energy. Furukawa also derived the dispersion relation of equation (5.28) for the DE model. Now

$$\langle n_{\boldsymbol{k}\uparrow}\rangle=\int_{-\infty}^{\mu}\mathrm{d}\epsilon A_{\boldsymbol{k}}(\epsilon) \tag{5.31}$$

where $A_{\boldsymbol{k}}(\epsilon)$, given by equation (4.1), is calculated for the saturated ferromagnetic state at $T=0$. As in deriving $\sigma(\nu)$ we can replace the $\boldsymbol{k}$ sum in equation (5.29) by an energy integral. Hence, using the notation $A_E(\epsilon)$ introduced in equation (4.18),

$$D=-\frac{a^2}{6(n+2S)}\int_{-W}^{W}\mathrm{d}E\int_{-\infty}^{\mu}\mathrm{d}\epsilon E D_{\mathrm{e}}(E)A_E(\epsilon)\,. \tag{5.32}$$

As in chapter 4 we have approximated the simple cubic density of states by the elliptic density of states $D_{\mathrm{e}}(E)$. For simplicity and to match the other calculations in this work, in particular that of the optical conductivity, we calculate $A_E(\epsilon)$, and hence the double integral in equation (5.32) which represents the average kinetic energy K, in the limit $S = \infty$. However, in the prefactor in equation (5.32) we put $S = 3/2$ as is appropriate for the localized Mn spins. This corresponds to calculating the Bloch wall stiffness constant[2] ($\propto D(n+2S)$), which is a static quantity, in the limit $S \to \infty$ but retaining the essential finiteness of the spin in the dynamical quantity D. Otherwise we use the same parameters as in chapter 4, except that we now take $a = 4\text{Å}$. In section 4.2 we used $a = 5\text{Å}$, for consistency with earlier work on conductivity [21, 20], but 4Å is closer to the Mn–Mn distance in the pseudocubic manganites.

In figure 5.2 we plot the spin-wave stiffness D at $T = 0$ as a function of electron-phonon coupling g/W. The reason for the striking decrease of D with g/W, particularly in the range $0.1 < g/W < 0.2$ applicable to the manganites, is clear from equation (5.29). For $g/W = 0$, the pure DE model, $\langle n_{\boldsymbol{k}\uparrow}\rangle = 1$ for $\boldsymbol{k}$ within the Fermi surface and $\langle n_{\boldsymbol{k}\uparrow}\rangle = 0$ otherwise. This is due to the fact that the second term $J\sum_i \boldsymbol{\sigma}_i \cdot \boldsymbol{S}_i$ in Hamiltonian (2.16) becomes a constant shift in energy, and we therefore have a system of non-interacting particles occupying a Fermi sphere in $\boldsymbol{k}$ space at $T = 0$. The negative quantity K in this case is the full non-interacting one-electron energy of the ferromagnetic state which drives the DE mechanism. For larger g/W, $\langle n_{\boldsymbol{k}\uparrow}\rangle$ is more spread out over the whole zone and $|K|$ decreases. In an extreme limit where electrons are localized at sites, $\langle n_{\boldsymbol{k}\uparrow}\rangle$ is constant throughout the zone and hence $D = 0$. In fact, for the DE model, D can be calculated exactly from equation (5.32). As discussed above, $\langle n_{\boldsymbol{k}\uparrow}\rangle$ is just the Fermi distribution function which simplifies to a step function at $T = 0$. Hence, from equation (5.32), we have

$$\begin{aligned} D &= -\frac{a^2}{3\pi W^2(n+2S)} \int_{-W}^{\mu} \mathrm{d}\epsilon \left(W^2 - \epsilon^2\right)^{1/2} \epsilon \\ &= \frac{a^2}{9\pi W^2(n+2S)} \left(W^2 - \mu^2\right)^{3/2} . \end{aligned} \tag{5.33}$$

If we take the usual values for the parameters $W = 1\text{eV}$, $n = 0.5$ and $S = 3/2$, we get

$$D = \frac{2a^2 W}{63\pi} \approx 161.68\text{meV}\text{Å}^2 . \tag{5.34}$$

Here we set $\mu = 0$ which is correct for $n = 0.5$ and $S = \infty$, the limit in which the integral in equation (5.33) has been evaluated. This numerical value of D for $g/W = 0$ agrees well with the curve in figure 5.2.

The behaviour of D in the Holstein-DE model is very similar to that of T_{C}, as calculated by Green [20] (see figure 3.5). The main difference is in the extreme strong-coupling limit where T_{C} becomes very small at $g/W \approx 0.35$ whereas D is decreasing quite slowly. The slow decrease of D is exactly what one expects from equation (5.29) and small-polaron theory, where the kinetic energy $K \sim g^{-2}$ [68]. T_{C} seems to be

[2] This constant is defined as the static energy of a Bloch wall which separates two domains of opposite spin polarization in a magnetically ordered solid (see e.g. Ashcroft and Mermin [67]).

determined more by the width of the narrow polaron band around the Fermi level, which decreases exponentially with g. Thus one may expect that $D/(k_B T_C)$ increases with increasing g, and thus with decreasing T_C. This is found experimentally, as discussed later.

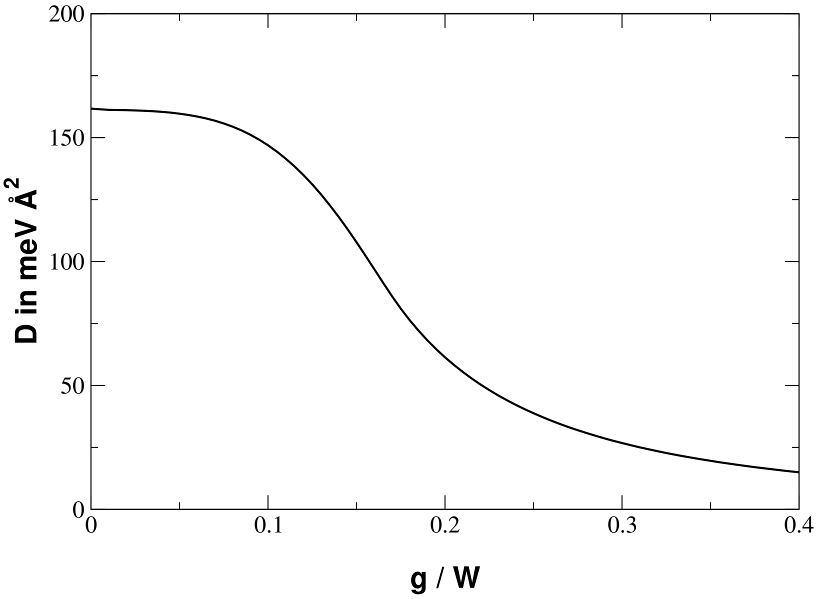

Figure 5.2.: The spin-wave stiffness D versus electron-phonon coupling g in the saturated ferromagnetic state at $T = 0$. The plot is for $S = J = \infty$, $W = 1$eV, $n = 0.5$ and $a =4$Å.

Green and Edwards [21, 31] find that, in the DE model with $n = 0.5$, T_C only increases by 5% when S increases from 3/2 to ∞. A similar insensitivity to S for $S \geq 3/2$ is expected in the Holstein-DE model. Hence, from equation (5.32) with $A_E(\epsilon)$ taken in the $S \to \infty$ limit as discussed, we have $\delta = D/(k_B T_C a^2) \propto (S + \frac{1}{2}n)^{-1}$. This is similar to the result $\delta = \frac{1}{2}(s+1)^{-1}$ for the spin s nearest neighbour simple cubic Heisenberg model, with follows from equations (5.13) and (5.14). Using values of T_C accurate to within about 1% [69] we find an improved Heisenberg value of $\delta = 0.286$ for $s = 3/2$, and $\delta = 0.258$ for an interpolated $s = 1.75$ which models the spin per site $S + \frac{1}{2}n$ in the present model. In the present calculations for D/a^2, together with those of Green [20] for T_C, we find, for $S = 3/2$ $\delta \approx 0.24$ for $g/W = 0.1$ and $\delta \approx 0.29$ for $g/W = 0.16$. With $a = 4$Å these values correspond to $D/(k_B T_C) \approx 3.9$ and 4.6Å^2, respectively. The agreement of these values of δ with the Heisenberg model suggests that for moderate g/W the ferromagnetic transition in the many-body CPA treatment of the Holstein-DE model is quite Heisenberg-like. However, this may not be the case for larger g/W where, as discussed above, δ increases rapidly with g/W.

To compare our theoretical results with experiment we first note that the simple spin-wave dispersion in equation (5.28), which is of the Heisenberg form, has been found to fit data on $La_{0.7}Pb_{0.3}MnO_3$ ($T_C = 355$K) throughout the Brillouin zone [70]. In this work the low temperature stiffness constant $D = 134$meVÅ^2 so that $D/(k_BT_C) = 4.4$Å^2. In LSMO, also with $x = 0.3$, Martin et al. [10] find $T_C = 378$K and $D \approx 188$meVÅ^2 (at 27K) so that $D/(k_BT_C) = 5.8$Å^2. $Pr_{0.63}Sr_{0.37}MnO_3$ seems to behave similarly with $T_C = 301$K, $D = 165$meVÅ^2, $D/(k_BT_C) = 6.4$Å^2 [71]. Although $D/(k_BT_C)$ in the last two materials is larger than in a Heisenberg model, their spin dynamics near T_C is quite conventional [10, 71]. However in some systems with lower T_C this is not the case, and $D/(k_BT_C)$ is considerably larger. Thus in LCMO, with $T_C = 250$K, $D = 170$meVÅ^2, $D/(k_BT_C) = 7.9$Å^2, the ferromagnetic transition seems not to be a standard second order one [72]. Also in NSMO, with $T_C = 198$K, $D = 165$meVÅ^2, $D/(k_BT_C) = 9.7$Å^2, the spin-wave stiffness constant does not collapse to zero at $T = T_C$ [71], just as in LCMO [72]. It is not clear whether such behaviour could occur within the Holstein-DE model or whether inhomogeneity due to disorder is important. However the larger values of $D/(k_BT_C)$ predicted by the model for strong electron-phonon coupling suggests that something unusual is going on. It is worth mentioning that D may be underestimated by the many-body CPA for an intermediate electron-phonon coupling such as $g/W = 0.16$ appropriate to LCMO. This is because spurious incoherent scattering near the Fermi level reduces the 'kinetic energy' K, and hence D. On the other hand equation (5.29) itself gives an upper bound to D which, in a better approximation will certainly be reduced. For the DE model, in approximations equivalent to the random phase approximation (RPA) [19, 66, 54], this is achieved by an additional negative term proportional to Δ^{-1} where $\Delta = JS$ is the Hartree-Fock exchange splitting between up and down spin bands. In the presence of an onsite Coulomb interaction U, $\Delta = JS + Un$ so that the negative term is considerably reduced. RPA estimates of D in a two-band model differ widely [54, 73]. For the one-band model with $J = \infty$ and $S = 3/2$ Golosov [74] has shown that D is reduced to about half its $S = \infty$ value, over a wide range of band-filling, when magnon-electron scattering processes are considered. A detailed discussion of spin waves in the DE and the Holstein-DE model is given by Edwards [8].

Appendix

A. Computational details

A.1. Green function and self-energy

As discussed in chapter 3, for $J = \infty$, in the paramagnetic or the saturated ferromagnetic state, the Green function for finite e_g band width $2W$ can be calculated from the CPA equation

$$G = G^{\mathrm{AL}}(\epsilon - W^2 G/4) \tag{A.1}$$

which has to be solved for G self-consistently. Here G^{AL} is given by equations (3.39)–(3.45). As a starting point for the iteration of the CPA equation we take the Green function for the pure DE model, for $J = \infty$, given by equation (3.31). Equation (A.1) is then iterated until the required accuracy[1] for G is reached.

For practical reasons G is calculated on a lattice of energy-points with the number of points determined by the accuracy. Once we know $G(\epsilon)$ it is easy to obtain the self-energy from

$$\Sigma_\sigma(\epsilon) = \epsilon - G^{-1}(\epsilon) - \frac{W^2 G(\epsilon)}{4} \tag{A.2}$$

which follows from equation (3.27).

With the Green function and the self-energy we can calculate the density of states, the spectral function, the optical conductivity and the spin-wave stiffness constant.

A.2. Integrations

The double integrals appearing in the formulas for the optical conductivity and the spin-wave stiffness are calculated using an extension of **Simpsons's Rule** to a double integral over a rectangular area. The formula can be found, for example, in Burden and Faires [75] and we have chosen the lattice points (x_i, y_i) used there as the mesh points for the Green function and the self-energy.

Simple one-dimensional integrals, which are for example necessary to determine the chemical potential by integration over the density of states, where evaluated using a standard **Gauß-Legendre** routine from the Numerical Recipes [76].

[1] Since the Green function G is complex-valued, the (relative) error is calculated for the modulus of G.

B. Spin waves

B.1. Normalization of the one-magnon state

As spin operators of local and itinerant moments commute we have

$$\begin{aligned}[S^+_{-\boldsymbol{q}} + \sigma^+_{-\boldsymbol{q}}, S^-_{\boldsymbol{q}} + \sigma^-_{\boldsymbol{q}}] &= [S^+_{-\boldsymbol{q}}, S^-_{\boldsymbol{q}}] + [\sigma^+_{-\boldsymbol{q}}, \sigma^-_{\boldsymbol{q}}] \\ &= 2S^z(0) + 2\sigma^z(0)\,,\end{aligned}$$

where we have used the commutation relations from equations (5.4) and (5.5). From equations (5.3), with $\boldsymbol{k} = 0$, we obtain

$$S^z(0)\,|F\rangle = \sum_i S^z_i\,|F\rangle = NS\,, \tag{B.1}$$

since $|F\rangle$ denotes the state with all local spins (with magnitude S) pointing in the z direction. We also have

$$\begin{aligned}\sigma^z(0) = \sum_i \sigma^z_i &= \frac{1}{2}\sum_i (n_{i\uparrow} - \underbrace{n_{i\downarrow}}_{0}) \\ &= \frac{1}{2}\sum_i n_{i\uparrow} = \frac{1}{2} nN\end{aligned}$$

where we have used $n_\uparrow = \sum_i \langle n_{i\uparrow}\rangle = n$, $n_\downarrow = 0$.

B.2. Proof of $[H, S^-_{\boldsymbol{q}} + \sigma^-_{\boldsymbol{q}}] = [H_0, S^-_{\boldsymbol{q}} + \sigma^-_{\boldsymbol{q}}]$

The Hamiltonian of the Holstein-DE model is

$$H = H_0 \underbrace{- J\sum_i \boldsymbol{S}_i \cdot \boldsymbol{\sigma}_i}_{A} \underbrace{- g\sum_i n_i \left(b^\dagger_i + b_i\right)}_{B} + \underbrace{\omega \sum_i b^\dagger_i b_i}_{C}\,. \tag{B.2}$$

The last term in equation (B.2) trivially commutes with the spin lowering operators since it only contains phonon operators. Term B contains phonon and conduction electron operators and consequently commutes with the local spin $S_{\boldsymbol{q}}^-$. Hence we are left with

$$\begin{aligned}[C, S_{\boldsymbol{q}}^- + \sigma_{\boldsymbol{q}}^-] &= \sum_i [n_i(b_i^\dagger + b_i), \sigma_{\boldsymbol{q}}^-] \\ &= \sum_i (b_i^\dagger + b_i)[n_i, \sigma_{\boldsymbol{q}}^-]\,.\end{aligned}$$

To evaluate $[n_i, \sigma_{\boldsymbol{q}}^-]$, we use $n_{i\sigma} = N^{-1}\sum_{\boldsymbol{k}\sigma}\exp(\mathrm{i}\boldsymbol{k}\cdot\boldsymbol{R})n_{\boldsymbol{k}\sigma}$. Replacing $\sigma_{\boldsymbol{q}}^-$ according to equation (5.22) we get

$$\begin{aligned}[n_{\boldsymbol{k}\sigma}, \sigma_{\boldsymbol{q}}^-] &= \sum_p \left\{ a_{\boldsymbol{k}\sigma}^\dagger [a_{\boldsymbol{k}\sigma}, a_{\boldsymbol{p}\downarrow}^\dagger a_{\boldsymbol{p}+\boldsymbol{q}\uparrow}] + [a_{\boldsymbol{k}\sigma}^\dagger, a_{\boldsymbol{p}\downarrow}^\dagger a_{\boldsymbol{p}+\boldsymbol{q}\uparrow}] a_{\boldsymbol{k}\sigma} \right\} \\ &= \sum_p \left\{ \delta_{\boldsymbol{k}\boldsymbol{p}}\delta_{\sigma\downarrow} a_{\boldsymbol{k}\sigma}^\dagger a_{\boldsymbol{k}+\boldsymbol{q}\uparrow} - \delta_{\boldsymbol{k},\boldsymbol{p}+\boldsymbol{q}}\delta_{\sigma\uparrow} a_{\boldsymbol{k}-\boldsymbol{q}\downarrow}^\dagger a_{\boldsymbol{k}\sigma} \right\} \\ &= a_{\boldsymbol{k}\downarrow}^\dagger a_{\boldsymbol{k}+\boldsymbol{q}\uparrow} - a_{\boldsymbol{k}-\boldsymbol{q}\downarrow}^\dagger a_{\boldsymbol{k}\uparrow}\,.\end{aligned}$$

Using this result we obtain

$$\sum_i (b_i^\dagger + b_i)[n_i, \sigma_{\boldsymbol{q}}^-] = \frac{1}{N}\sum_i (b_i^\dagger + b_i) \sum_{\boldsymbol{k}\sigma} \mathrm{e}^{\mathrm{i}\boldsymbol{k}\cdot\boldsymbol{R}_i} \left\{ a_{\boldsymbol{k}\downarrow}^\dagger a_{\boldsymbol{k}+\boldsymbol{q}\uparrow} - a_{\boldsymbol{k}-\boldsymbol{q}\downarrow}^\dagger a_{\boldsymbol{k}\uparrow} \right\}\,.$$

As the second sum runs over all $\boldsymbol{k}$ we can make the substitution $\boldsymbol{k} \to \boldsymbol{k} + \boldsymbol{q}$ in the last term yielding $[C, S_{\boldsymbol{q}}^- + \sigma_{\boldsymbol{q}}^-] = 0$.

In a second step we have to show that $(S_{\boldsymbol{q}}^- + \sigma_{\boldsymbol{q}}^-)$ commutes with term A of equation (B.2). To this end, we again use the Fourier transform of spin operators (equations (5.3))

$$[A, S_{\boldsymbol{q}}^- + \sigma_{\boldsymbol{q}}^-] = \sum_{il} \mathrm{e}^{-\mathrm{i}\boldsymbol{q}\cdot\boldsymbol{R}_l} X + \sum_{im} \mathrm{e}^{-\mathrm{i}\boldsymbol{q}\cdot\boldsymbol{R}_m} Y \tag{B.3}$$

where $X = [\boldsymbol{S}_i \cdot \boldsymbol{\sigma}_i, S_l^-]$ and $Y = [\boldsymbol{S}_i \cdot \boldsymbol{\sigma}_i, \sigma_m^-]$. Exploiting equation (5.2) and the commutation relations of equations (5.4) we find

$$X = \delta_{il}\left\{\sigma_i^- S_i^z - \sigma_i^z S_i^-\right\}\,, \quad Y = \delta_{im}\left\{\sigma_i^z S_i^- - \sigma_i^- S_i^z\right\}\,.$$

Inserting this result in equation (B.3) shows that $[A, S_{\boldsymbol{q}} + \sigma_{\boldsymbol{q}}^-] = 0$.

Conclusions

The many-body CPA treatment of the Holstein-DE model has been used to investigate several spectral properties which may be compared with experimental data on the manganites. We have been able to supply the theory which was hinted at by Dessau et al. [47] in the discussion of their ARPES measurements on the layered manganite $La_{1.2}Sr_{1.8}Mn_2O_7$ in the low temperature ferromagnetic state. Broad spectral peaks lie either side of a pseudogap at the Fermi level and the pseudogap contains polaron subbands with exponentially small weight. One of these, at the Fermi level, is responsible for the poor metallic behaviour. We therefore agree with Alexandrov and Bratkovsky [77] that in this system, with unusually strong electron-phonon coupling, small polarons exist in the ferromagnetic state. However we find that small-polaron theory does not apply above or below T_{C} in a pseudocubic manganite like $Nd_{0.7}Sr_{0.3}MnO_3$ with intermediate coupling strength. In particular the small-polaron result that the activation energy of the high-temperature dc conductivity is one-quarter of the peak photon energy in optical conductivity $\sigma(\nu)$ is found not to hold, in agreement with experiments on NSMO. The observed shift in spectral weight of $\sigma(\nu)$ to lower energy on going into the ferromagnetic state is found to occur, although it is somewhat suppressed by spurious incoherent scattering at $T = 0$ which is a defect of the theory. A rigorous upper bound is derived for spin-wave energies at $T = 0$ in the Holstein-DE model. It is shown that the spin-wave stiffness constant D decreases with increasing electron-phonon coupling strength in a similar way to T_{C}. However, for strong coupling the ratio $D/(k_{\mathrm{B}}T_{\mathrm{C}})$ increases quite rapidly with increasing coupling strength, i.e. with decreasing T_{C}. This trend is found experimentally.

Bibliography

[1] G. H. Jonker and J. H. V. Santen, Physica **16**, 337 (1950).

[2] J. H. Van Santen and G. H. Jonker, Physica **16**, 599 (1950).

[3] C. Zener, Phys. Rev. **82**, 403 (1951).

[4] P. W. Anderson and H. Hasegawa, Phys. Rev. **100**, 675 (1955).

[5] J. Volger, Physica **20**, 49 (1954).

[6] J. M. D. Coey, M. Viret, and S. von Molnár, Advances in Physics **48**, 167 (1999).

[7] A. P. Ramirez, J. Phys.: Condens. Matter **9**, 8171 (1997).

[8] D. M. Edwards, Advances in Physics **51**, 1259 (2002).

[9] S. Satpathy, Z. S. Popović, and F. R. Vukajlovič, Phys. Rev. Lett. **76**, 960 (1996).

[10] M. C. Martin, G. Shirane, Y. Endoh, K. Hirota, Y. Moritomo, and Y. Tokura, Phys. Rev. B **53**, 14285 (1996).

[11] A. Moreo, S. Yunoki, and E. Dagotto, Science **283**, 2034 (1999).

[12] E. L. Nagaev, Phys. Uspekhi **39**, 781 (1996).

[13] Y. Tomioka, A. Asamitsu, H. Kuwuhara, Y. Moritomo, and Y. Tokura, Phys. Rev. B **53**, R1689 (1996).

[14] P. Schiffer, A. P. Ramirez, W. Bao, and S.-W. Cheong, Phys. Rev. Lett. **75**, 3336 (1995).

[15] A. Urushibara, Y. Moritomo, T. Arima, A. Asamitsu, G. Kido, and Y. Tokura, Phys. Rev. B **51**, 14103 (1995).

[16] D. N. McIlroy, C. Waldfried, J. Zhang, J.-W. Choi, F. Foong, S. H. Liou, and P. A. Dowben, Phys. Rev. B **54**, 17438 (1996).

[17] W. Nolting, *Viel-Teilchen-Theorie*, volume 7 of *Grundkurs Theoretische Physik* (Vieweg, 1997), 4th edition.

[18] A. J. Millis, P. B. Littlewood, and B. I. Shraiman, Phys. Rev. Lett. **74**, 5144 (1995).

[19] N. Furukawa, in *Physics of Manganites*, edited by T. A. Kaplan and S. D. Mahanti (Kluwer, New York, 1999), p 1.

[20] A. C. M. Green, Phys. Rev. B **63**, 205110 (2001).

[21] D. M. Edwards, A. C. M. Green, and K. Kubo, J. Phys.: Condens. Matter **11**, 2791 (1999).

[22] W. Nolting, *Quantentheorie des Magnetismus*, volume 1 (B G Teubner, 1986).

[23] A. J. Millis, R. Müller, and B. I. Shraiman, Phys. Rev. B **54**, 5405 (1996).

[24] G. D. Mahan, *Many-particle Physics* (Plenum Press, 1990), second edition.

[25] T. Holstein, Ann. Phys. (N.Y.) **8**, 325; **8**, 343 (1959).

[26] T. Holstein, Ann. Phys. (N.Y.) **8**, 343 (1959).

[27] H. Röder, J. Zang, and A. R. Bishop, Phys. Rev. Lett. **76**, 1356 (1996).

[28] J. Zang, A. R. Bishop, and H. Röder, Phys. Rev. B **53**, R8840 (1996).

[29] J. D. Lee and B. I. Min, Phys. Rev. B **55**, 12 454 (1997).

[30] A. S. Alexandrov and A. M. Bratkovsky, J. Phys.: Condens. Matter **11**, 1989 (1999).

[31] A. C. M. Green and D. M. Edwards, J. Phys.: Condens. Matter **11**, 10511 (1999), *erratum*, 2000, 12, 9107.

[32] A. J. Millis, B. I. Shraiman, and R. Müller, Phys. Rev. Lett. **77**, 175 (1996).

[33] J. Ranninger, Phys. Rev. B **48**, 13 166 (1993).

[34] K. Held and D. Vollhardt, Phys. Rev. Lett. **84**, 5168 (2000).

[35] A. J. Millis, R. Müller, and B. I. Shraiman, Phys. Rev. B **54**, 5389 (1996).

[36] S. Ciuchi, F. de Pasquale, S. Fratini, and D. Feinberg, Phys. Rev. B **56**, 4494 (1997).

[37] A. Georges, G. Kotliar, W. Krauth, and M. J. Rosenberg, Rev. Mod. Phys. **68**, 13 (1996).

[38] K. Kubo, J. Phys. Soc. Jpn. **36**, 32 (1974).

[39] H. Sumi, J. Phys. Soc. Jpn. **36**, 770 (1974).

[40] V. Janiš, Z. Phys. B. Condens. Matter **83**, 227 (1991).

[41] J. K. Freericks, M. Jarrell, and D. J. Scalapino, Europhys. Lett. B **25**, 37 (1994).

[42] W. Gasser, E. Heiner, and K. Elk, *Greensche Funktionen in der Festkörper- und Vielteilchenphysik* (Wiley-VCH, 2001).

[43] J. Hubbard, Proc. Roy. Soc. **281**, 401 (1964).

[44] R. J. Elliot, J. A. Krumhansl, and P. L. Leath, Rev. Mod. Phys. **46**, 465 (1974).

[45] D. Emin and T. Holstein, Ann. Phys. (N.Y.) **53**, 439 (1969).

[46] Bronshtein and Semendyayev, *Handbook of Mathematics* (Verlag Harri Deutsch, 1985), 3rd edition.

[47] D. S. Dessau, T. Saitoh, C.-H. Park, Z.-X. Shen, P. Villella, N. Hamada, Y. Moritomo, and Y. Tokura, Phys. Rev. Lett. **81**, 192 (1998).

[48] V. Perebinos and P. B. Allen, Phys. Rev. Lett. **85**, 5178 (2000).

[49] A. Moreo, S. Yunoki, and E. Dagotto, Phys. Rev. Lett. **83**, 2773 (1999).

[50] T. Pruschke, M. Jarrell, and J. K. Freericks, Advances in Physics **44**, 187 (1995).

[51] W. Chung and J. K. Freericks, Phys. Rev. B **57**, 11955 (1998).

[52] A. Chattopadhyay, A. J. Millis, and S. Das Sarma, Phys. Rev. B **61**, 10738 (2000).

[53] T. Pruschke, D. L. Cox, and M. Jarrell, Phys. Rev. B **47**, 3553 (1993).

[54] M. Quijada, J. Černe, J. R. Simpson, H. D. Drew, K. H. Ahn, A. J. Millis, R. Shreekala, R. Ramesh, M. Rajeswari, and T. Venkatesan, Phys. Rev. B **58**, 16093 (1998).

[55] S. G. Kaplan, M. Quijada, H. D. Drew, D. B. Tanner, G. C. Xiong, R. Ramesh, C. Kwon, and T. Venkatesan, Phys. Rev. Lett. **77**, 2081 (1996).

[56] H. J. Lee, J. H. Jung, Y. S. Lee, J. S. Ahn, T. W. Noh, K. H. Kim, and S.-W. Cheong, Phys. Rev. B **60**, 5251 (1999).

[57] G.-m. Zhao, D. J. Kang, W. Prellier, M. Rajeswari, H. Keller, T. Venkatesan, and R. L. Greene, Phys. Rev. B **63**, 060402(R) (2000), see also cond-mat/9912355.

[58] A. C. M. Green (unpublished).

[59] S. Ishihara, M. Yamanaka, and N. Nagaosa, Phys. Rev. B **56**, 686 (1997).

[60] F. Mack and P. Horsch, in *Physics of Manganites*, edited by T. A. Kaplan and S. D. Mahanti (Kluwer, New York, 1999), p 103.

[61] W. Nolting, *Quantentheorie des Magnetismus*, volume 2 (B G Teubner, 1986).

[62] E. L. Nagaev, Sov. Phys. Solid State **11**, 2249 (1970).

[63] E. L. Nagaev, Phys. Rev. B **58**, 827 (1998).

[64] K. Kubo and N. Ohata, J. Phys. Soc. Jpn. **33**, 21 (1972).

[65] N. Furukawa, J. Phys. Soc. Jpn. **65**, 1174 (1996).

[66] X. Wang, Phys. Rev. B **57**, 7427 (1998).

[67] N. W. Ashcroft and N. D. Mermin, *Solid State Physics* (Saunders College Publishing, 1976).

[68] A. S. Alexandrov and N. F. Mott, Rep. Prog. Phys. **57**, 1197 (1994).

[69] G. S. Rushbrooke and P. J. Wood, Molec. Phys. **1**, 257 (1958).

[70] T. G. Perring, G. Aeppli, S. M. Hayden, S. A. Carter, J. P. Remeika, and S.-W. Cheong, Phys. Rev. Lett. **77**, 711 (1996).

[71] J. A. Fernandez-Baca, P. Dai, H. Y. Hwang, C. Kloc, and S.-W. Cheong, Phys. Rev. Lett. **80**, 4012 (1998).

[72] J. W. Lynn, R. W. Erwin, J. A. Borchers, Q. Huang, A. Santoro, J.-L. Peng, and Z. Y. Li, Phys. Rev. Lett. **76**, 4046 (1996).

[73] G.-m. Zhao, Phys. Rev. B **62**, 11639 (2000).

[74] D. I. Golosov, Phys. Rev. Lett. **84**, 3974 (2000).

[75] R. L. Burden and J. D. Faires, *Numerical Analysis* (Brooks / Cole Publishing Company, 1997), 6th edition.

[76] W. H. Press, *Numerical Recipes in C* (Cambridge University Press, 1988).

[77] A. S. Alexandrov and A. M. Bratkovsky, J. Phys.: Condens. Matter **11**, L531 (1999).

Acknowledgments

Naturally, there are many people who deserve a few words of thanks for their help and support during the last years and especially during the work on this diploma thesis.

The first of these belong to **Prof. David M Edwards**, who supervised, guided and inspired my research work at Imperial College. It was a very instructive and fruitful collaboration and a great pleasure and honour to work with him. Second, I am very grateful to my supervisor, **Prof. Wolfgang von der Linden**, who gave me the opportunity to work at Imperial College and who sparked my interest in strongly-correlated electron systems. I am also deeply indebted to **Prof. Hans Gerd Evertz** for all his advice and help in the last two years. I am grateful to **Dietrich Meyer** for answering so many physical and computational questions during my stay at IC. I want to thank **Winfried Koller**, **Alex Prüll** and **Prof. Ewald Schachinger** for fruitful discussion. My work was financially supported by a **Förderungsstipendium** from the Faculty of Natural Sciences at Technical University Graz, a grant from the **Industriellenvereinigung Steiermark** and a scholarship from the **Steiermärkische Landesregierung**. Moreover half of my stay in London was supported by the **Department of Mathematics** at IC by means of an IAESTE summer working placement. I want to thank my friend **Philipp Huber** for inspiring me to study physics. **Antonio Völker** from HyperGra provided the figure on the title page. Last but definitely not least, I am very grateful to my fiancée, **Kathrin Weinhandl**, who helped me with her unlimited love, and to my parents, **Ferdinand** and **Verena Hohenadler**, for their love and financial support in all the years.

Typeset by $\LaTeX\,2_\varepsilon$, the **KOMA**-script and
$\mathcal{A}\mathcal{M}\mathcal{S}$-TEX the TEX macro system of the American Mathematical Society.